OPTIMIZING THE PERFORMANCE OF NEURAL INTERFACE DEVICES WITH HYBRID POLY(3,4-ETHYLENE DIOXYTHIOPHENE) (PEDOT)

by

Chin-chen Kuo

A dissertation submitted to the Faculty of the University of Delaware in partial fulfillment of the requirements for the degree of Doctor of Philosophy in Materials Science and Engineering

Winter 2017

OPTIMIZING THE PERFORMANCE OF NEURAL INTERFACE DEVICES

WITH

HYBRID POLY(3,4-ETHYLENE DIOXYTHIOPHENE) (PEDOT)

by

Chin-chen Kuo

Approved: _____

Darrin J. Pochan, Ph.D.
Chair of the Department of Materials Science and Engineering

Approved: _____

Babatunde A. Ogunnaike, Ph.D.
Dean of the College of Engineering

Approved: _____

Ann L. Ardis, Ph.D.
Senior Vice Provost for Graduate and Professional Education

I certify that I have read this dissertation and that in my opinion it meets the academic and professional standard required by the University as a dissertation for the degree of Doctor of Philosophy.

Signed: _____

David C. Martin, Ph.D.
Professor in charge of dissertation

I certify that I have read this dissertation and that in my opinion it meets the academic and professional standard required by the University as a dissertation for the degree of Doctor of Philosophy.

Signed: _____

Darrin J. Pochan, Ph.D.
Member of dissertation committee

I certify that I have read this dissertation and that in my opinion it meets the academic and professional standard required by the University as a dissertation for the degree of Doctor of Philosophy.

Signed: _____

Chaoying Ni, Ph.D.
Member of dissertation committee

I certify that I have read this dissertation and that in my opinion it meets the academic and professional standard required by the University as a dissertation for the degree of Doctor of Philosophy.

Signed: _____

Jeffrey L. Caplan, Ph.D.
Member of dissertation committee

ACKNOWLEDGMENTS

I first would like to acknowledge my adviser, Prof. David Martin, for his support throughout journey of my Ph.D. degree. I especially like to appreciate his guidance style. When I was a first-year rookie in his group, he showed us his typical guidance that "as long as you don't blow up the lab, go ahead to try any crazy ideas". That is, in my Ph.D. life, we have some successful projects, some failed projects, some crazy projects and some discoveries we don't even know yet how to interpret. Those ups and downs put my Ph.D. together. He showed me his passion in pursuing knowledge, which inspired me the most not only on the research field but also for my future life. This thesis would not be possible without his guidance and support.

I would like to thank to my committee members, Prof. Darrin Pochan, Prof. Chaoying Ni, and Dr. Jeffrey Caplan for their suggestions on my dissertation. I also like to thank to my collaborators. I especially thank Prof. Amy Griffin in Department of Psychology for her guidance in the animal studies. Dr. Jeffery Caplan, Deborah Powell, Jean Ross in Bioimaging Center of Delaware Biotechnology of Institute, Dr. Chaoying Ni, Dr. Fei Deng, and Dr. Jen Sloppy in Keck lab helped me with their professional expertise on image acquistion.

I have been fortunate to have great group members, Dr. Lianqi Ouyang, Dr. Jinglin Liu, Dr. Bin Wei and Jing Qu. For the research-wise, we have been through a lot of brainstorming, discussions and challenges. For my personal life, they have been always my great support through all these years. I like to thank to our previous group members, Dr. Bong-sup Shim, Dr. Jinghang Wu, Dr. Katie Feldman, Dr. Laura Povlich

and Dr. Charles Shaw, who helped me to learn things in the lab during my first year. I also want to thank Charlie Garbini, our lab coordinator, for his effort to keep us safe and ensuring we don't blow up the lab.

Moreover, I would like to thank a lot of friends for bringing happiness and fulfillment to my graduate student life: Hsu-Ying Chen, Chun-Yen Hsu, Hui-Ting Chung, Ching-Lung Chen, Sunny Yang, Wei-Fan Kuan, and Jenn Fang Su. I also want to thank to my parents and my parents-in-law for their understanding and support on my graduate study. Finally, I would like to thank my wife, Chia-tzu Lin, and my lovely girl, Riko Kuo, who might be the reason why I have to spend one more year for my Ph.D. but it is totally worth it.

This work has been financially supported by the NIH, DARPA, and the University of Delaware.

TABLE OF CONTENTS

LIST OF TABLES ix
LIST OF FIGURES x
ABSTRACT xiv

Chapter

1 CONJUGATED POLYMERS AS NEURAL INTERFACING MATERIALS 1

1.1 Neural Interfaces and Neural Electrodes 1
1.2 Chronic Foreign Body Response in the Central Nervous System 2
1.3 Conducting Polymers as Softer, More Conductive and Biocompatible Neural Interfacing Materials 3

1.3.1 PEDOT as a Neural Interfacing Material 4

1.4 Challenges of PEDOT 5

1.4.1 Mechanical Failures of PEDOT Coating 5

1.4.1.1 Cohesion of PEDOT- Cracking 6
1.4.1.2 Adhesion of PEDOT Coating- Delamination 8
1.4.1.3 Challenges of Quantifying Mechanical Properties from a PEDOT Thin Film 9

1.4.2 Mechanical Mismatch Between PEDOT Coating and Tissues: Foreign Body Response 10
1.4.3 EDOT- Lack of Biological Cues 14

1.5 Motivations and Objectives 16
1.6 Outline of the Thesis 18

REFERENCES 24

2 NANOSCALE MECHANICAL TESTING OF ELECTROCHEMICALLY DEPOSITED PEDOT THIN FILMS BY *IN SITU* FOCUSED ION BEAM/SCANNING ELECTRON MICROSCOPY (FIB/SEM) 34

2.1 Introduction 34
2.2 Materials and Methods 37

2.2.1 Electrochemical Deposition 37
2.2.2 Specimen Preparation 37
2.2.3 AFM-QNM Measurements 37
2.2.4 Data Analysis 38
2.2.5 Results and Discussion 38
2.2.6 Force and Elongation of EC-PEDOT during Tensile Test 40
2.2.7 Stress-Strain Curve of EC-PEDOT 41
2.2.8 Other Methods to Obtain Mechanical Properties of PEDOT 42
2.2.9 *In Situ* Test in TEM 46
2.2.10 Beam Damage 46

2.3 Conclusions 47

REFERENCES 54

3 ELECTROCHEMICAL DEPOSITION OF PEDOT IN ADIPOSE-DERIVED STEM CELL (ADSC) PRODUCED EXTRACELLULAR MATRIX (ECM)……...58

3.1 Introduction 58
3.2 Materials and Methods 62

3.2.1 ECM Fabrication and Characterization 62
3.2.2 *In Situ* Polymerization of PEDOT into ECM Constructs 63
3.2.3 PEDOT-ECM Characterizations: Electrical Properties 63
3.2.4 PEDOT-ECM Characterizations: Surface Morphology 64
3.2.5 *In Vitro* Cell Culture Tests 64

3.3 Results and Discussions 65

3.3.1 Fabrication of ECM 65
3.3.2 *In Situ* Polymerization of PEDOT into ECM Film 66
3.3.3 SEM Observations 68
3.3.4 Electrical Properties 69
3.3.5 *In Vitro* Study-PC12 Adhesion Test 70

3.4 Conclusions 71

REFERENCES 80

4 *IN SITU* POLYMERIZATION OF PEDOT IN LOW MODULUS HYDROGELS FOR NEURAL INTERFACES 85

4.1 Introduction 85
4.2 Materials and Methods 90

4.2.1 Fabrication EDOT-gel Coated Electrodes 90
4.2.2 *In Situ* Polymerization of PEDOT in Hydrogels 91
4.2.3 PEDOT-gel Characterizations: Electrical Properties 92
4.2.4 PEDOT-gel Characterizations: Morphology 92
4.2.5 PEDOT-gel Characterizations: Mechanical Properties 93
4.2.6 *In Vitro* Cell Culture Tests: PC12 94
4.2.7 Animal Study Design 95

4.3 Results and Discussion 96

4.3.1 Mechanical Properties 97
4.3.2 Morphologies of PEDOT-gel 98
4.3.3 Electrical Properties 100
4.3.4 *In Vivo* Study 102

4.4 Conclusions 105

REFERENCES 115

5 CONCLUSIONS AND FUTURE DIRECTIONS 121

5.1 Conclusions 121
5.2 Future Directions 123

5.2.1 Conductive Micro-organism Coated Electrodes 123
5.2.2 *In Situ* Observations of PEDOT Electrochemical Polymerization 125

REFERENCES 131

LIST OF TABLES

Table 2.1 Comparison of different mechanical characterization methods 53

LIST OF FIGURES

Figure 1.1 Examples of PEDOT delamination and cracking. (a-d) PEDOT delamination (Abidian et al., 2010) (e) PEDOT cracking after ETO sterilization (Green et al., 2013a). 20

Figure 1.2 (a) Impedance amplitude of PEDOT and PEDOT-co-EPh copolymers as a function of frequency; (b) impedance amplitude at 1 Hz and 1 kHz for the PEDOT-co-EPh copolymers as a function of EPh content; dashed lines indicate the impedance amplitude of bare Pt electrode at 1 Hz (red) and 1 kHz (black), respectively. (deposition charge: 288 mC/cm^2) (Ouyang et al, 2015) 21

Figure 1.3 AFM-QNM modulus distribution. (top) AFM image of the polymer films (2 μm by 2 μm); (bottom) AFM-QNM DMT modulus distribution of PEDOT, 0.1% EPh and 0.5% EPh (Ouyang et al., 2015)… 22

Figure 1.4 Schematic of using PEDOT-amine as the adhesion promoting layer. (a) PEDOT deposition on solid substrates. (b) PEDOT deposition on PEDOT-amine layer. (Ouyang et al., in review) 23

Figure 1.5 Optical images of PEDOT films on ITO and on PEDOT-amine layer before and after sonication adhesion test. (Wei et al, 2015) 23

Figure 2.1 Tensile test in SEM chamber of EC-PEDOT specimen; (a) to (c) Schematic of fabrication of the EC-PEDOT dog bone specimen; (d) (e) attached both side of the specime to the force sensor for force measurement and the OmniProbe for operation. (f) the high resolutuon SEM image of in situ tensile test setup in SEM chamber. 48

Figure 2.2 (a) to (c) real time SEM images showing the tensile test of EC-PEDOT; (d) high magnification of gauge elongation during the tensile test……49

Figure 2.3 Stress (top) and strain (bottom) change with respect with time of EC-PEDOT during tensile test 50

Figure 2.4 Stress-strain curves of *in situ* tensile test. (a) stress-strain curves with different gauge thickness of 350, 450 and 750 nm. (b) stress-strain curves from three tests with exactly the same gauge thickness of 450 nm……..... 51

Figure 2.5 AFM QNM^{TM} modulus distribution of EC-PEDOT by different calibration method and probe force constant (left) . AFM image of the polymer film (1 μm by 1μm) (right). 52

Figure 3.1 (a) preparation scheme for ECM scaffolds and *in situ* PEDOT polymerization in ECM (b) Optical image of a free standing ECM prepared with AA & A2P culture for 2 weeks. 72

Figure 3.2 SEM images shows PEDOT deposition on gold electrode and under ECM film by using traditional electrode design. The insulated ECM film allows portion of the ions transportation but blocked all electron transportation limiting the conductive pathways during signal transmission. 73

Figure 3.3 Bright-field images (top) and schematic diagram (bottom) of *in situ* PEDOT polymerization in ECM film with different deposition time..... 74

Figure 3.4 SEM images of (a) ECM, (b) PEDOT-ECM showing the PEDOT clusters aggregated along ECM fibers, (c) PEDOT-ECM with lower magnification showing that PEDOT filled up the space between ECM fibers and (d) the schematic diagram of PEDOT-ECM 75

Figure 3.5 (a) SEM images of the interface between ECM and PEDOT-ECM with detail morphology correlated with (b) optical image of the sample..... 76

Figure 3.6 Impedance spectra for bare gold electrodes (red dash), PEDOT coated electrodes (blue), PEDOT-ECM coated electrodes (pink to red with respect to different deposition time) vs AC frequency..... 77

Figure 3.7 Differentiated PC12 attachment on various substrates for 4 days..... 78

Figure 3.8 The differentiation of PC12s on PEDOT-ECM modified electrodes. PC12s were differentiated for 7 days in NGF added medium. (a) Fluorescence image of differentiated PC12 cells on PEDOT-ECM substrate. The long neuritis confirms the high degree of differentiation. (b) SEM images of the detailed neurites of cells interacting with PEDOT-ECM coating. The arrows indicate axons attached to the PEDOT-ECM coated surface, not on the bare electrode..... 79

Figure 4.1 AFM QNM™ height and modulus distribution of dehydrated PEDOT-ECM. Scan size is 2 μm by 2 μm. The maximum of the DMT modulus of PEDOT-ECM is about 900 MPa which is significantly larger than cortex tissue. 106

Figure 4.2 The schematic of in situ PEDOT polymerization into hydrogel. (a) premix EDOT monomer with with agarose gel to form a EDOT-agarose gel. (b) apply potential to the system to oxidize EDOT to PEDOT, deposited on substrate in the beginning and then on the gel fibers. (c) dehydrate PEDOT-ECM using air dry method to collapse the PEDOT-gel structure, raising the modulus to allow safe implantation. (d) After implantation, reswell the PEDOT-gels with body fluid from the tissue. 107

Figure 4.3 Set up of the working electrode and counter electrode. the position of the PEDOT-gel coated cannula tip (working) was inserted into one hemisphere and the bare electrode (counter) was inserted into the other…. 108

Figure 4.4 (Top) the optical images showing the progress of PEDOT polymerized into hydrogels. The maximum thickness of PEDOT cloud in the gel was about 350 μm. (bottom) the thickness plot with respect with charge density confirming that PEDOT was initially deposited on the electrode as a thin film then at charge density of 0.8 C/cm^2, PEDOT starts to grow out to the hydrogel matrix. 109

Figure 4.5 The mechanical analysis of PEDOT-gel in (a) hydrated condition by rheometer and (b) dehydrated condition by AFM-QNM. The arrows indicate the mechanical modulus of rat hippocampus and stainless steel for the reference. 110

Figure 4.6 Swelling ratio of agarose gel and PEDOT-gel at different gel concentration at 0.5% and 1.0%. The presence of PEDOT inhibits the re-swelling ratio to about 30-50% of pure agarose gel. 111

Figure 4.7 SEM images of (a) hydrated PEDOT-gel (b) re-hydrated PEDOT-gel in DI water obtained by using WET SEM holder. Samples were images in the initial hydrated condition and then air dried in the room temperature overnight. The same samples were then immersed in DI water and imaged by SEM. 111

Figure 4.8 SEM images of (a) agarose gel and (b) PEDOT-gel prepared by critical point dry method. An obvious boundary between the PEDOT and PEDOT-gel interface was observed confirming the initial PEDOT thin film deposition on electrodes. 112

Figure 4.9 Electrical properties of PEDOT-gel was examined by EIS and CV. For EIS, (a) impedance amplitude and (b) phase angle of bare electrode, PEDOT coated, and PEDOT-gel coated electrode was compared over the frequency range between 1 Hz to 10kHz was. (c) CV was swept between -0.6 to 0.8 V for 20 cycles. 112

Figure 4.10 Viability tests of PC12 cells on bare, PEDOT coated and PEDOT-gel coated electrodes. PC12s were stained with live/dead viability kit where red represents dead cells and green represents live cells. 113

Figure 4.11 In vivo impedance of bare, PEDOT coated and PEDOT-gel coated electrodes implanted in rat hippocampus as working electrode in one hemisphere and a counter electrode in the other hemisphere. The recordings were taken and averaged every other day (three times a week) until 9 weeks of implantation. The data recorded at week 1, 2, 4 and 9 were plotted among 9 individual test (n=9). 114

Figure 5.1 Impedance spectra with respect with processing time for Geobacter deposition on Pt-Ir electrode shows that the impedance is lower with more Geobacter-derived material deposited. The embedded plot is the impedance spectra of a bare Pt-Ir electrode for reference. 127

Figure 5.2 (Right) the corresponding current recording during crystals formation. A significant drop of current reading was recorded where crystals were observed under optical microscope. (left) optical micrographs of the electrochemical deposition of PEDOT on a 25 micron diameter gold wire in the presence of agarose gel under potentiostatic condition of (a) 0, (b) 10 minutes, (c) 20 minutes, and (d) 30 minutes deposition time. After 20 minutes, birefringent, needle-shaped crystals were initially observed and then saturated after 30 minutes deposition. 128

Figure 5.3 Crystal length with respect to the hydrogel concentration and PSS concentration. The results suggested that without PSS or higher concentration of PSS, no crystals were observed in the system. (N=2 for each group. 3 images were analyzed from each sample. There were about 60-80 counts from each image. The final value is averaged from 300-500 countings) 129

Figure 5.4 TEM micrographs of PEDOT-crystals formed in the hydrogel. 130

ABSTRACT

This thesis describes methods for improving the performance of poly(3,4-ethylenedioxythiophene) (PEDOT) as a direct neural interfacing material. The chronic foreign body response is always a challenge for implanted bionic devices. After long-term implantation (typically 2-4 weeks), insulating glial scars form around the devices, inhibiting signal transmission, which ultimately leads to device failure. The mechanical mismatch at the device-tissue interface is one of the issues that has been associated with chronic foreign body response. Another challenge for using PEDOT as a neural interface material is its mechanical failure after implantation. We observed cracking and delamination of PEDOT coatings on devices after extended implantations.

In the first part of this thesis, we present a novel method for directly measuring the mechanical properties of a PEDOT thin film. Before investigating methods to improve the mechanical behavior of PEDOT, a comprehensive understanding of the mechanical properties of PEDOT thin film is required. A PEDOT thin film was machined into a dog-bone shape specimen with a dual beam FIB-SEM. With an OmniProbe, this PEDOT specimen could be attached onto a force sensor, while the other side was attached to OmniProbe. By moving the OmniProbe, the specimen could be deformed in tension, and a force sensor recorded the applied load on the sample simultaneously. Mechanical tensile tests were conducted in the FIB-SEM chamber along with *in situ* observation. With precise force measurement from the force sensor and the

corresponding high resolution SEM images, we were able to convert the data to a stress-strain curve for further analysis. By analyzing these stress-strain curves, we were able to obtain information about PEDOT including the Young's modulus, strength of failure, strain to failure, and toughness (energy to failure). This information should be useful for future material selection and molecular design for specific applications.

The second section of this thesis is mainly focused on developing a soft and conductive material by in situ PEDOT polymerization into soft matrix. First, PEDOT was *in situ* polymerized into extracellular matrix (ECM) as a conductive, soft, and bioactive material for neural interfacing. ECM is basically a matrix of proteins which provides biological cues with the potential to promote neural attachment. We modified the electrode to a needle shape, which could be inserted into the ECM film. The limited surface area on the electrode and the close contact with ECM made it possible to polymerize PEDOT into the ECM more easily. The conductivity of PEDOT-ECM was confirmed to be similar to intrinsic PEDOT. A cell adhesion test using the PC12 cell line was used to evaluate its biocompatibility. PEDOT-ECM shows improved cell adhesion for PC12 cells, as compared either bare metal electrodes or PEDOT coated surfaces. In the future this approach may be elevated to an " autologous" concept, where the ECM could be derived from the host patients themselves to further reduce the foreign body response.

Second, low modulus hydrogels were used as templates for PEDOT polymerization. EDOT monomers were premixed into agarose hydrogels. The

electrochemical polymerization was typically conducted in potentiostatic (constant voltage) mode with working voltage of 2 V. After 0.8 C/cm^2 charge density, a significant dark blue cloud was observed indicating that PEDOT was in situ polymerized into hydrogel matrix. A series of studies was conducted to confirm the improved mechanical properties, electrical properties and biocompatibility of the PEDOT-gel as compared to the typical solid PEDOT. Animal studies were conducted to evaluate the performance of PEDOT-gel coated electrode *in vivo*. Rats were used as the animal model with 3 rats in each group of bare electrode, PEDOT-coated, and PEDOT-gel coated electrode (n=9). The *in vivo* impedance was used to confirm the performance of the implanted electrodes. The results showed that the impedance had a significant increase after 4 weeks with the bare and solid PEDOT-coated electrode. This is consistent with the typical glial scar encapsulation around the electrode leading to an impedance increase. PEDOT-gel presents consistently low impedance along with 10 weeks implantation implying there was much less reactive response around the insertion site. These *in vivo* experiments on PEDOT-gels suggest that PEDOT-gels are promising neural interfacing materials for patients clinically.

Chapter 1

CONJUGATED POLYMERS AS NEURAL INTERFACING MATERIALS

1.1 Neural Interfaces and Neural Electrodes

Neural interfaces are external electronic devices that interface with neural tissue to provide communication or to deliver electric stimulation for medical therapy. One of the major applications is for bionic limb prostheses that may send electrical signals to perform motor functions (Nicolelis, 2003) or sense information about the environment (Saal & Bensmaia, 2015). Practically, neural electrodes can be directly inserted into the central nervous system (CNS) by surgery. The CNS includes the brain, spinal cord and retina of bilaterian animals. Its function is to process the information received from the peripheral nervous system (PNS) and send the integrated signals back to the distal motor and sensory end organs. Neural electrodes work as a bridge to maintain communication between machines and tissues. Another major application of neural interfaces is the treatment of neurological disorders such as Parkinson's disease, depression, Alzheimer's disease and stroke. Here, passing electric stimulation can suppress or alleviate symptoms according to previous reports (Herrington, Cheng, & Eskandar, 2016). There has been considerable interest in the development of various types of neural electrodes clinically and commercially to help the millions of potential patients.

Certain neural electrodes such as deep brain stimulation (DBS) electrodes and microfabricated cortical electrodes require long-term implantation in the CNS.

Experimentally, this extended period of implantation leads to loss of function of the devices. This dysfunction has been associated with scar encapsulation on the electrode surface, blocking signal communication between tissues and electrodes (Vetter, Williams, Hetke, Nunamaker, & Kipke, 2004) and a concomitant loss of the targeted neurons in a region ~150 microns proximal to the probe surface (Biran, Martin, & Tresco, 2005). There are several requirements that have to be considered for the design of more reliable neural electrodes. First, they should provide stable, sensitive communication with relatively weak neural signals. Second, they should have long-term biocompatibility to avoid accumulated glial scar encapsulation. Third, the electrodes should be stable under physical and electrochemical challenges *in vivo*. Those requirements significantly constrain the potential neural electrode designs and associated materials selections.

1.2 Chronic Foreign Body Response in the Central Nervous System

Neural interfacing methods can be generally divided into two types: non-invasive methods such as electroencephalography (EEG) (Khushaba et al., 2013), electrooculography (ECog), and electromyography (EMG) (Buzsáki, Anastassiou, & Koch, 2012); and invasive methods such as implantable intracortical electrodes. Although the non-invasive methods cause significantly less injury to the brain, they are limited by their relatively slower information transfer rate and lower spatial resolution (del R. Milan & Carmena, 2010). While intracortical electrodes provide faster information transfer rates and better signal resolution direct to the active neurons (Ryu & Shenoy, 2009), severe foreign body responses have been found after

implantation which has been associated with the ultimate dysfunction of electrodes (Gilja et al., 2011)(Biran et al., 2005).

After device implantation, reactive microglia have been found near the implantation site. Reactive microglia have both M-1 and M-2 states. The M-1 state is known to secrete neurotoxic agents that may lead to neuronal death. On the other hand, the astrocytes synthesize glial fibrillary acidic protein (GFAP) that accelerates astrocyte proliferation and accumulation near the implantation site. After that, the activated astrocytes replace neurons and secrete bioactive agents that inhibit neuron growth, thus leading to scar formation. Previous work has shown that GFAP+ astrocytes accumulated about ~150 um near the electrode site after 2 weeks of implantation and kept growing over the next 8 weeks, as indicated in Figure 1.1 (Biran et al., 2005). These processes form a glial sheath around the implanted electrode that blocks communication between devices and tissues (Winslow, Christensen, Yang, Solzbacher, & Tresco, 2010). There are several hypotheses describing the contribution to the chronic foreign body response such as bioactivity of the electrode surface, the size of electrodes, and the mechanical strain at the interface. One of the most significant concerns is the mechanical mismatch between the stiff inorganic substrate and soft living tissue near the interface (Moshayedi et al., 2014).

1.3 Conducting Polymers as Softer, More Conductive and Biocompatible Neural Interfacing Materials

To address the issue of the mechanical mismatch near the implantation interface, soft, compliant and highly conductive materials are desired. Previous studies have shown that the device function time can be significantly improved by coating a soft, electron-ion conductive polymer layer on the devices (Cui & Martin, 2003a) to

buffer the mechanical mismatch. Conducting polymers have demonstrated to be useful in neural recording (Ludwig, Uram, Yang, Martin, & Kipke, 2006) neural stimulation (Cui, 2007)(Forciniti, Ybarra, Zaman, & Schmidt, 2014), neural regeneration (Subramanian, Krishnan, & Sethuraman, 2012)(Zhu et al., 2011), and controlled drug delivery (Abidian, Kim, & Martin, 2006).

When conducting polymers are deposited on substrates, they form rough, nano-fibrous morphologies that dramatically increase the effective surface area, allowing more efficient charge transport and hence signal transmission. After coating with conducting polymers, the impedances of the electrode were decreased over the whole frequency range (1-10 kHz), with the most significant drops in the biologically important low frequency range below 1 kHz (Cui, Hetke, Wiler, Anderson, & Martin, 2001). The charge storage capacity (CSC) of conducting polymer-coated electrodes was also substantially improved. Lower impedances and higher CSCs also means the devices require lower voltages to communicate with tissue, which helps to avoid damage during electrical stimulation (Wilks, Richardson-Burns, Hendricks, Martin, & Otto, 2009).

1.3.1 PEDOT as a Neural Interfacing Material

Many conducting polymers, such as poly(pyrrole) (PPy) and poly(aniline) (PANI) (Bhadra, Khastgir, Singha, & Lee, 2009) have been thoroughly investigated. The diethoxy-substituted thiophene poly(3,4-ethylene dioxythiophene) (PEDOT) has received particular interest as a reliable material for interfacing electronic biomedical devices with neural tissue because of its excellent chemical stability and high conductivity. In recent years, PEDOT has been studied with a variety of cell lines such as neurons (Richardson-Burns et al., 2007b) and myocytes (Miriani, Abidian, &

Kipke, 2008). Salto et al also showed that PEDOT could be used to control the adhesion and growth density of neural stem cells (Saltó et al., 2008). Comprehensive studies about the biocompatibility of PEDOT were conducted to show the improvement of cells adhesion, growth, and differentiation.

Researchers have also investigated various ways to reduce the inflammatory response including the controlled release of anti-inflammatory drugs such as dexamethasone into the system to reduce the scar formation (Abidian et al., 2006) , or immobilizing protein growth factors on the device surface to attract neural growth (D.-H. Kim, Richardson-Burns, Hendricks, Sequera, & Martin, 2007). Researchers have also learned to synthesize derivatives of PEDOT such as PEDOT-OH and PEDOT-acid. These added functional groups allow for the possibility to make chemical modifications (such as the attachment of integrin-binding peptides) that can improve cell attachment (Povlich et al., 2012). Those strategies significantly improve the performance and length the duration of the implanted devices. However, the improvements are still limited for chronic body reactions after extended implantations.

1.4 Challenges of PEDOT

1.4.1 Mechanical Failures of PEDOT Coating

One of the biggest challenges for using PEDOT as a neural interfacing material is its mechanical failure after implantation. There are several ways to prepare PEDOT as a coating on devices, but generally, PEDOT films are relatively fragile. It has been found that there can be substantial cracking and delamination of PEDOT coatings from substrates after extended implantations (Abidian, Corey, Kipke, & Martin, 2010).

Sterilization and chronic stimulation has also been associated with the mechanical failure of PEDOT coatings, as shown in figure 1.1 (Green et al., 2011) (Cui, 2007). This issue is evidently more serious when the PEDOT films were interfaced with peripheral nerves where the electrodes underwent intensive muscle movements (Kung et al., 2014). These mechanical failures of PEDOT coatings may not only decrease the performance of the devices but also leave the PEDOT residuals behind presenting a potential risk to the patients. Therefore, it is of considerable interest to create more mechanically reliable materials for neural interfaces. One of the particular challenges is the need to measure the mechanical properties and failure mechanisms of PEDOT, and use this information to design and synthesize improved materials.

1.4.1.1 Cohesion of PEDOT- Cracking

The typical mechanical failures of PEDOT coatings can potentially be addressed by either improving the inherent cohesive strength of the coating or the adhesion between the coating and substrate. It was suggested that most mechanical failures are associated with the decohesion of PEDOT film. The failure strength of PEDOT is related to ambient moisture content, temperature, and the stress undertaken (Dupont, Novoa, Voroshazi, & Dauskardt, 2014). While it is difficult to control the environmental moisture and temperature during implantation, we could create a more robust PEDOT film to endure larger operating stresses in vivo. We synthesized EPh monomer, an EDOT crosslinking agent, following Idzik et al's procedure (Idzik, Beckert, Golba, Ledwon, & Lapkowski, 2010). EPh was successfully copolymerized with EDOT to create a crosslinked PEDOT coating on electrodes (Ouyang et al., 2015a).

It was proved by other reports that with its electronic and ionic conductivity and large surface area, PEDOT coatings can significantly decrease the impedance of metallic electrodes in vitro (Martin et al., 2010) and in vivo (Ludwig et al., 2011). However, we found that the EPh-crosslinked PEDOT copolymers were less conductive then intrinsic PEDOT alone. As Figure 1.1 (a) shows, with 0.2% EPh monomer in the feed ratio, the copolymer coating exhibited similar impedance magnitude as intrinsic PEDOT coating. With a further increase feed ratio of EPh in the system, the impedance also increased. When the feed ratio was 1%, the low frequency impedance magnitude was similar to bare electrodes, while it was slightly larger at higher frequencies (>1E+04 Hz). Figure 1.1 (b) shows the impedance magnitude at 1 Hz and 1 kHz for different EPh feed ratios. It indicates that at 1%, the impedance of EPh PEDOT coating became larger than bare metal electrodes. Then the impedance saturated at about 10% or larger EPh feed ratio. To maintain good conductive pathways between the devices and tissues, a feed ratio of lower than 0.2% of EPh was needed .

At 0.2% of the crosslinker feed ratio, the electrical properties of crosslinked PEDOT were comparable to unmodified PEDOT, while the mechanical stiffness and strength were improved (Fig 1.2). PeakForce QNMTM AFM results showed that the modulus of EPh PEDOT coating increased with respect to the EPh feed ratio. It was found that the indentation modulus calculated from QNMTM mode with DMT model for PEDOT was 0.75 ± 0.16 GPa. The film deposited at 0.1% EPh had a modulus of 1.35 ± 0.48 GPa. However, at 0.5% EPh, the modulus became 4.9 ± 2.1 GPa, which was 5 times larger than the PEDOT film. Other reports from our lab also confirmed the tensile strength of 0.5% EPh PEDOT coating was 147±92 MPa which was 3 times larger than intrinsic PEDOT film (Qu, Ouyang, Kuo, & Martin, 2016). Theses studies

confirmed that the cohesive strength of PEDOT film could be improved by adding an appropriate amount of crosslinking agent into the system.

1.4.1.2 Adhesion of PEDOT Coating- Delamination

Another mechanical failure of PEDOT film is due to the relatively poor adhesion of PEDOT coating on metal electrodes. During electrochemical polymerization process, EDOT monomers are oxidized to radical cations near the electrode. These radical cations can react with another cations to form dimers, and then to polymers (Martin et al., 2010). These insoluble oligomers and polymers are then deposited on the electrode surface without strong bonding between PEDOT and electrode surface.

To improve the adhesion of PEDOT on electrode surfaces, our lab proposed the idea of an "adhesion promoter layer" by functionalizing PEDOT with an amine or carboxylic acid (Wei, Liu, Ouyang, Kuo, & Martin, 2015). Wei et al's report illustrates the idea of covalently bond PEDOT-acid with hydroxyl groups on the substrate surface. Ultrasonication tests showed that the adhesion of the PEDOT layer was greatly improved as compared with PEDOT films on unmodified surface. However, this method required hydroxyl groups on the surface to anchor PEDOT-acid such as ITO or stainless steel. This limits somewhat the selection of appropriate electrode materials. We also proposed another idea of grafting an adhesion promoting layer by using PEDOT-amine. Figure 1.3 illustrates the idea of using PEDOT-amine as the adhesion promoting layer. After it, PEDOT can be electrochemical polymerized on the PEDOT-amine layer. Figure 1.4 shows the optical images of PEDOT film on ITO and modified ITO before and after sonication after a period of time. It indicated

that with the adhesion promoting layer, PEDOT films were strongly adherent on the substrates.

1.4.1.3 Challenges of Quantifying Mechanical Properties from a PEDOT Thin Film

As mentioned above, researchers have developed several methods to address the issue of mechanical failure of PEDOT films (Wei et al., 2015)(Ouyang et al., 2015b). However, quantitative data about mechanical properties and failure modes of PEDOT films is still limited. In order to fully understand the use of conjugated polymers for these applications, it would be useful to have mechanical testing methods that could be used on extremely small samples similar in size to the devices and tissues, as well as their interfaces. Previous methods have examined much larger samples such as cast PEDOT/PSS (Chen et al., 2011), but we wanted to be able to examine extremely small volumes of sample as the thin film coating on devices. It would also be useful to obtain information about delamination and fracture modes. This is particularly important for electrochemically deposited PEDOT films that need to be deposited onto electrically conducting substrates.

Here, we describe methods for machining electrochemically deposited, relatively thick films of PEDOT, and interfacing the resulting specimens with a mechanical testing apparatus in a dual beam FIB/SEM. While the technique is slow and labor-intensive, it has provided unprecedented information about the tensile properties of these conjugated polymer films.

1.4.2 Mechanical Mismatch Between PEDOT Coating and Tissues: Foreign Body Response

When looking at the interface, there is a striking mechanical mismatch between the "hard" inorganic, metallic or semiconducting, electron conductive interface and "soft", organic, ionically conductive tissue. One advantage of employing PEDOT as an interfacing material with neural tissue is that it has a relatively low modulus. The typical Young's modulus of PEDOT is around 2 GPa which is much lower than traditional metallic materials such as gold, platinum or stainless steel (~ 100 GPa). This soft polymer coating on electrodes has been shown to significantly improve cell adhesion *in vitro* and *in vivo* (Ouyang, Shaw, Kuo, Griffin, & Martin, 2014). In addition, using this relatively softer polymer coating as the interface significantly decreases the mechanical mismatch between the hard electrode and the soft tissue, which is expected to help reduce the chronic foreign body response (Moshayedi et al., 2014).

However, even when the devices are modified with PEDOT, there is still a 6 order of magnitude difference in the modulus between the solid polymer coating and the surrounding neural tissue (Fig 1.3). The chronic foreign body response is therefore likely to be somewhat alleviated but not resolved. Hence, there is a continued need for even softer coatings. To further reduce the mechanical modulus of implants, it has been suggested to use hydrogels to replace traditional metallic materials (Peppas, Hilt, Khademhosseini, & Langer, 2006)(Drury & Mooney, 2003). Previous studies also showed that using Zwitterionic hydrogels in implantation can reduce the scar encapsulation formation for 3 months or more (Zhang et al., 2013)**.** The results support the idea of using hydrogels to mitigate chronic body reactions.

However, hydrogels are not able to provide conductive pathways for signal transmission, making them not well suited for neural interfacing.

For neural interface applications, the materials must facilitate charge transport both electronically and ionically. Previous reports have demonstrated various methods to create conductive hydrogels by using conducting polymers. Researchers have chemically developed intrinsically conducting hydrogels through chemical synthesis by utilizing conducting moieties on hydrogel monomers or by using precursors (Pan et al., 2012) (Mawad et al., 2012). Those chemically synthesized conductive hydrogels presented significantly lower conductivities than traditional CP films. Pan et al showed a conductivity of 0.11 S/cm from their conductive hydrogel which was 4 orders of magnitude lower than PEDOT/PSS (>200 S/cm). In addition, the chemical synthesis involved several toxic chemicals which would present potential risks to potential hosts.

Other reports demonstrated physical methods, by mixing conducting polymer suspensions during hydrogel crosslinking, to create conducting polymer blends in hydrogel (Press et al., 1999). By this method, the mixed CP suspension was only electrostatically attached to the hydrogel backbones. The integration between the CP suspension and hydrogel matrix is likely too weak to maintain a reliable CP/hydrogel blend. Besides that, the results showed that the conductivity of this CP/hydrogel blend was much lower than intrinsic PEDOT(Åsberg & Inganäs, 2003). The decreased conductivity would limit its use as a material for neural interfacing.

Another method to fabricate conducting polymer hydrogels is to add oxidant into the hydrogel solution with the CP monomer in order to polymerize CP simultaneously with hydrogel crosslinking. These CP hydrogels can be used for

biosensing applications due to their high conductivity and uniform deposition (Ismail, Martínez, Al Harrasi, Kim, & Otero, 2011). However chemical deposition of the CP onto the hydrogel backbone caused the hydrogel to become more brittle and fragile. In a later report, Dai at al. developed a double layer hydrogel network to improve its durability. (Dai et al., 2010)(Dai, Qing, Lu, & Xia, 2009). Although the chemical deposition method provided good conductivity, the process required strong oxidizing agents for polymerization. These oxidants will also function as a dopants for the CP polymerized in the hydrogel. After being polymerized in the hydrogel, the oxidant will begin to diffuse out over time. It is difficult to remove these biologically hazardous oxidants from those gels with normal rinsing. The residual chemicals may cause the damage to exposed tissues. Therefore the chemical deposition of CP hydrogels is not well suited for biological interfacing applications.

Green et al. recently developed a hybrid of CP polymerized on anionic hydrogel to make highly integrated and robust CP/hydrogels (Green et al., 2012a). However, these CP/hydrogel showed a relatively high modulus in the range of 1000 MPa which is 2 fold larger than cortex tissues making this hydrogel still an issue for implantation. Soichiro et al. have demonstrated electrochemically polymerized CP in hydrogels. However, from their results, most of the CP was concentrated near the electrode surface (~ 10 μm) (Sekine, Ido, Miyake, Nagamine, & Nishizawa, 2010) (Ido et al., 2012). This CP/hydrogel thickness is far less than the known scar encapsulation characteristic thickness which would make it difficult if not impossible for the CP/hydrogel to obtain signals if the typical amount of scar formation occurred (~150 μm).

We have shown that PEDOT can be directly polymerized into tissue matrix to create a conductive pathway without the use of any rigid substrates or scaffolds (Ouyang et al., 2014). By this method, we are able to significantly lower the mechanical mismatch during implantation. This method required the infusion of EDOT monomer into cortex before polymerization. However, previous report confirmed that EDOT monomers were toxic to cells in vitro (Richardson-Burns et al., 2007b). It is still unknown if EDOT monomers will cause long term damage to host body. This method required additional extensive studies before it can be put into practical clinical use. Without further study to clarify the potential damage to the tissues exposed to EDOT monomers, a prepared polymerized PEDOT coated electrode is a more suitable method for implantation.

Previously, our lab developed a CP-hydrogel with high conductivity by an electrochemical method (Dong-Hwan Kim, Abidian, & Martin, 2004). We found that after the deposition of 506 mC/cm^2 of charge, the impedance was even lower (10^4 Ω at 1 KHz) than that of thin film CP deposition (10^5 Ω for PPy thin film) (Dong-Hwan Kim et al., 2004). Abidian et al. have also used similar methods to fabricate conducting polymer-hydrogel conduits for axonal growth to provide an encapsulated environment for peripheral nerve regeneration (Abidian et al., 2012). This method is relatively easy to fabricate and avoids many of the chemical synthesis steps hence increasing the biocompatibility of the material. However, in these previous studies, the information of mechanical properties of conductive hydrogel is limited. The effect of mechanical modulus to the foreign body response has yet to be confirmed.

In this study, we reproduced this method on an extremely low modulus agarose hydrogel (~2 kPa) to create a conducting hydrogel by the in situ polymerization of

PEDOT. PEDOT could polymerize into the hydrogel matrix as far as 350 μm in diameter. With this large size of the PEDOT-gel, the signal communication can go well beyond the typical characteristic thickness of the glial scar (~150 μm), hence allowing the material to obtain an electrical signal even scar encapsulation occurs. Additionally, agarose gels have been reported to enhance cell adhesion, proliferation, as well as neural outgrowth (Ying Luo & Shoichet, 2004). A detailed study of the morphology, electrical properties, mechanical properties, and swelling properties of PEDOT-agarose gels are presented here. These PEDOT-hydrogel constructs exhibited extremely low modulus, which can potentially reduce the chronic body reaction to the implanted material. They also provide electrical conductivity, creating effective neural interfaces between electronic biomedical devices and living tissue.

1.4.3 EDOT- Lack of Biological Cues

To maintain a good signal transmission between devices and tissues, the foreign body response is a primary concern. With a mitigated foreign body response, one could expect to maintain efficient conductive pathways between tissues and devices. Researchers have also proposed creating biologically active material that could attract more neurons to the electrode surfaces.

Thus far, bioactive materials have been developed from synthetic biodegradable polymers such as PGA and PLGA (Freed et al., 1994), natural polymers such as collagen (Parenteau-Bareil, Gauvin, & Berthod, 2010), dextran (De Groot et al., 2001), and hyaluronic acid (Collier, Camp, Hudson, & Schmidt, 2000), to tissue engineering scaffolds made from acellular tissues (Farwell, Giachelli, Ph, & Ratner, 2006)(Badylak, 2002). Among them, synthetic polymers provide biodegradability but

little bioactivity due to its residual chemicals, acid moieties, and microscale particulates from degradation. As for natural polymers and acellular tissues, they are often exhaustively xenogeneic and allogeneic. Without proper operation and sterilization, they will bring the potential risks of pathogen transmission and undesirable inflammatory reactions.

As described earlier, researchers have demonstrated that PEDOT could be polymerized within hydrogels, forming PEDOT-hydrogel composites that further lower the mechanical modulus of devices (Dong-Hwan Kim, Wiler, Anderson, Kipke, & Martin, 2010)(Chikar et al., 2012)(Green et al., 2012b). To add biological cues, Green et al designed a "living electrode" idea based on integrating living cells in the conducting polymers-hydrogel composites to enhance their biological activity (R. A. Green et al., 2013). This idea is to bring neural attraction during implantation by the presence of cultured neural cells in the implant. However, there is no further study to confirm its biological response in vitro or in vivo.

Researchers have investigated the incorporation of biologically active materials into conducting polymers to both reduce the mechanical mismatch and promote neuron adhesion near the implants. Previous studies have shown that collagen, laminin, or other kinds of natural polymers can significantly improve the cell adhesion and reduce the inflammatory response (Xiao, Li, Wang, Shi, & Ooi, 2010a).We have shown that co-deposition of polypyrrole (PPy) and synthetic peptides significantly enhanced neural attachment in vivo(Cui, Wiler, Dzaman, Altschuler, & Martin, 2003). Alternatively, dopants with functional groups, such as chondroitin sulfate can be codeposited with PPy. Collagen fibers can then be immobilized onto the coating through the carboxylic acid groups on side chains of the dopant (X. Liu, Yue, Higgins,

& Wallace, 2011). Improved cell adhesion was also shown in this study. However, the bioactive materials are typically from heterogonous sources. Without extensive purification and sterilization, they may also be prone to pathogen transmission and severe immune responses.

Here in this study, we report the decoration of adipose stem cell derived extracelluar matrix (ECM) with the conducting polymer PEDOT. This ADSC-derived ECM was used a demonstration that ECM could be fabricated from any cultured cell type, and used as a scaffold for PEDOT polymerization. PEDOT was electrochemically deposited into the matrix to form conducting pathways. In the future, we expect that similar methods could be used to create an autologous ECM using cells directly extracted from the host, thus minimizing the potential risk of immune responses (Hongxu Lu, Hoshiba, Kawazoe, & Chen, 2011). This tissue-like ECM film provides a mechanical buffer layer at the device-tissue interface. In addition, it also provides biological and topological signals to promote regeneration at the interface.

1.5 Motivations and Objectives

To extend the functional use time of neural electrodes, robust and reliable interfacing materials are required. With the nature of PEDOT structure, the relatively low intrinsic cohesive strength limits its use as a neural interfacing material, especially for long-term implantations. It is therefore desirable to improve the mechanical properties of PEDOT coatings for chronic applications. Therefore, in this study we

modified the PEDOT coating with a crosslinker to improve its cohesive strength. In addition, we also developed an innovative method to investigate the local mechanical properties of PEDOT thin films using machining of samples in a dual beam FIB/SEM. While experimentally tedious, the approach provides a comprehensive understanding of a conducting polymer thin film's mechanical behavior that should be useful for future material design.

A continuing issue for neural interfacing materials is the associated chronic foreign body response in vivo. It is a biological response related to multiple factors. Researchers have investigated many methods to alleviate this issue such as decreasing the probe size, decreasing the probe stiffness, modifying the surface with biological cues, or delivering anti-inflammatory drugs to inhibit glial scar growth. However, there is no single method that has been found to totally resolve this issue. Biological response is a series of complicated events. Previously, we demonstrated that PEDOT could be polymerized into hydrogels forming a soft and conductive material for neural interfacing. Here we further improve the original design to achieve an ultra low modulus PEDOT-gel. We used an animal study to evaluate its performance in rat hippocampus. In addition to that, we also proposed a method to electrochemical polymerize PEDOT into a bioactive ECM template. Providing biological cues to the implants, we expected to create an improved cell adhesion surface to attract and attach neurons on the electrodes.

1.6 Outline of the Thesis

This thesis mainly discusses the performance of PEDOT coatings of interest for use in neural electrodes. The continuing problems of current neural interfaces can be classified into two topics: the mechanical instability of PEDOT coatings and the foreign body response caused by the large mechanical mismatch of implants. This thesis is focused on methods to characterize the mechanical properties of PEDOT thin film and the in situ polymerization of PEDOT in soft materials to reduce the mechanical modulus.

As discussed earlier, we have studied the characteristics of crosslinked PEDOT including its electrical, mechanical properties as well as its biocompatibility. A multifunctional EDOT derivative (EPh) was copolymerized with EDOT to create a crosslinked PEDOT coating on electrodes. At 0.2% of the crosslinker feed ratio, the electrical properties of crosslinked PEDOT were comparable to unmodified PEDOT, while the mechanical stiffness and strength were improved. We investigated the properties of crosslinked PEDOT film. However, the information of the toughness of this polymer thin film coating was still limited. Mechanical toughness is the major factor which can be used to describe the cracking behavior of a thin film coating on devices.

Therefore, in Chapter 2, an innovative nano-scale mechanical testing method was introduced. Taking advantage of a state-of-art dual beam FIB-SEM (focused ion beam - scanning electron microscope), we were able to conduct an in situ tensile test in the SEM chamber and obtain stress-strain curves. From this data were we able to estimate the modulus and strengths of the sample, and compare these results with other methods.

Chapter 3 describes a method to *in situ* polymerize PEDOT into an extracelluar matrix (ECM) as a soft and bioactive material for neural interfaces. The electrical and mechanical properties of PEDOT-ECM were examined. We found that this PEDOT-ECM film presented an improved cell adherent surface for PC12 cells, implying that it would be a more bioactive surface for neural interfacing.

Chapter 4 describes the *in situ* polymerization of PEDOT into ultra low modulus agarose hydrogels. An animal study was employed to evaluate the performance of these PEDOT-gels *in vivo*. The results were studied by using *in vivo* impedance. The results show improved performance from PEDOT-gel electrode as compared to traditional materials. The precise mechanisms of how PEDOT polymerizes into the gel matrix are still unknown.

A summary of results from each chapter and potential future work are described in Chapter 5. For example, we are hoping to be able to examine the *in situ* polymerization of the PEDOT in gels in more detail in the future, using corroborative optical and electron microscopy.

FIGURES

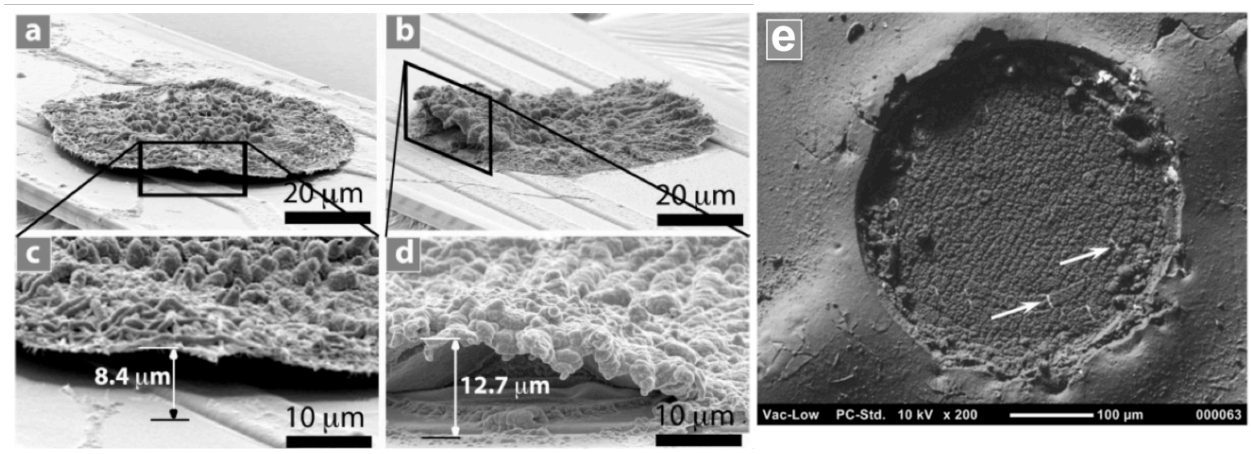

Figure 1.1 Examples of PEDOT delamination and cracking. (a-d) PEDOT delamination (Abidian et al., 2010) (e) PEDOT cracking after ETO sterilization (Green et al., 2013a).

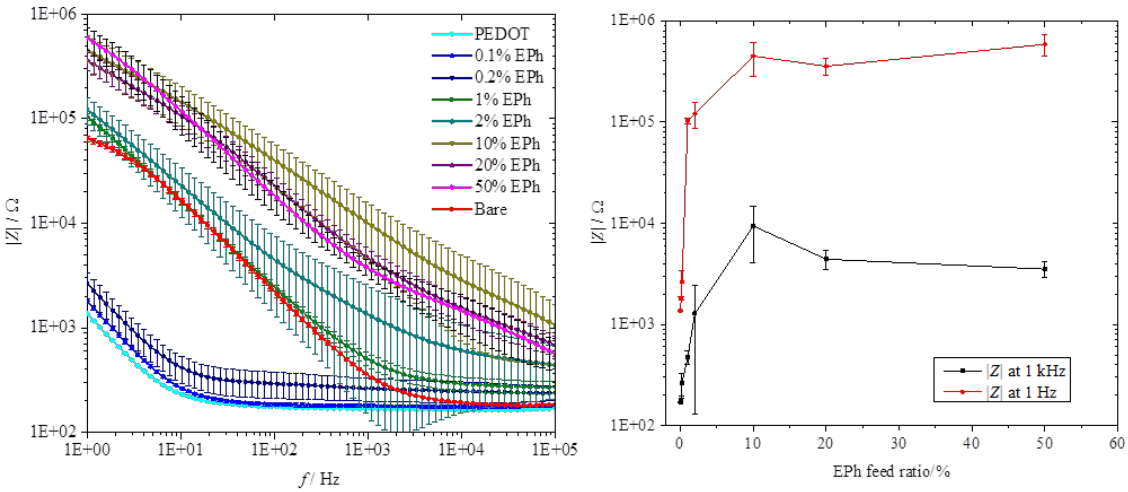

Figure 1.2 (a) Impedance amplitude of PEDOT and PEDOT-co-EPh copolymers as a function of frequency; (b) impedance amplitude at 1 Hz and 1 kHz for the PEDOT-co-EPh copolymers as a function of EPh content; dashed lines indicate the impedance amplitude of bare Pt electrode at 1 Hz (red) and 1 kHz (black), respectively. (deposition charge: 288 mC/cm^2) (Ouyang et al, 2015)

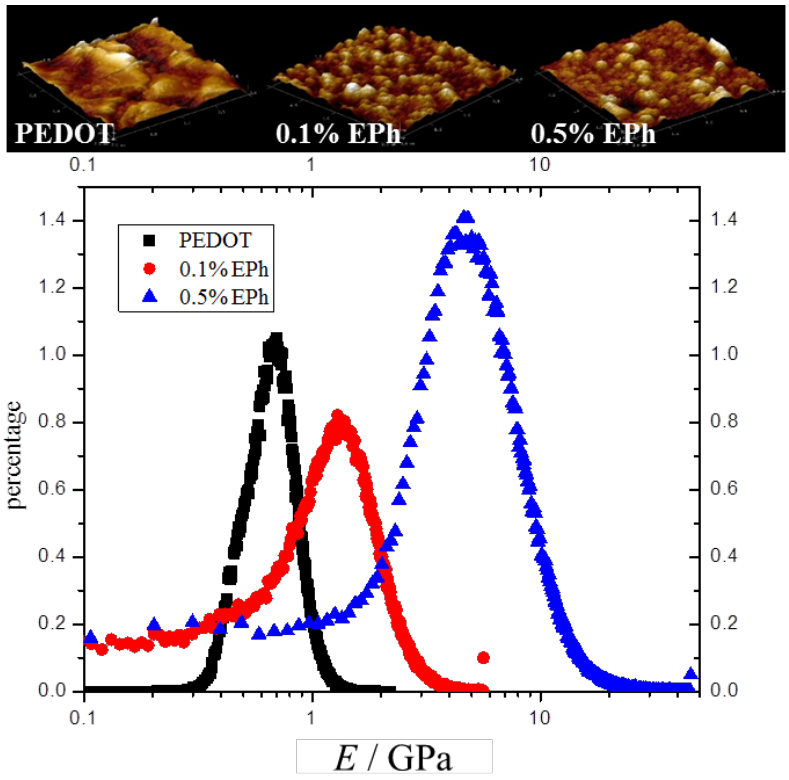

Figure 1.3 AFM-QNM modulus distribution. (top) AFM image of the polymer films (2 μm by 2 μm); (bottom) AFM-QNM DMT modulus distribution of PEDOT, 0.1% EPh and 0.5% EPh (Ouyang et al., 2015)

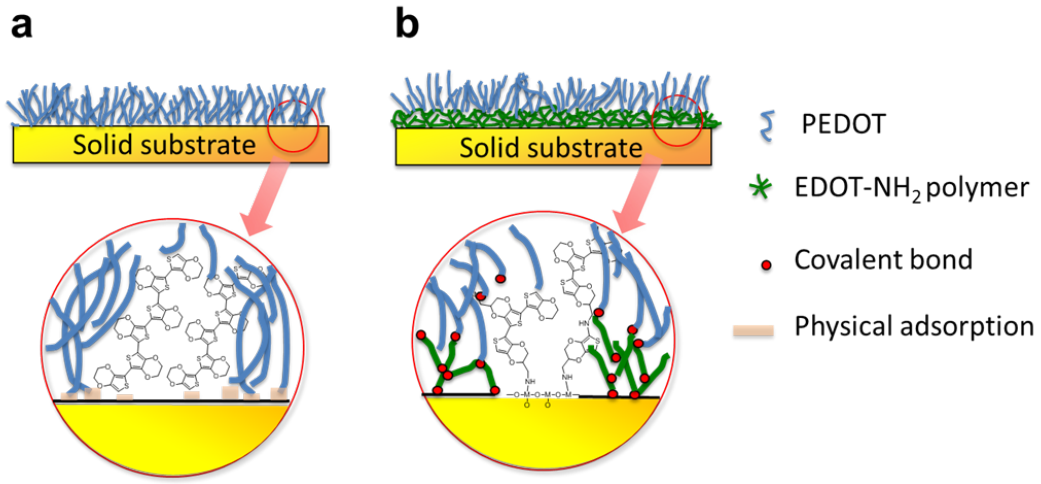

Figure 1.4 Schematic of using PEDOT-amine as the adhesion promoting layer. (a) PEDOT deposition on solid substrates. (b) PEDOT deposition on PEDOT-amine layer. (Ouyang et al., in review)

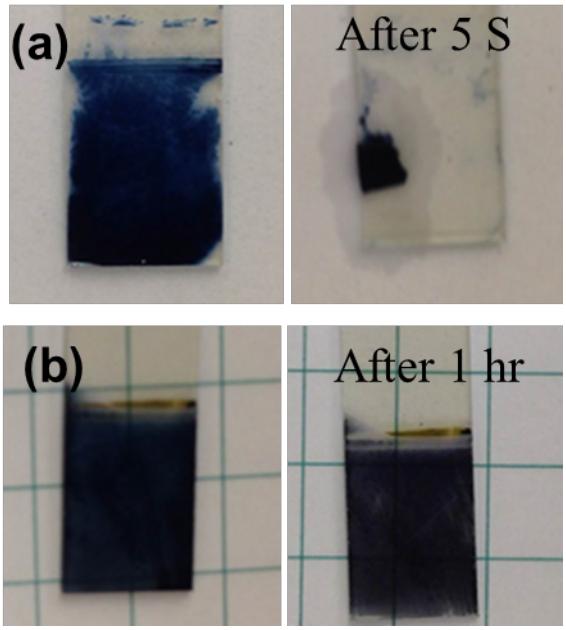

Figure 1.5 Optical images of PEDOT films on ITO and on PEDOT-amine layer before and after sonication adhesion test. (Wei et al, 2015)

REFERENCES

Abidian, M. R., Corey, J. M., Kipke, D. R., & Martin, D. C. (2010). Conducting-polymer nanotubes improve electrical properties, mechanical adhesion, neural attachment and neurite outgrowth of neural electrodes. *Small*, *6*(3), 421–429. http://doi.org/10.1002/smll.200901868

Abidian, M. R., Daneshvar, E. D., Egeland, B. M., Kipke, D. R., Cederna, P. S., & Urbanchek, M. G. (2012). Hybrid conducting polymer-hydrogel conduits for axonal growth and neural tissue engineering. *Advanced Healthcare Materials*, *1*(6), 762–7. http://doi.org/10.1002/adhm.201200182

Abidian, M. R., Kim, D.-H., & Martin, D. C. (2006). Conducting-Polymer Nanotubes for Controlled Drug Release. *Advanced Materials (Deerfield Beach, Fla.)*, *18*(4), 405–409. http://doi.org/10.1002/adma.200501726

Åsberg, P., & Inganäs, O. (2003). Hydrogels of a conducting conjugated polymer as 3-D enzyme electrode. *Biosensors and Bioelectronics*, *19*(3), 199–207. http://doi.org/10.1016/S0956-5663(03)00220-3

Badylak, S. F. (2002). The extracellular matrix as a scaffold for tissue reconstruction. *Seminars in Cell & Developmental Biology*, *13*(5), 377–383. http://doi.org/10.1016/S1084

Bhadra, S., Khastgir, D., Singha, N. K., & Lee, J. H. (2009). Progress in preparation, processing and applications of polyaniline. *Progress in Polymer Science*, *34*(8), 783–810. http://doi.org/10.1016/j.progpolymsci.2009.04.003

Biran, R., Martin, D. C., & Tresco, P. a. (2005). Neuronal cell loss accompanies the brain tissue response to chronically implanted silicon microelectrode arrays. *Experimental Neurology*, *195*(1), 115–26. http://doi.org/10.1016/j.expneurol.2005.04.020

Buzsáki, G., Anastassiou, C. a, & Koch, C. (2012). The origin of extracellular fields and currents--EEG, ECoG, LFP and spikes. *Nature Reviews. Neuroscience*, *13*(6), 407–20. http://doi.org/10.1038/nrn3241

Chen, C. H., Torrents, A., Kulinsky, L., Nelson, R. D., Madou, M. J., Valdevit, L., & Larue, J. C. (2011). Mechanical characterizations of cast Poly(3,4-ethylenedioxythiophene): Poly(styrenesulfonate)/Polyvinyl Alcohol thin films. *Synthetic Metals*, *161*(21-22), 2259–2267. http://doi.org/10.1016/j.synthmet.2011.08.031

Chikar, J. a, Hendricks, J. L., Richardson-Burns, S. M., Raphael, Y., Pfingst, B. E., & Martin, D. C. (2012). The use of a dual PEDOT and RGD-functionalized alginate hydrogel coating to provide sustained drug delivery and improved cochlear implant function. *Biomaterials*, *33*(7), 1982–90. http://doi.org/10.1016/j.biomaterials.2011.11.052

Collier, J. H., Camp, J. P., Hudson, T. W., & Schmidt, C. E. (2000). Synthesis and characterization of polypyrrole-hyaluronic acid composite biomaterials for tissue engineering applications. *Journal of Biomedical Materials Research*, *50*(4), 574–584. http://doi.org/10.1002/(SICI)1097-4636(20000615)50:4<574::AID-JBM13>3.0.CO;2-I

Cui, X. (2007). Poly (3,4-ethylenedioxythiophene) for chronic neural stimulation. *IEEE Trans Neural Syst Rehabil Eng.*, *15*(4), 502–8. http://doi.org/10.1109/TNSRE.2007.909811.

Cui, X., Hetke, J. F., Wiler, J. a., Anderson, D. J., & Martin, D. C. (2001). Electrochemical deposition and characterization of conducting polymer polypyrrole/PSS on multichannel neural probes. *Sensors and Actuators A: Physical*, *93*(1), 8–18. http://doi.org/10.1016/S0924-4247(01)00637-9

Cui, X., & Martin, D. C. (2003). Electrochemical deposition and characterization of poly(3,4-ethylenedioxythiophene) on neural microelectrode arrays. *Sensors and Actuators B: Chemical*, *89*(1-2), 92–102. http://doi.org/10.1016/S0925-4005(02)00448-3

Cui, X., Wiler, J., Dzaman, M., Altschuler, R. a, & Martin, D. C. (2003). In vivo studies of polypyrrole/peptide coated neural probes. *Biomaterials*, *24*(5), 777–87. Retrieved from http://www.ncbi.nlm.nih.gov/pubmed/12485796

Dai, T., Qing, X., Lu, Y., & Xia, Y. (2009). Conducting hydrogels with enhanced mechanical strength. *Polymer*, *50*(22), 5236–5241. http://doi.org/10.1016/j.polymer.2009.09.025

Dai, T., Qing, X., Zhou, H., Shen, C., Wang, J., & Lu, Y. (2010). Mechanically strong conducting hydrogels with special double-network structure. *Synthetic Metals*, *160*(7-8), 791–796. http://doi.org/10.1016/j.synthmet.2010.01.024

De Groot, C. J., Van Luyn, M. J. A., Van Dijk-Wolthuis, W. N. E., Cad??e, J. A., Plantinga, J. A., Otter, W. Den, & Hennink, W. E. (2001). In vitro biocompatibility of biodegradable dextran-based hydrogels tested with human fibroblasts. *Biomaterials*, *22*(11), 1197–1203. http://doi.org/10.1016/S0142-9612(00)00266-0

del R. Milan, J., & Carmena, J. (2010). Invasive or Noninvasive: Understanding Brain-Machine Interface Technology. *IEEE Engineering in Medicine and Biology Magazine*, *29*(1), 16–22. http://doi.org/10.1109/MEMB.2009.935475

Drury, J. L., & Mooney, D. J. (2003). Hydrogels for tissue engineering: scaffold design variables and applications. *Biomaterials*, *24*(24), 4337–4351. http://doi.org/10.1016/S0142-9612(03)00340-5

Dupont, S. R., Novoa, F., Voroshazi, E., & Dauskardt, R. H. (2014). Decohesion kinetics of PEDOT:PSS conducting polymer films. *Advanced Functional Materials*, *24*, 1325–1332. http://doi.org/10.1002/adfm.201302174

Farwell, D. G., Giachelli, C. M., Ph, D., & Ratner, B. D. (2006). Matrix Tissue Scaffold. *Tissue Engineering*, *12*(2).

Forciniti, L., Ybarra, J., Zaman, M. H., & Schmidt, C. E. (2014). Schwann cell response on polypyrrole substrates upon electrical stimulation. *Acta Biomaterialia*, *10*(6), 2423–2433. http://doi.org/10.1016/j.actbio.2014.01.030

Freed, L. E., Vunjak-Novakovic, G., Biron, R. J., Eagles, D. B., Lesnoy, D. C.,

Barlow, S. K., & Langer, R. (1994). Biodegradable Polymer Scaffolds for Tissue Engineering. *Nature Biotechnology*, *12*(7), 689–693. http://doi.org/10.1038/nbt0794-689

Gilja, V., Chestek, C. A., Diester, I., Henderson, J. M., Deisseroth, K., & Shenoy, K. V. (2011). Challenges and opportunities for next-generation intracortically based neural prostheses. *IEEE Transactions on Biomedical Engineering*, *58*(7), 1891–1899. http://doi.org/10.1109/TBME.2011.2107553

Green, R. a, Hassarati, R. T., Goding, J. a, Baek, S., Lovell, N. H., Martens, P. J., & Poole-Warren, L. a. (2012a). Conductive hydrogels: mechanically robust hybrids for use as biomaterials. *Macromolecular Bioscience*, *12*(4), 494–501. http://doi.org/10.1002/mabi.201100490

Green, R. a, Matteucci, P. B., Hassarati, R. T., Giraud, B., Dodds, C. W. D., Chen, S., … Lovell, N. H. (2013a). Performance of conducting polymer electrodes for stimulating neuroprosthetics. *Journal of Neural Engineering*, *10*(1), 016009. http://doi.org/10.1088/1741-2560/10/1/016009

Green, R. A., Lim, K. S., Henderson, W. C., Hassarati, R. T., Martens, P. J., Lovell, N. H., & Poole-Warren, L. A. (2013). Living electrodes: tissue engineering the neural interface. *Conference Proceedings : ... Annual International Conference of the IEEE Engineering in Medicine and Biology Society. IEEE Engineering in Medicine and Biology Society. Annual Conference*, *2013*, 6957–6960. http://doi.org/10.1109/EMBC.2013.6611158

Green, R., Duan, C., Hassarati, R., Goding, J., Byrnes-Preston, P., Suaning, G. J., … Lovell, N. H. (2011). Electrochemical stability of poly(ethylene dioxythiophene) electrodes. *2011 5th International IEEE/EMBS Conference on Neural Engineering, NER 2011*, 566–569. http://doi.org/10.1109/NER.2011.5910611

Herrington, T. M., Cheng, J. J., & Eskandar, E. N. (2016). Mechanisms of deep brain stimulation. *JOURNAL OF NEUROPHYSIOLOGY*, *115*(1), 19–38. http://doi.org/10.1152/jn.00281.2015

Ido, Y., Takahashi, D., Sasaki, M., Nagamine, K., Miyake, T., Jasinski, P., &

Nishizawa, M. (2012). Conducting Polymer Microelectrodes Anchored to Hydrogel Films. *ACS Macro Letters*, *1*(3), 400–403. http://doi.org/10.1021/mz2002406

Idzik, K. R., Beckert, R., Golba, S., Ledwon, P., & Lapkowski, M. (2010). Synthesis by Stille cross-coupling procedure and electrochemical properties of C3-symmetric oligoarylobenzenes. *Tetrahedron Letters*, *51*(18), 2396–2399. http://doi.org/10.1016/j.tetlet.2010.02.051

Ismail, Y. a., Martínez, J. G., Al Harrasi, A. S., Kim, S. J., & Otero, T. F. (2011). Sensing characteristics of a conducting polymer/hydrogel hybrid microfiber artificial muscle. *Sensors and Actuators B: Chemical*, *160*(1), 1180–1190. http://doi.org/10.1016/j.snb.2011.09.044

Khushaba, R. N., Wise, C., Kodagoda, S., Louviere, J., Kahn, B. E., & Townsend, C. (2013). Consumer neuroscience: Assessing the brain response to marketing stimuli using electroencephalogram (EEG) and eye tracking. *Expert Systems with Applications*, *40*(9), 3803–3812. http://doi.org/10.1016/j.eswa.2012.12.095

Kim, D.-H., Abidian, M., & Martin, D. C. (2004). Conducting polymers grown in hydrogel scaffolds coated on neural prosthetic devices. *Journal of Biomedical Materials Research. Part A*, *71*(4), 577–85. http://doi.org/10.1002/jbm.a.30124

Kim, D.-H., Richardson-Burns, S. M., Hendricks, J. L., Sequera, C., & Martin, D. C. (2007). Effect of Immobilized Nerve Growth Factor on Conductive Polymers: Electrical Properties and Cellular Response. *Advanced Functional Materials*, *17*(1), 79–86. http://doi.org/10.1002/adfm.200500594

Kim, D.-H., Wiler, J. a, Anderson, D. J., Kipke, D. R., & Martin, D. C. (2010). Conducting polymers on hydrogel-coated neural electrode provide sensitive neural recordings in auditory cortex. *Acta Biomaterialia*, *6*(1), 57–62. http://doi.org/10.1016/j.actbio.2009.07.034

Kung, T., Langhals, N. B., Martin, D. C., Johnson, P. J., Cederna, P. S., & Urbanchek, M. G. (2014). Regenerative peripheral nerve interface viability and signal transduction with an implanted electrode. *Plastic and Reconstructive Surgery*,

133(6), 1380–94. http://doi.org/10.1097/PRS.0000000000000168

Liu, X., Yue, Z., Higgins, M. J., & Wallace, G. G. (2011). Conducting polymers with immobilised fibrillar collagen for enhanced neural interfacing. *Biomaterials*, *32*(30), 7309–17. http://doi.org/10.1016/j.biomaterials.2011.06.047

Lu, H., Hoshiba, T., Kawazoe, N., & Chen, G. (2011). Autologous extracellular matrix scaffolds for tissue engineering. *Biomaterials*, *32*(10), 2489–99. http://doi.org/10.1016/j.biomaterials.2010.12.016

Ludwig, K. a, Langhals, N. B., Joseph, M. D., Richardson-Burns, S. M., Hendricks, J. L., & Kipke, D. R. (2011). Poly(3,4-ethylenedioxythiophene) (PEDOT) polymer coatings facilitate smaller neural recording electrodes. *Journal of Neural Engineering*, *8*, 014001. http://doi.org/10.1088/1741-2560/8/1/014001

Ludwig, K. a, Uram, J. D., Yang, J., Martin, D. C., & Kipke, D. R. (2006). Chronic neural recordings using silicon microelectrode arrays electrochemically deposited with a poly(3,4-ethylenedioxythiophene) (PEDOT) film. *Journal of Neural Engineering*, *3*, 59–70. http://doi.org/10.1088/1741-2560/3/1/007

Luo, Y., & Shoichet, M. S. (2004). A photolabile hydrogel for guided three-dimensional cell growth and migration. *Nature Materials*, *3*(4), 249–53. http://doi.org/10.1038/nmat1092

Martin, D. C., Wu, J., Shaw, C. M., King, Z., Spanninga, S. a., Richardson-Burns, S., … Yang, J. (2010). The Morphology of Poly(3,4-Ethylenedioxythiophene). *Polymer Reviews*, *50*(3), 340–384. http://doi.org/10.1080/15583724.2010.495440

Mawad, D., Stewart, E., Officer, D. L., Romeo, T., Wagner, P., Wagner, K., & Wallace, G. G. (2012). A Single Component Conducting Polymer Hydrogel as a Scaffold for Tissue Engineering. *Advanced Functional Materials*, *22*(13), 2692–2699. http://doi.org/10.1002/adfm.201102373

Miriani, R. M., Abidian, M. R., & Kipke, D. R. (2008). Cytotoxic analysis of the conducting polymer PEDOT using myocytes. *Conference Proceedings : ... Annual International Conference of the IEEE Engineering in Medicine and Biology Society. IEEE Engineering in Medicine and Biology Society. Conference*,

2008, 1841–4. http://doi.org/10.1109/IEMBS.2008.4649538

Moshayedi, P., Ng, G., Kwok, J. C. F., Yeo, G. S. H., Bryant, C. E., Fawcett, J. W., … Guck, J. (2014). The relationship between glial cell mechanosensitivity and foreign body reactions in the central nervous system. *Biomaterials*, *35*(13), 3919–3925. http://doi.org/10.1016/j.biomaterials.2014.01.038

Nicolelis, M. a L. (2003). Neural Circuits. *Neuroscience*, *4*(May), e27488. http://doi.org/10.1016/j.conb.2011.07.004.Specificity

Ouyang, L., Kuo, C., Farrell, B., Pathak, S., Wei, B., Qu, J., & Martin, D. C. (2015a). Poly[3,4-ethylene dioxythiophene (EDOT)-co-1,3,5-tri[2-(3,4-ethylene dioxythienyl)]-benzene (EPh)] copolymers (PEDOT-co-EPh): optical, electrochemical and mechanical properties. *J. Mater. Chem. B*, *3*(25), 5010–5020. http://doi.org/10.1039/C5TB00053J

Ouyang, L., Shaw, C. L., Kuo, C.-C., Griffin, A. L., & Martin, D. C. (2014). In vivo polymerization of poly(3,4-ethylenedioxythiophene) in the living rat hippocampus does not cause a significant loss of performance in a delayed alternation task. *Journal of Neural Engineering*, *11*(2), 026005. http://doi.org/10.1088/1741-2560/11/2/026005

Pan, L., Yu, G., Zhai, D., Lee, H. R., Zhao, W., Liu, N., … Bao, Z. (2012). Hierarchical nanostructured conducting polymer hydrogel with high electrochemical activity. *Proceedings of the National Academy of Sciences of the United States of America*, *109*(24), 9287–92. http://doi.org/10.1073/pnas.1202636109

Parenteau-Bareil, R., Gauvin, R., & Berthod, F. (2010). Collagen-based biomaterials for tissue engineering applications. *Materials*, *3*(3), 1863–1887. http://doi.org/10.3390/ma3031863

Peppas, N. a., Hilt, J. Z., Khademhosseini, a., & Langer, R. (2006). Hydrogels in Biology and Medicine: From Molecular Principles to Bionanotechnology. *Advanced Materials*, *18*(11), 1345–1360. http://doi.org/10.1002/adma.200501612

Povlich, L. K., Cho, J. C., Leach, M. K., Corey, J. M., Kim, J., & Martin, D. C.

(2012). Synthesis, copolymerization and peptide-modification of carboxylic acid-functionalized 3,4-ethylenedioxythiophene (EDOTacid) for neural electrode interfaces. *Biochimica et Biophysica Acta*. http://doi.org/10.1016/j.bbagen.2012.10.017

Press, A., Williams, D. J., Sohn, J. E., Marder, S. R., Josse, D., Zyss, J., … Goddard, W. A. (1999). Conducting Polymer Hydrogels as 3D Electrodes : Applications for Supercapacitors ** By Soumyadeb Ghosh * and Olle Inganäs, (14), 1214–1218.

Qu, J., Ouyang, L., Kuo, C. C., & Martin, D. C. (2016). Stiffness, strength and adhesion characterization of electrochemically deposited conjugated polymer films. *Acta Biomaterialia*, *31*, 114–121. http://doi.org/10.1016/j.actbio.2015.11.018

Richardson-Burns, S. M., Hendricks, J. L., Foster, B., Povlich, L. K., Kim, D.-H., & Martin, D. C. (2007). Polymerization of the conducting polymer poly(3,4-ethylenedioxythiophene) (PEDOT) around living neural cells. *Biomaterials*, *28*(8), 1539–52. http://doi.org/10.1016/j.biomaterials.2006.11.026

Ryu, S. I., & Shenoy, K. V. (2009). Human cortical prostheses: lost in translation? *Neurosurgical Focus*, *27*(1), E5. http://doi.org/10.3171/2009.4.FOCUS0987

Saal, H. P., & Bensmaia, S. J. (2015). Biomimetic approaches to bionic touch through a peripheral nerve interface. *Neuropsychologia*, *79*, 344–353. http://doi.org/10.1016/j.neuropsychologia.2015.06.010

Saltó, C., Saindon, E., Bolin, M., Kanciurzewska, A., Fahlman, M., Jager, E. W. H., … Berggren, M. (2008). Control of neural stem cell adhesion and density by an electronic polymer surface switch. *Langmuir : The ACS Journal of Surfaces and Colloids*, *24*(24), 14133–8. http://doi.org/10.1021/la8028337

Sekine, S., Ido, Y., Miyake, T., Nagamine, K., & Nishizawa, M. (2010). Conducting polymer electrodes printed on hydrogel. *Journal of the American Chemical Society*, *132*(38), 13174–5. http://doi.org/10.1021/ja1062357

Subramanian, A., Krishnan, U. M., & Sethuraman, S. (2012). Axially aligned

electrically conducting biodegradable nanofibers for neural regeneration. *Journal of Materials Science. Materials in Medicine*, *23*(7), 1797–809. http://doi.org/10.1007/s10856-012-4654-y

Vetter, R. J., Williams, J. C., Hetke, J. F., Nunamaker, E. a, & Kipke, D. R. (2004). Chronic neural recording using silicon-substrate microelectrode arrays implanted in cerebral cortex. *IEEE Transactions on Bio-Medical Engineering*, *51*(6), 896–904. http://doi.org/10.1109/TBME.2004.826680

Wei, B., Liu, J., Ouyang, L., Kuo, C.-C., & Martin, D. C. (2015). Significant Enhancement of PEDOT Thin Film Adhesion to Inorganic Solid Substrates with EDOT-Acid. *ACS Applied Materials & Interfaces*, *7*(28), 15388–94. http://doi.org/10.1021/acsami.5b03350

Wilks, S. J., Richardson-Burns, S. M., Hendricks, J. L., Martin, D. C., & Otto, K. J. (2009). Poly(3,4-ethylenedioxythiophene) as a Micro-Neural Interface Material for Electrostimulation. *Frontiers in Neuroengineering*, *2*(June), 7. http://doi.org/10.3389/neuro.16.007.2009

Winslow, B. D., Christensen, M. B., Yang, W.-K., Solzbacher, F., & Tresco, P. a. (2010). A comparison of the tissue response to chronically implanted Parylene-C-coated and uncoated planar silicon microelectrode arrays in rat cortex. *Biomaterials*, *31*(35), 9163–72. http://doi.org/10.1016/j.biomaterials.2010.05.050

Xiao, Y., Li, C. M., Wang, S., Shi, J., & Ooi, C. P. (2010). Incorporation of collagen in poly(3,4-ethylenedioxythiophene) for a bifunctional film with high bio- and electrochemical activity. *Journal of Biomedical Materials Research. Part A*, *92*(2), 766–72. http://doi.org/10.1002/jbm.a.32412

Zhang, L., Cao, Z., Bai, T., Carr, L., Ella-Menye, J.-R., Irvin, C., … Jiang, S. (2013). Zwitterionic hydrogels implanted in mice resist the foreign-body reaction. *Nature Biotechnology*, (October 2012). http://doi.org/10.1038/nbt.2580

Zhu, Y., Wang, A., Patel, S., Kurpinski, K., Diao, E., Bao, X., … Li, S. (2011). Engineering bi-layer nanofibrous conduits for peripheral nerve regeneration. *Tissue Engineering. Part C, Methods*, *17*(7), 705–15.

http://doi.org/10.1089/ten.tec.2010.0565

Chapter 2

NANOSCALE MECHANICAL TESTING OF ELECTROCHEMICALLY DEPOSITED PEDOT THIN FILMS BY *IN SITU* FOCUSED ION BEAM/SCANNING ELECTRON MICROSCOPY (FIB/SEM)

2.1 Introduction

The advantages of interfacing conducting polymers with biological systems include their high electronic and ionic conductivity, excellent biocompatibility, and versatile organic chemistry. They are especially attractive in the applications such as neural interfaces (Cui, Lee, et al., 2001; Ludwig et al., 2006), biosensing (Oh, Kwon, & Jang, 2013)(Gerard, Chaubey, & Malhotra, 2002), and tissue engineering (D.-H. Kim et al., 2007)(C E Schmidt, Shastri, Vacanti, & Langer, 1997). Coated on neural probes, conducting polymers such PEDOT provide a relatively soft interface with high surface area. This polymer interface helps to reduce the mechanical mismatch between rigid devices and soft neural tissues (Cui et al., 2003)(Biran et al., 2005)(Cui & Martin, 2003a), and has been shown to significantly improve the performance of the neural probes both *in vivo* and *in vitro* (Cui & Martin, 2003b)(Wilks, Richardson-burns, Hendricks, Martin, & Otto, 2009)(Ludwig et al., 2006)(Wilks, Richardson-burns, et al., 2009).

However, in certain situations it has been observed that PEDOT coatings may delaminate from the substrate or crack after extended implantations *in vivo* (Cui, 2007). The cracking of PEDOT after ethylene oxide (EtO) sterilization and electrical stimulation was also reported (Green et al., 2013b). These mechanical failures of

PEDOT might decrease the efficiency of charge transport, and hence lead to device failure. Moreover, leaving behind residual pieces of cracked PEDOT films in tissues could cause potential risks for patients. Different methods have been investigated to improve the mechanical properties of PEDOT. In our previous work, we demonstrated that crosslinking PEDOT with a tri-functional EDOT derivative (EPh) led to a more robust film without sacrificing its electrical properties (Ouyang et al., 2015b). In order to further understand the mechanical stability of PEDOT and to evaluate the strategies addressing this issue, it is necessary to have more precise characterization methods to measure the local mechanical properties such as Young's modulus, fracture strength and toughness.

Performing mechanical tests on electrochemically deposited PEDOT is challenging since it is difficult to use traditional methods to obtain free-standing PEDOT thin films. Several indirect methods have been reported for measuring the mechanical properties of PEDOT thin films. Indentation methods, such as nanoindentation (H. Lu, Wang, Ma, Huang, & Viswanathan, 2003; Yang & Martin, 2006) or atomic force microscopy Quantitative Nanomechanical Mapping (AFM-QNM^{TM}) (Ouyang et al., 2015a)(Hassarati et al., 2014) have been employed to estimate the modulus of PEDOT thin films on substrates. These methods are complicated by the need to determine the geometry of the indentation tip, the cantilever spring constant and the film surface roughness. In addition, none of these methods can be used to obtain the properties related to failure, such as tensile strength or toughness.

It is also necessary to take into account the potential inconsistencies between bulk properties of macroscopic films and thin films coated on solid substrates. For

macroscopic films, the internal defects and inhomogeneity of film thickness due to deposition methods may lead to experimental errors in measurements of the polymers' mechanical properties. To understand the mechanical failures of films that are typically coated on microelectrodes, nanoscale mechanical testing methods are of great interest.

In this chapter, we describe the development and evaluation of methods to examine the local mechanical properties of electrochemically deposited PEDOT thin films. We prepared dog bone-shaped specimens for nanoscale tensile testing using a focused ion beam (FIB). Electrochemically deposited PEDOT was sectioned with the FIB into dog-bone shapes that were several hundred nanometers in size, similar to typical thickness of PEDOT. The specimens were *in situ* transferred to a nanoscale tensile testing system in the SEM with a nano-manipulating tungsten probe (OmniProbe). The deformation measurements were directly observed and recorded in the SEM chamber, and the stresses on the sample were measured with a calibrated load cell. The Young's modulus and fracture strength of this nano-engineered PEDOT specimen were obtained. By integrating the corresponding area under the stress-strain curve, the tensile toughness (total energy to failure) could also be estimated. The results help us to further analyze the strength, stiffness, and toughness of PEDOT and its derivatives. To corroborate the FIB-SEM results, we also used AFM QNM to collect mechanical modulus from PEDOT coatings prepared by the same protocol.

2.2 Materials and Methods

2.2.1 Electrochemical Deposition

Electrochemically polymerized PEDOT films (EC-PEDOT) were deposited on 25 μm diameter gold wires. A potentiostat (ModuLab, Solartron Analytical) was used to generate the electrical potential required to oxidize the EDOT monomer. Solutions were prepared with a concentration of 0.01 M EDOT monomer with 0.1 wt% PSS as the counter ions in DI water. The deposition proceeded at 2 V for 10 hours in a three-electrode cell using platinum foil as a counter electrode. The final thickness of the PEDOT was about 100 μm. The thicknesses of EC-PEDOT films were confirmed by optical microscopy and SEM.

2.2.2 Specimen Preparation

EC-PEDOT samples on the gold wire were transferred into to a Zeiss Auriga 60 CrossBeam Focused Ion Beam (FIB)/Scanning Electron Microscope (SEM) equipped with a nano-manipulation OmniProbe. The specimen was imaged at an accelerating voltage of 3 kV. FIB was employed to mill the sample to a dog-bone shape for tensile testing. First, a thin plate with dimensions of 5 μm x 3 μm with a desired thickness (ranging from 350 nm to 700 nm) was milled from its bulk parent body. The OmniProbe was used to pick up the specimen for further polishing. The sample gauge was trimmed to the designed width and length then the sample was further polished into the precise thickness with ion beam at 30 kV / 5pA.

2.2.3 AFM-QNM Measurements

The quantitative nanomechanical (QNM) modulus was calculated by PeakForce QNM^{TM} AFM mode with Nanoscope Dimension 3100 software on a

Bioscope Catalyst (Bruker Nano/ Veeco) Atomic Force Microscop (AFM). All samples were measured at room temperature in the dry state. AFM probe with specific force constants ranging from 5 N/m to 200 N/m were used to indent the sample surface to a depth of about 1-2 nm. The measurements were averaged from 5 samples of EC-PEDOT.

2.2.4 Data Analysis

The analysis of strain to failure measurements in the SEM was conducted with Tracker software (OSP Java framework). A specific video frame was marked and tracked during real time video recording. In most cases, the edge of the dog bone shaped specimen was used as the reference frame since it proved to be reliably and reproducibly located. An origin was set at the marked video frame with a calibrated scale bar in SEM. The precise frame moving distance was determined at each time point. Once the dog bone shaped specimen of PEDOT was broken, the recording was automatically stopped since there was then no matching frame in the video. After stress-time and strain-time curves were obtained, the open source software, Engauge Digitizer was used to converted plots to data points.

2.2.5 Results and Discussion

It has been demonstrated in previous studies that the mechanical properties of PEDOT films is influenced greatly by the dopants (Baek, Green, & Poole-Warren, 2014). In this study, the electrochemically polymerized PEDOT (EC-PEDOT) was doped with a polymeric dopant, PSS. It has been reported that this dopant gives the largest modulus to PEDOT (Baek et al., 2014). In order to get enough PEDOT to

section a specimen, the required thickness of the parent body is at least 80 μm. The deposition proceeded at 2 V for 10 hours. For these long time depositions, the corresponding current drops dramatically after a few hours. We found that a minimum deposition voltage of 2 V was required to create a >80 μm thickness PEDOT coating.

We used the focused ion beam to section the EC-PEDOT into dog-bone shaped specimens for the *in situ* tensile tests. As illustrated in Figure 2.1, a 80-100 μm EC-PEDOT film was deposited onto 25 μm diameter gold wire electrochemically. A rectangular shaped film (15 μm in length, 10 μm in with and 2 μm in thickness) was cut out from the bulk EC-PEDOT by using the finely controlled gallium beam (1 nA) (Fig. 2.1 (b)). A 600 pA milling current was then used to carve this film into the desired dog-bone shape of the specimen (Fig. 2.1 (c)). The OmniProbe was used to pick the dog-bone specimen up from the bulk sample. The dog-bone specimen was mounted onto the OmniProbe by using platinum deposition (Fig. 2.1 (c)). The OmniProbe with the dog-bone specimen attached was brought close to the force sensor (Nanoscience) and then mounted by platinum deposition (Fig. 2.1 (d)). In order to obtain a thinner area for the force concentration, a lower intensity beam of 5 pA was used for the fine milling. After all these processes, in order to have a uniform force applied to the specimen cross section, the attachment to the OmniProbe was cut through by FIB and then again using Pt to bond to the other end of the specimen (Fig. 2.1 (e)). Figure 2.1 (f) shows the actual experimental setup in SEM chamber with the force sensor on the right and the OmniProbe on the left. While moving the OmniProbe to the left, a capacitance based force sensor recorded the voltage change in the system for the EC-PEDOT stress analysis.

A Labview programmed code controlled the voltage output and a data acquisition system was used to monitor the voltage change from the force sensor during the tensile testing process. The OmniProbe was translated with a speed of 0.1 μm/sec. As an example, Figure 2.2 (a-c) shows a series of SEM images taken at different time points during one of the tests. Figure 2.2 (d) shows the gauge strain change during the corresponding test.

2.2.6 Force and Elongation of EC-PEDOT during Tensile Test

In this particular example, the initial voltage was 1.65 V before testing. The voltage was monitored during the tensile test until the specimen was broken where voltage dropped to its initial value. For this sample, a 0.1 V increase represents an increase of 50 μN from the load sensor. The cross-section area of the gauge was confirmed from SEM images for each test. Figure 2.3 (top) shows the calculated stress change with respect with time during the test. The stress was initially zero and then increased to about 300 MPa almost linearly. It is noted that the voltage before the test was not the zero-force voltage. To precisely calculate the corresponding stress, the value after tensile test is the correct zero-force voltage. This difference was evidently due to some residual stress induced in the sample due to the Pt deposition at the edge of the specimen. Before Pt deposition, the OmniProbe was approached close to specimen without directly contacting each other. Then Pt deposition was used to fill up the gap between PEDOT and the probe leading to the compression to the specimen. Therefore, the zero-force voltage in this test was 1.68 V instead of 1.65 V, corresponding to an initial residual force of 15 μN.

In order to precisely estimate tensile strains, the video analysis software Tracker (OSP Java framework) was employed to analyze the recorded video clips. A

specific video frame could be "marked" and "tracked". The moving distance was calibrated using the SEM image scale bar. The origin was set to be on the marked frame for easier calculations. The relative position of the marked frame was recorded with respect to processing time. When calculating the strain, the values of y-axis change were neglected because their variations were significantly less than x-axis (typically there was less than a 0.03 μm change in the y-axis as compared with ~0.35 μm in x-axis). In this example, the tracking point of the sample moved about 0.3 μm before tensile rupture. From the recorded data points, we determined information about the associated elongation of the EC-PEDOT specimen during the tensile test. The dimensions of the gauge could be obtained from the high resolution SEM images. After converting the deformation behavior to strain and the known dimensions of the sample, we were able to obtain the strain change with respect with time for these EC-PEDOT thin films (Figure 2.3 bottom) .

2.2.7 Stress-Strain Curve of EC-PEDOT

By normalizing the process time in Fig 2.3 (top) and (bottom), stress-strain curves could be obtained. Figure 2.4 (a) shows the stress-strain curves for EC-PEDOT with different gauge thicknesses. In this study, 3 different specimens with different gauge thickness of 350 nm, 450 nm, and 750 nm were tested. With linear fitting, the average Young's modulus and tensile strength was calculated to be 5.0 ± 1.0 GPa and 270 ± 70 MPa from these three measurements. To further confirm the reproducibility of the method, three exactly identical EC-PEDOT specimens were examined using the same method. The corresponding stress-strain curves are shown in figure 2.4 (b) with hollow marks. After linear fitting, the Young's modulus of the EC-PEDOT was

calculated to be 5.4 ± 0.3 GPa and the tensile strength was 320 ± 19 MPa. The mechanical properties from these two tests are similar, indicating the reproducibility of this method.

Despite the importance of Young's modulus and tensile strength, EC-PEDOT toughness has not been investigated previously. From stress-strain curve, we could calculate the tensile toughness by integrating the area under the stress-strain curve. In this case, since the stress-strain curve was linear we used linear fitting to estimate the tensile toughness. The averaged toughness so determined was 7.16 ± 2.78 MPa.

2.2.8 Other Methods to Obtain Mechanical Properties of PEDOT

As mentioned earlier, there are several indirect methods available for measuring the mechanical properties of PEDOT films. Table 3.1 is a list of the current method used to measure PEDOT mechanical properties as well as their advantages and disadvantages. It is worth noting that the value of modulus obtained from this *in situ* tensile testing method is somewhat larger than that determined by other methods. As described earlier, nanoscale specimens are expected to contain less defects leading to a larger strength of failure. Another important factor is the relative humidity (rH) as Lang et al (Lang, Naujoks, & Dual, 2009) discussed in their report. With lower rH, the measured modulus was expected to be larger. In the in-situ tensile test of the present work, tests were conducted under vacuum environment in a SEM chamber. It is expected that the modulus measured from in-situ tensile test may be larger than tests conducted in an ambient environment with certain rH.

Due to the difficulty of obtaining a sufficient size of EC-PEDOT for tensile test, Lang et al reported a bulk size tensile test on a Baytron P spin casted film. With proper operations, a cast film of Baytron P with sufficient size can be peeled off as a

freestanding film for a bulk tensile test. They found that PEDOT modulus was highly affected by relative humidity (rH) (Lang et al., 2009). The Young's modulus was increased from 0.9±0.2 GPa at 55% rH to 2.8±0.5 GPa at 23% rH. The strength was also increased from 22.2±4 MPa to 53.2±9.5 MPa respectively. However, this method can only be applied to spun cast Baytron P film, and can not be adapted to EC-PEDOT. It should also be noted that Baytron P is an aqueous suspension of a chemically oxidized PEDOT:PSS in polyelectrolyte complex with excess PSS for better dispersion (Lövenich, 2014). Therefore, it is expected that the mechanical behaviors of solution cast chemically polymerized PEDOT and electrochemical polymerized PEDOT would be different.

Baek et al used nano-indentation to measure the modulus of PEDOT with different dopants (Baek et al., 2014). The results suggest that with larger dopants, the mechanical modulus increases. The indentation modulus of PEDOT doped with PSS was measured as 3.23 ± 1.00 GPa (Baek et al., 2014). However, the results are not consistent from group to group (Yang & Martin, 2006). Reports have discussed how the influence of surface roughness can greatly affect the measurements of mechanical properties (Jiang, Su, & Feng, 2008)(J. Y. Kim et al., 2007). PEDOT surfaces have a bumpy and nano-fibrous morphology with characteristic size of a few nanometers which implies that roughness factor cannot be ignored in the test which scattered the results. In addition, in later publications from the same group, the authors suggested that the indentation tip is too large (~20-50 nm) compared with the morphology of PEDOT surface which lead to an overestimation of the modulus (Hassarati et al., 2014).

AFM QNM may be a more reliable method because the size of AFM QNM probe is relatively smaller (~ 8 nm) that of nano-indentation probes. However, the limitations of this method involve some calibration methods and selection of probes. Figure 2.5 shows the distribution of the data points over the region examined on EC-PEDOT using probes with different force constants as well as different calibration methods.

For the relative calibration method, a 2.7 GPa polystyrene was used as the standard material. The measured modulus was 4 GPa and 7 GPa with 5N/m and 40 N/m force constant respectively. It is noted that Green et al also used AFM QNM to estimate the mechanical modulus of EC-PEDOT with different size of counter ions. The results show that larger dopants lead to a larger modulus from 68.0 MPa with perchlorate to 214.8 MPa with PSS (Hassarati et al., 2014). In their study, the calibration of tips was performed on a relatively soft PDMS standard (~1 MPa). The relative calibration method forces the value of ratio $K/R^{0.5}$ to be correct at given indentation depth. This assumes limited modulus difference between standards and the samples to be measured. As the modulus of PEDOT was expected to be around hundreds of MPa to several GPa range, we found that the modulus varied dramatically with different calibration standard materials. In order to measure this large range of modulus change in a consistent manner, a universal calibration method was adopted in our study. The force constant of the cantilever was calibrated through thermal tuning and the precise tip radius was measured through analyzing standard TiO_2 samples.

Figure 2.5 shows the measured DMT modulus from universal calibration methods with different probe force constants. The moduli so obtained were 1.5 GPa, 4.2 GPa, and 9 GPa with 5, 40, and 200 N/m force constants respectively. These

results imply that the measurement may show deviations if not choosing the proper probe for target samples. The measurements of modulus from AFM QNM are more reliable than from nano-indentation only with proper calibration and probes; however, the PEDOT strength and toughness is still unknown. Without considering strength and toughness, it is difficult to describe the durability of PEDOT coating.

To better understand the mechanical behavior of EC-PEDOT, a universal stress-strain curve is necessary in order to estimate modulus, strength, and toughness. However, the methods mentioned above only provided information about the modulus. A thin film cracking method developed in our group tried to provide a more thorough mechanical characterization method (Qu et al., 2016). By observing fracture strain, and the PEDOT film crack spacing during the crack saturated state, both the cohesive and adhesive strength could be obtained (Agrawal & Raj, 1990). The estimated Young's modulus of PEDOT films was 2.6 ± 1.4 GPa, the strain to failure was round 2%, and the tensile strength was measured to be 56 ± 27 MPa. The interfacial shear strength, which is essential to estimate the film adhesion, was estimated to be 0.7 ± 0.3 MPa. However, by introducing a gold/palladium thin coating to make the ductile substrate conductive for electrochemical deposition, the complexity of the system was increased, which would affect accuracy of the interfacial shear strength. Also, since this method is not a direct tensile test of PEDOT film, the Young's modulus results calculated from the rule of mixtures might be affected, too.

With the in situ tensile test presented in the work, we will be able to have more quantitative understanding about EC-PEDOT.

2.2.9 *In Situ* Test in TEM

Tian et al (Tian et al., 2012) reported an *in situ* TEM tensile test on a metallic glasses (MG) to explore the ideal elastic limit of MG. In the report, they claimed that the electron beam didn't cause significant effects to the sample during the *in situ* observation. To confirm this, they did tests with the beam on and off showing consistent results. However, TEM observation is still difficult to be applied to polymers based materials like PEDOT. Research shows that PEDOT will degrade under high acceleration voltage used in TEM in just a few seconds (Martin et al., 2010). SEM is thus a more suitable method to perform an *in situ* observations and characterizations for polymer based materials.

2.2.10 Beam Damage

It is noted that it there might be beam damage to the PEDOT structure while ion milling the dog bone shape specimens with the gallium beam. To address this issue, a relatively low current beam was used when polishing samples to minimize the possible beam damage. It is reasonable to assume that the beam effect on PEDOT is uniform along the surface. Samples were made with different cross-section areas which means the affected part of sample is fixed. With different sizes of the sample, the ratio of non-FIBed/ FIBed is varied hence this should lead to a different mechanical behaviour if there is any structural damage. If there is any obvious beam damage, the corresponding results should be different. However, in this report, the measured modulus and the strength with different size samples were similar, within our experimental error. These results suggest that if there is some beam damage, there was no significant effect to the mechanical properties of PEDOT, at least under the

conditions used in this experiment. The following are some possible explanations: First, the damage of FIB is mainly from the heat generated by Ga ion beam energy in the sample. The reported temperature rise of FIB is about 330 ºC at 30 kV/ 0.1 nA and 1000 ºC at 30 kV/ 1 nA on aPt/W thermocouple junction (Shukla et al., 2009). In the experiment, a low beam current of 5 pA was used which was 20 times lower than the reported values. Therefore, it is reasonable that the temperature rise is under the temperature of thermal stability limitation of PEDOT which has been reported to be around 380 K (Hokazono, Anno, & Toshima, 2014) Also, there was a large tungsten tip with high thermal conductivity in local contact with PEDOT specimen. Any heat generated during milling was likely conducted away to the relatively large tungsten probe. To conclude, we have used the lowest power of FIB to minimize the beam damage, and have found that there was no significant effect on the mechanical behaviour of EC-PEDOT.

2.3 Conclusions

Studies of the mechanical properties of electrochemically deposited PEDOT films, especially its tensile strength and toughness, are limited due to the difficulty of obtaining a free standing samples. In this study, we reported a novel tensile testing method within a FIB-SEM chamber that allowed us to perform *in situ* observations and simultaneous measurements of the mechanical behaviour of EC-PEDOT. In addition, an AFM QNM method was employed to corroborate the values of modulus so obtained. With the better understanding of PEDOT mechanical behavior provided by this approach, we hope to be able to optimize the performance of these and related materials with new variations in chemistry and processing.

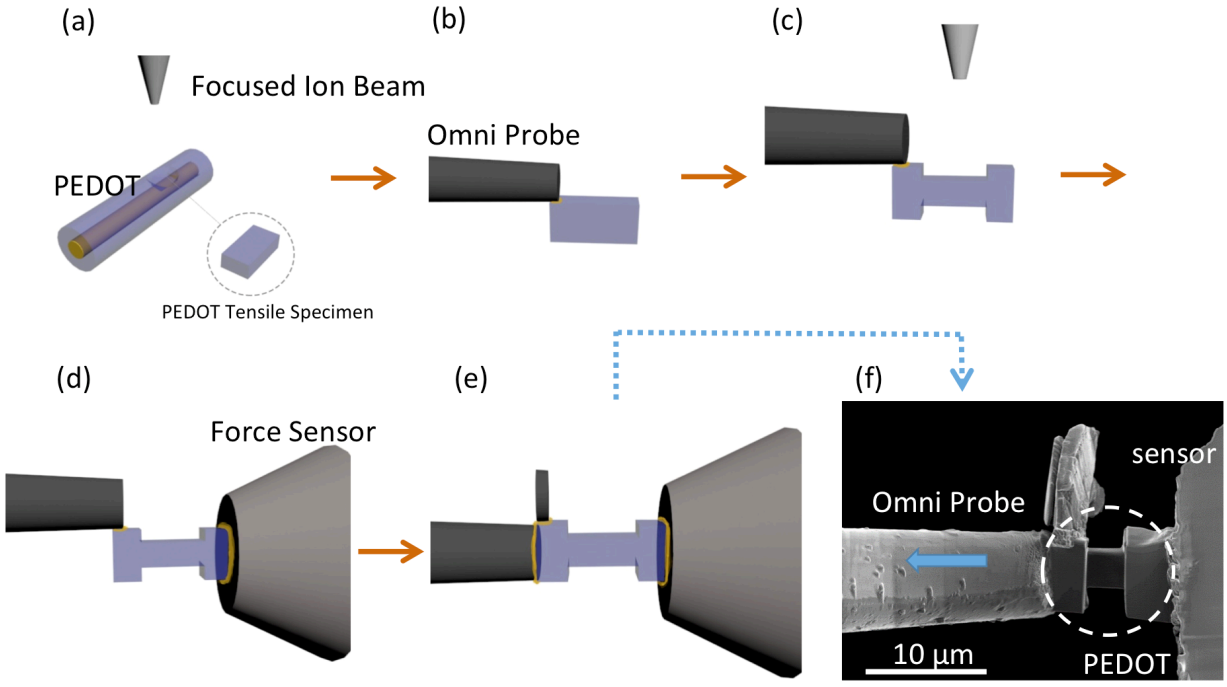

Figure 2.1 Tensile test in SEM chamber of EC-PEDOT specimen; (a) to (c) Schematic of fabrication of the EC-PEDOT dog bone specimen; (d) (e) attached both side of the specime to the force sensor for force measurement and the OmniProbe for operation. (f) the high resolutuon SEM image of in situ tensile test setup in SEM chamber.

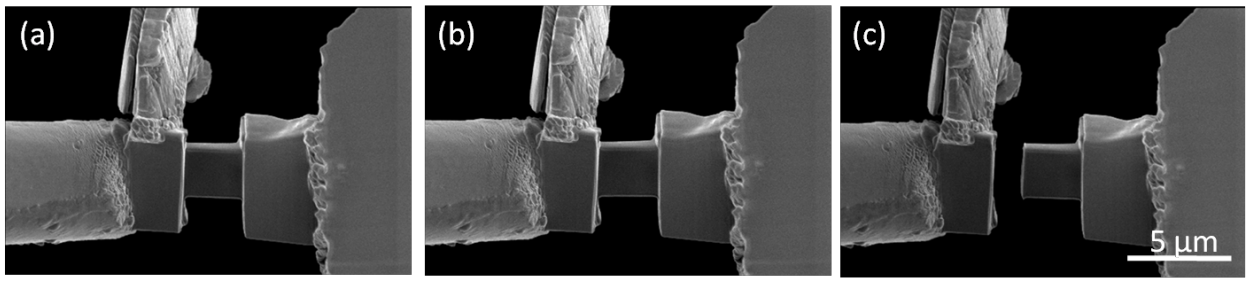

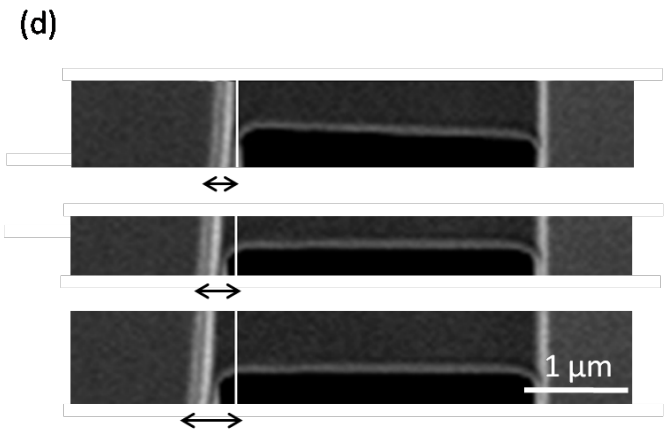

Figure 2.2 (a) to (c) real time SEM images showing the tensile test of EC-PEDOT; (d) high magnification of gauge elongation during the tensile test

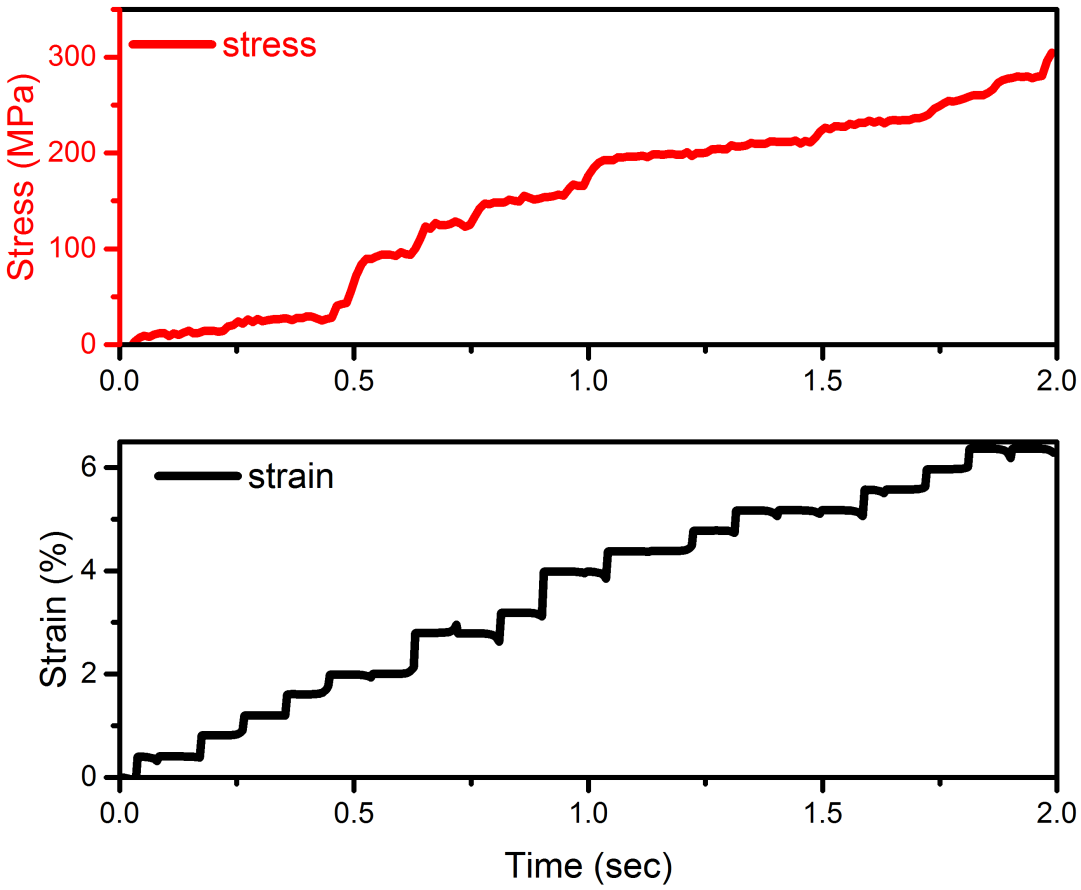

Figure 2.3 Stress (top) and strain (bottom) change with respect with time of EC-PEDOT during tensile test

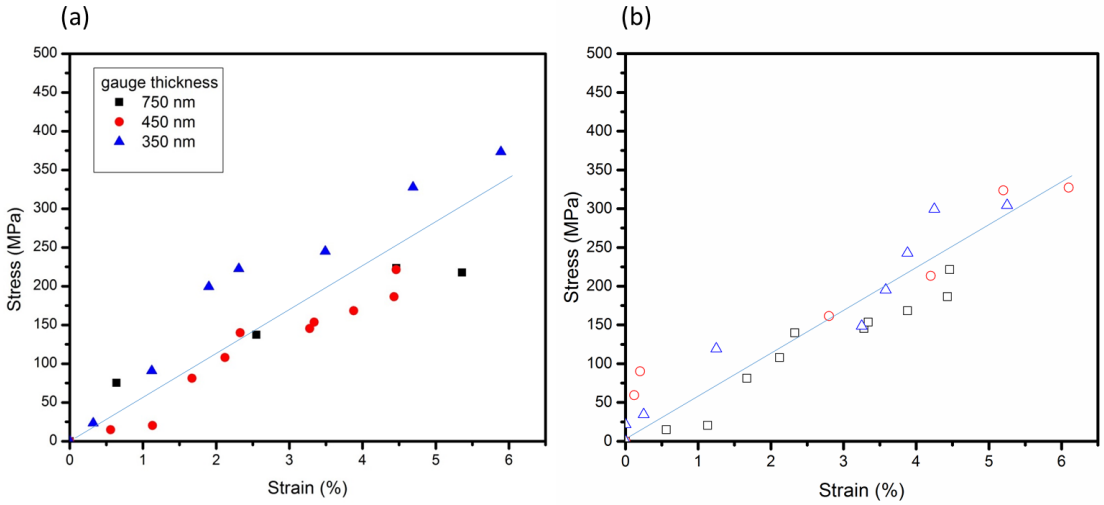

Figure 2.4 Stress-strain curves of *in situ* tensile test. (a) stress-strain curves with different gauge thickness of 350, 450 and 750 nm. (b) stress-strain curves from three tests with exactly the same gauge thickness of 450 nm

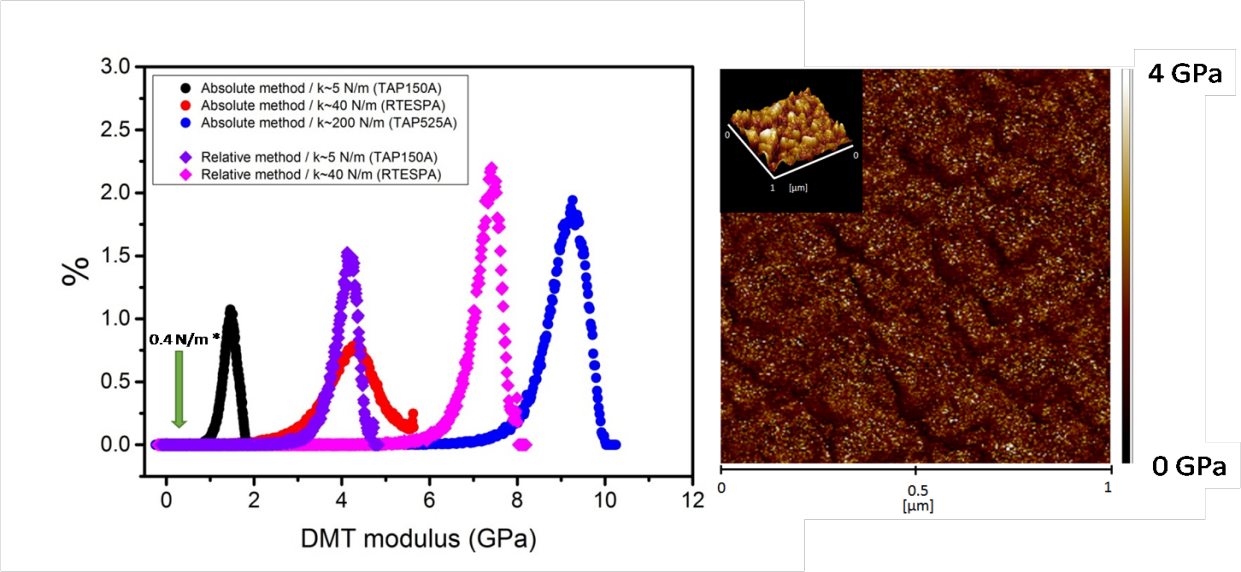

Figure 2.5 AFM QNM^{TM} modulus distribution of EC-PEDOT by different calibration method and probe force constant (left) . AFM image of the polymer film (1 µm by 1µm) (right).

TABLE

	Materials	dopants	Modulus	Tensile Strength	Pros	Cons
In situ tensile test	EC-PEDOT	PSS	5 ± 1.0 GPa	270 ± 70 MPa	1. Micro scale mechanical properties 2. Direct measurements 3. Able to obtain tensile strength	1. Vacuum environment 2. Complicated operation
AFM QNM	EC-PEDOT	PSS	1.2 ± 0.3 GPa	N/A	1. Small probe size 2. Statistic data over the examined area	1. No tensile strength 2. DMT modulus 3. Highly depend on the calibration standard materials/ spring constant of the probe
Nano-indentation	EC-PEDOT	PSS	3.2±1.0 GPa	N/A	1. Easy to perform	1. Large probe size lead to an overestimation of modulus 2. Require flat surface 3. No tensile strength
Traditional tensile test	Baytron P	PSS	2.8±0.5 GPa at 23%rH	53.2±9.5 MPa at 23%rH	1. Easy to perform 2. Able to obtain tensile strength	1. Not able to measure EC-PEDOT
Thin film cracking	EC-PEDOT	$LiClO_4$	2.6 ± 1.4 GPa	56 ± 27 MPa	1. Able to obtain both the tensile and interfacial shear strength 2. Easy to perform	1. An indirect method 2. The complexity of the system increases the inaccuracy of the method.

Table 2.1 Comparison of different mechanical characterization methods

REFERENCES

Agrawal, D., & Raj, R. (1990). Ultimate shear strengths of copper-silica and nickel-silica interfaces. *Materials Science and Engineering: A*, *126*, 125–131.

Baek, S., Green, R. a., & Poole-Warren, L. a. (2014). Effects of dopants on the biomechanical properties of conducting polymer films on platinum electrodes. *Journal of Biomedical Materials Research - Part A*, *102*(August), 2743–2754. http://doi.org/10.1002/jbm.a.34945

Biran, R., Martin, D. C., & Tresco, P. a. (2005). Neuronal cell loss accompanies the brain tissue response to chronically implanted silicon microelectrode arrays. *Experimental Neurology*, *195*(1), 115–26. http://doi.org/10.1016/j.expneurol.2005.04.020

Cui, X. (2007). Poly (3,4-ethylenedioxythiophene) for chronic neural stimulation. *IEEE Trans Neural Syst Rehabil Eng.*, *15*(4), 502–8. http://doi.org/10.1109/TNSRE.2007.909811.

Cui, X., Lee, V. a., Raphael, Y., Wiler, J. a., Hetke, J. F., Anderson, D. J., & Martin, D. C. (2001). Surface modification of neural recording electrodes with conducting polymer/biomolecule blends. *Journal of Biomedical Materials Research*, *56*, 261–272. http://doi.org/10.1002/1097-4636(200108)56:2<261::AID-JBM1094>3.0.CO;2-I

Cui, X., & Martin, D. C. (2003a). Electrochemical deposition and characterization of poly(3,4-ethylenedioxythiophene) on neural microelectrode arrays. *Sensors and Actuators B: Chemical*, *89*(1-2), 92–102. http://doi.org/10.1016/S0925-4005(02)00448-3

Cui, X., & Martin, D. C. (2003b). Fuzzy gold electrodes for lowering impedance and improving adhesion with electrodeposited conducting polymer films. *Sensors and Actuators, A: Physical*, *103*, 384–394. http://doi.org/10.1016/S0924-4247(02)00427-2

Cui, X., Wiler, J., Dzaman, M., Altschuler, R. a, & Martin, D. C. (2003). In vivo studies of polypyrrole/peptide coated neural probes. *Biomaterials*, *24*(5), 777–87. Retrieved from http://www.ncbi.nlm.nih.gov/pubmed/12485796

Gerard, M., Chaubey, A., & Malhotra, B. D. (2002). Application of conducting polymers to biosensors. *Biosensors and Bioelectronics*, *17*, 345–359. http://doi.org/10.1016/S0956-5663(01)00312-8

Green, R. a, Matteucci, P. B., Hassarati, R. T., Giraud, B., Dodds, C. W. D., Chen, S., … Lovell, N. H. (2013). Performance of conducting polymer electrodes for stimulating neuroprosthetics. *Journal of Neural Engineering*, *10*, 016009. http://doi.org/10.1088/1741-2560/10/1/016009

Hassarati, R. T., Goding, J. a., Baek, S., Patton, A. J., Poole-Warren, L. a., & Green, R. a. (2014). Stiffness quantification of conductive polymers for bioelectrodes. *Journal of Polymer Science Part B: Polymer Physics*, *52*(9), 666–675. http://doi.org/10.1002/polb.23465

Hokazono, M., Anno, H., & Toshima, N. (2014). Thermoelectric properties and thermal stability of PEDOT:PSS films on a polyimide substrate and application in flexible energy conversion devices. *Journal of Electronic Materials*, *43*(6), 2196–2201. http://doi.org/10.1007/s11664-014-3003-y

Jiang, W. G., Su, J. J., & Feng, X. Q. (2008). Effect of surface roughness on nanoindentation test of thin films. *Engineering Fracture Mechanics*, *75*(17), 4965–4972. http://doi.org/10.1016/j.engfracmech.2008.06.016

Kim, D.-H., Richardson-Burns, S. M., Hendricks, J. L., Sequera, C., & Martin, D. C. (2007). Effect of Immobilized Nerve Growth Factor on Conductive Polymers:

Electrical Properties and Cellular Response. *Advanced Functional Materials*, *17*(1), 79–86. http://doi.org/10.1002/adfm.200500594

Kim, J. Y., Kang, S. K., Lee, J. J., Jang, J. Il, Lee, Y. H., & Kwon, D. (2007). Influence of surface-roughness on indentation size effect. *Acta Materialia*, *55*, 3555–3562. http://doi.org/10.1016/j.actamat.2007.02.006

Lang, U., Naujoks, N., & Dual, J. (2009). Mechanical characterization of PEDOT:PSS thin films. *Synthetic Metals*, *159*, 473–479. http://doi.org/10.1016/j.synthmet.2008.11.005

Lövenich, W. (2014). PEDOT-properties and applications. *Polymer Science Series C*, *56*(1), 135–143. http://doi.org/10.1134/S1811238214010068

Lu, H., Wang, B., Ma, J., Huang, G., & Viswanathan, H. (2003). Measurement of creep compliance of solid polymers by nanoindentation. *Mechanics Time-Dependent Materials*, *7*(3-4), 189–207. http://doi.org/10.1023/B:MTDM.0000007217.07156.9b

Ludwig, K. a, Uram, J. D., Yang, J., Martin, D. C., & Kipke, D. R. (2006). Chronic neural recordings using silicon microelectrode arrays electrochemically deposited with a poly(3,4-ethylenedioxythiophene) (PEDOT) film. *Journal of Neural Engineering*, *3*, 59–70. http://doi.org/10.1088/1741-2560/3/1/007

Martin, D. C., Wu, J., Shaw, C. M., King, Z., Spanninga, S. a., Richardson-Burns, S., … Yang, J. (2010). The Morphology of Poly(3,4-Ethylenedioxythiophene). *Polymer Reviews*, *50*(3), 340–384. http://doi.org/10.1080/15583724.2010.495440

Oh, W.-K., Kwon, O. S., & Jang, J. (2013). Conducting Polymer Nanomaterials for Biomedical Applications: Cellular Interfacing and Biosensing. *Polymer Reviews*, *53*(July), 407–442. http://doi.org/10.1080/15583724.2013.805771

Ouyang, L., Kuo, C., Farrell, B., Pathak, S., Wei, B., Qu, J., & Martin, D. C. (2015a). Poly[3,4-ethylene dioxythiophene (EDOT)-co-1,3,5-tri[2-(3,4-ethylene dioxythienyl)]-benzene (EPh)] copolymers (PEDOT-co-EPh): optical,

electrochemical and mechanical properties. *J. Mater. Chem. B*, *00*, 1–11. http://doi.org/10.1039/C5TB00053J

Qu, J., Ouyang, L., Kuo, C. C., & Martin, D. C. (2016). Stiffness, strength and adhesion characterization of electrochemically deposited conjugated polymer films. *Acta Biomaterialia*, *31*, 114–121. http://doi.org/10.1016/j.actbio.2015.11.018

Schmidt, C. E., Shastri, V. R., Vacanti, J. P., & Langer, R. (1997). Stimulation of neurite outgrowth using an electrically conducting polymer. *Proceedings of the National Academy of Sciences of the United States of America*, *94*(August), 8948–8953. http://doi.org/10.1073/pnas.94.17.8948

Shukla, N., Tripathi, S. K., Banerjee, A., Ramana, a. S. V., Rajput, N. S., & Kulkarni, V. N. (2009). Study of temperature rise during focused Ga ion beam irradiation using nanothermo-probe. *Applied Surface Science*, *256*, 475–479. http://doi.org/10.1016/j.apsusc.2009.07.024

Tian, L., Cheng, Y.-Q., Shan, Z.-W., Li, J., Wang, C.-C., Han, X.-D., … Ma, E. (2012). Approaching the ideal elastic limit of metallic glasses. *Nature Communications*, *3*, 609. http://doi.org/10.1038/ncomms1619

Wilks, S. J., Richardson-burns, S. M., Hendricks, J. L., Martin, D. C., & Otto, K. J. (2009). Poly (3 , 4-ethylenedioxythiophene) as a micro-neural interface material for electrostimulation, *2*(June), 1–8. http://doi.org/10.3389/neuro.16.007

Yang, J., & Martin, D. (2006). Impedance spectroscopy and nanoindentation of conducting poly(3,4-ethylenedioxythiophene) coatings on microfabricated neural prosthetic devices. *Journal of Materials Research*, *21*(5), 1124–1132. http://doi.org/10.1557/jmr.2006.0145

ELECTROCHEMICAL DEPOSITION OF PEDOT IN ADIPOSE DERIVED STEM CELL (ADSC) PRODUCED EXTRACELLULAR MATRIX (ECM)

3.1 Introduction

Conducting polymers have attracted extensive interest for use in flexible electronic devices such as organic light emitting diodes (OLED) (W. H. Kim et al., 2002), solar cells (Huynh, 2002), transistors and biosensors (Dong-Hwan Kim et al., 2010)(Gerard et al., 2002) (Forrest, 2004). The alternating carbon-carbon double bonds in the conjugated molecular backbone create π-orbital overlap along the polymer chain. These delocalized electrons and associated counter ions lead to high electrical and ionic conductivity (Martin et al., 2010). In recent years, conducting polymers have shown great potential for directly interfacing bionic devices with living tissue (Richardson-Burns et al., 2007a)(R. A. Green, Lovell, Wallace, & Poole-Warren, 2008). Compared to metal or semiconductor electrodes, these polymers provide relatively soft, conformal and sensitive interfaces with large surface areas that are useful for both *in vitro* and *in vivo* applications. Many conducting polymers, such as poly(pyrrole) (PPy) (Cui, Lee, et al., 2001) and poly(aniline) (PANI) (Bhadra et al., 2009) have been investigated for neural interface applications. Among these polymers, the diethoxy-substituted thiophenepoly(3,4-ethylene dioxythiophene) (PEDOT) has

received particular interest as a reliable material for interfacing electronic biomedical devices with neural tissue due to its excellent chemical stability and high conductivity (Crispin & Marciniak, 2003).

In neural interface applications, the implantation typically requires inserting a hard, metallic or semiconductive electrode into soft, living, ionically conductive tissue. In chronic applications, the implants are usually associated with a glial scar encapsulation that has been associated with the loss of device function (Woolley, Desai, & Otto, 2013). The glial sheath creates a ~150 μm characteristic gap between devices and tissues, which is associated with an increase of impedance and eventually device failure (Biran, Martin, & Tresco, 2007). One of the possible reasons of this scar encapsulation is the large mechanical strain near the interface of rigid device and soft tissue (Subbaroyan, Martin, & Kipke, 2005) (Karumbaiah et al., 2013). The constant strain leads to a hostile environment for neural survival, therefore decreasing the neuron densities near the implants. The lack of biological signals for neuron growth can be another drawback of the devices (Anderson, Rodriguez, & Chang, 2008).

Conducting polymers has been investigated to interface devices and tissues due to its relatively low mechanical modulus and improved conductivity. Besides using conducting polymers alone, they can be polymerized with varied materials to tailor their properties for different purpose. Reports have demonstrated that PEDOT can be polymerized with hydrogel forming a PEDOT-hydrogel composite to further lower the mechanical modulus of devices (Kim et al., 2010)(Chikar et al., 2012)(Green et al., 2012b). Green et al designed a “living electrode” idea based on integrating living cells

in the conducting polymers-hydrogel composites to enhance biological activity (R. A. Green et al., 2013). This idea is to bring up neural compatibility during implantation by the presence of cultured neural cells in the implant. However, there is no further study to confirm its biological response in vitro or in vivo. Other studies also investigate to control the morphology of conducting polymer by using different template to trigger cells stimulation. Yang et al used PS spheres as the template during PEDOT deposition and then dissolve to make a microporous PEDOT surface to control cell dispersion potentially (Yang & Martin, 2004). Abidian et al also reported a method to fabricate a soft, control-releasing materials by polymerizing PEDOT into electrospun fibers with alginate hydrogel(Abidian & Martin, 2009). Those polymer composites emphasize on its physical characteristic for better neural interfacing applications, however, the contribution of biological cues is not yet discussed. In this study, extracellular matrix, a bioactive template, was used to make conducting polymers composites to provide a better biological compatibility during implantation.

Thus far, bioactive materials have been developed from synthetic biodegradable polymers such as PGA and PLGA (Freed et al., 1994), natural polymers such as collagen (Parenteau-Bareil et al., 2010), dextran (De Groot et al., 2001), and hyaluronic acid (Collier et al., 2000), to tissue engineering scaffolds made from acellular tissues (Farwell et al., 2006)(Badylak, 2002). Among them, synthetic polymers provide biodegradability but little bioactivity due to its residual chemicals, acid moieties, and microscale particulates from degradation. As for the natural polymers and acellular tissues, they are often exhaustively xenogeneic and allogeneic. Without proper operation and sterilization, they will bring potential risk of pathogen transmission and undesirable inflammatory reaction. In this study, our target is to

improve the chronic performance of electronic biomedical devices. We developed an extracelluar matrix film (ECM) derived from adipose-derived stem cells (ADSC) that was subsequently incorporated with PEDOT. This method creates a soft, biologically active and conductive material that is interest for directly interfacing devices with tissue.

Researchers have investigated the incorporation of biologically active materials into conducting polymers to both reduce the mechanical mismatch and promote neuron adhesion near the implants. Previous studies have shown that collagen, laminin, or other kinds of natural polymers can significantly improve the cell adhesion and reduce the inflammatory response (Xiao et al., 2010a).We have shown that co-deposition of polypyrrole (PPy) and synthetic peptides significantly enhanced neural attachment in vivo(Cui et al., 2003). Alternatively, dopants with functional groups, such as chondroitin sulfate can be codeposited with PPy. Collagen fibers can then be immobilized onto the coating through the carboxylic acid groups on side chains of the dopant. (X. Liu et al., 2011). Improved cell adhesion was also shown in this study.

However, the bioactive materials are typically from heterogonous sources. Without extensive purification and sterilization, they may be prone to pathogen transmission and severe immune responses. Here in this study, we report the decoration of adipose derived stem cell extracelluar matrix (ECM) with conducting polymer, PEDOT. This ADSC-derived ECM was used a demonstration that ECM could be fabricated from a cultured cell line, and used as a scaffold for PEDOT polymerization. In the future, we expect that similar methods could be used to create an autologous ECM using cells directly extracted from the host, thus minimizing the

potential risk of immune responses (Hongxu Lu et al., 2011). This tissue-like ECM film provides a layer of mechanical buffer at the interface. In addition, it also provides biological and topological signals to promote regeneration at the interface. PEDOT was electrochemically deposited into the matrix to form conducting pathways. The morphology of the *in situ* polymerized films was confirmed by optical and scanning electron microscopy. The electrochemical properties of the composites were investigated by Electrochemical Impedance spectroscopy (EIS). The improvement of cell adhesion was confirmed by differentiated PC12 cells *in vitro*.

3.2 Materials and Methods

3.2.1 ECM Fabrication and Characterization

Adipose derived stem cells (ADSC) were obtained from Lonza (Walkersville, MD). Cells were cultured in a 75 cm^2 culture flask with ADSC growth medium from passage 2. ADSC growth medium was prepared by adding the contents of the SingleQuots ® to the basal medium. Cells at passage 4-7 were collected by trypsin/EDTA for ECM fabrication.

A gold-sputtered wafer was used as the template to fabricate ECM. The ECM fabrication protocol was adapted from previously published studies (Hongxu Lu et al., 2011). After the ADSC cells were fully confluent and adherent to the substrate, ascorbic acid (150 μg/ml) and ascorbate-2-phodphate (150 μg/ml) were added to the culture medium to stimulate ECM fabrication. After 5 days of culture in the ascorbate containing medium, a white dense layer was seen to deposit on the substrate. Samples were rinsed with phosphate buffered saline (PBS) and DI water (Millipore, Bedford,

MA). Cell-ECM constructs were immersed in NH_4OH (25 mM) solution for decellularization. The constructs were immersed in ammonia solution for 20 mins and then rinsed with DI water to wash off the detached cells. The decellularization steps were repeated 5-6 times until were no cells left behind in optical microscope observations.

3.2.2 *In Situ* Polymerization of PEDOT into ECM Constructs

The ECM film was stored in DI water to retain its structure. To prevent drying, samples were placed in a 37ºC incubator for further process. An EDOT monomer solution was prepared with 0.01 M EDOT and 0.1 wt% PSS as the counter ions in DI water. Samples were dipped into the EDOT monomer solution overnight for further electrochemical polymerization. A platinum needle electrode was used as the working electrode inserted into the ECM film while another large platinum/iridium foil was placed next to the ECM film as the counter electrode. A potentiostat (ModuLab, Solartron Analytical) was used to generate the electrical potential required to oxidize EDOT monomer. The deposition proceeded at 2 V for up to 4 hours leading to a dark blue deposition in the ECM film. The extent of the *in situ* polymerization could be observed under optical microscope due to the significantly dark color change.

3.2.3 PEDOT-ECM Characterizations: Electrical Properties

Electrochemical characterization including CV and EIS was conducted with the Solartron in a three-electrode cell. For EIS, samples were used as the working electrode, an imbedded platinum/iridium foil was acted as the counter electrode, and a saturated Ag/AgCl electrode as the reference electrode was placed next to the working electrode. A 2 mV sinusoidal AC signal was applied to the system with frequency

range from 1 to 10 kHz. Both impedance amplitude and phase angle were collected. For CV, the samples were scanned from -0.6 to 0.8 V to remain inside the water window.

3.2.4 PEDOT-ECM Characterizations: Surface Morphology

Static contact angles were used to confirm the presence of PEDOT deposition in the ECM. A 5 μL drop of DI water was applied to the surface of bare gold, PEDOT, and PEDOT-ECM. The corresponding contact angles were analyzed using NIH ImageJ with an open source plug-in, Drop Snake Analysis.

SEM images of PEDOT-ECM films and cultured cells were acquired with a Zeiss Auriga 60 Focused Ion Beam- Scanning Electron Microscope (FIB-SEM). To enhance the contrast in SEM observation, osmium was used to stain ECM and cells. In order to retain the ECM structure under SEM, samples were prepared critical point dry method. We choose ethanol as the intermediate fluid during the drying process. To replace the water with ethanol, samples were immersed intoa series of water-ethanol mixtures with 10%, 25%, 50%, 75%, 90% and 100% ethanol respectively for 1 hour. Samples were stored in 100% ethanol for more than 24 hours before critical point drying.

Optical and fluorescence microscopy were performed on a Nikon Eclipse LV100 POL microscope equipped with a Nikon Intensilight C-HGFI lamp. The images were collected via a Nikon DS-Ri1 camera.

3.2.5 *In Vitro* Cell Culture Tests

PEDOT-ECM samples were prepared by depositing onto gold-coated silicon substrates (approximately 0.2 cm^2). For each group, 3 independent samples were

prepared for each test. Prior to cell seeding, the samples were sterilized by immersing into for ethanol overnight. To investigate the effect of cell adhesion of PEDOT-ECM and ECM modified surface, no cell adherent promoter such as collagen, poly-l-lysine were added. Rat pheochromocytoma cells expressing green fluorescent protein (PC-12-Turbo-GFP, Marin Pharm) were seeded onto the samples at a density of 2×10^4 per well through a 22 gauge needle to dispense the cells. The cells were cultured in growth medium (RPMI 1640 (Corning Cellgro) plus 5% fetal calf serum (FCS), 10% horse serum (HS), 2 mM L-alanyl-L-glutamine, 1% Pen-Strep and 1% non-essential amino acids (NEAA)) overnight before switching to differentiation medium (RPMI 1640 with 150 ng/mL NGF, 1% FCS and 1% HS). For cell adhesion tests, the cell numbers were calculated before switching to differentiation medium. The detailed morphology of the neurite were examined by SEM. Samples were stained with osmium to increase the contrast and then dehydrated in the critical point dryer for SEM observation.

3.3 Results and Discussions

3.3.1 Fabrication of ECM

Figure 3.1 (a) shows the specific process steps used to fabricate the ECM. The ECM was produced from adipose derived stem cells (ADSC). After the cells were cultured for 5 days (about passage 4) , AA and A2P were added to the medium to accelerate the cell metabolism to produce more extracellular proteins. Another 6 days of culture in the treated medium result in a white thick (about 10-100 μm) film on the substrate. Cells were then removed by the combination of freeze-thaw cycling and ammonium hydroxide. The freeze-thaw cycling causes the repeating ice formation in the cell body. After repeated freeze-thaw cycling, cells were broken into small debris.

Ammonium hydroxide solution helped to break the connection between intracellular and extracellular matrix. With complete washing steps in DI water, cell debris can be totally washed away, leaving left the ECM film for further process. Finally, PEDOT was introduced into the ECM film by electrochemical polymerization.

As shown in Figure 3.1 (b), through this method, ECM could be obtained as a free-standing film with estimated thickness of 10-100 μm. In this process, AA and A2P were necessary to induce enough protein production. Without the additives, only limited amounts of ECM were obtained. The ECM films could be stored in DI water for a few weeks. After a few weeks storage of in DI water, the films still retained their integrity.

3.3.2 *In Situ* Polymerization of PEDOT into ECM Film

The electrochemical deposition of conducting polymers into templates often requires coating a conducting metallic electrode with the templates before the actual deposition. When ECM was initially grown on gold-coated wafer substrates, the underlying substrates then served as the working electrodes for the polymerization of EDOT monomer solution with a platinum foil as the counter electrode. When an anodic current was applied through the working electrode, we found that a uniform PEDOT could grow on the gold substrate, forming substrate-PEDOT-ECM sandwich layers. This could happen because naturally porous ECM allowed sufficient ion exchanges between the substrate and the electrolyte. SEM image shows ECM is cover on the PEDOT coating as shown in Figure 3.2. It could be a drawback to use as an electrode for neural interface since the extended neuritis were blocked by the insulated ECM film and cannot reach to the conductive part of the coating such as PEDOT and

electrode itself. This implies that no signal can be transmitted through neuritis to and from electrodes.

Alternatively, we found that by using a platinum needle as the working electrode, PEDOT could be locally deposited into the ECM. The ECM was first immersed in EDOT-containing solution. An epoxy-insulated platinum wire with only the tip exposed was then inserted into the ECM film. An anodic current was applied through the needle. Figure 3.2 shows the progress of *in situ* PEDOT deposition in ECM film as a function of deposition time. The top figures are optical microscope images and the bottom figures are the schematics representing the PEDOT electrochemical deposition condition. The thicker of the biofilm appears to be darker in the image. PEDOT presents a dark blue color due to its absorbing nature in the visible to near infrared light range. As shown in Fig. 3.2, PEDOT was firstly deposited on the exposed area of the working electrode, and then starts to polymerize outwards to the ECM film. It was typically a symmetric growth. After 4 hours of deposition, we observed that PEDOT polymerization approaches its saturation as the dark polymer boundary stopped moving forward. The final size of the dark PEDOT area could be up to several cm in diameter which is highly dependent on the structure of the ECM. As figure shows, the PEDOT tended to be much denser adjacent to the working electrode, where the polymerization initiated. We also found that with extensive polymerization of PEDOT, the PEDOT-ECM composite became more brittle. Under external mechanical deformation, the films cracked and lost its integrity. Consistent with our observation that PEDOT was denser near the center of deposition, we found that the most brittle part was also in the center. As more PEDOT deposition can provide better conductivity, it is important for this method to find the optimal conditions that both

retain the relative mechanical properties of the ACEM while enhance the good electric activity of the composite.

3.3.3 SEM Observations

The detailed surface morphologies of the films were investigated by SEM. Figure 3.3 (a) shows the ECM morphology under SEM observation. The ECM consisted of nanometer-sized fibers that were locally aligned the same direction. The estimated thickness of the ECM film was about 10-100 μm and was highly dependent on the cells condition and the concentration of AA and A2P. We observed no cell debris in the film, indicating that the decellularization process was successful. Figure 3.3 (b) shows that the PEDOT was deposited along the fibers of ECM as well as in the pores between ECM fibers. When PEDOT deposition was thin, it decorated the individual fibers of the ECM, creating a core-shell structure (Figure 3.3 (b) and (c)). Once PEDOT deposition became thick enough, it allowed the continued PEDOT growing on the film surface, forming a lumpy, cauliflower-like morphology that is typical of PEDOT electrochemicaly-deposited films (as indicated by the arrows in Figure 3.3 (c)). Figure 3.3 (d) shows a schematic of PEDOT deposition along the ECM fibers.

Macroscopically, we also observed cracking of the composite film. This could due to the brittleness of the composite when PEDOT deposition became too thick. It is worth mentioning that there were more fracture structures in the PEDOT-ECM than in the pure ECM. Since we used the same protocol to prepare samples for SEM imaging, it suggested that the fracture part of PEDOT-ECM is due to the PEDOT deposition. Those cracking can be contributed by two reasons. First, ECM itself is insulating.

During electrochemical deposition, the potential significantly increases around the insulated area. The particular high electrical potential can cause damage to the ECM structure. Second, *in situ* PEDOT may breaks ECM fibers. During *in situ* deposition, PEDOT was continuously deposited on the soft ECM fibers making the separate fibers form a large film. The large film was not strong enough to support all the mass on itself.

Figure 3.4 shows the interface of PEDOT-ECM and the intrinsic ECM. A clear boundary was observed in figure 3.4 (a). Higher magnification SEM images illustrates the detail morphology of PEDOT-ECM and intrinsic ECM. Figure 3.4 (b) shows the precise spot of (a) as indicated by the dark blue color where the boundary is.

3.3.4 Electrical Properties

The electrical properties of PEDOT-ECM were investigated with EIS. As shown in Figure 3.5, bare gold electrode had relatively high impedance at 1 to 1k Hz range. At 1 kHz, the impedance magnitude of gold was around 500 Ohm. We found that PEDOT coating decreased the impedance to ~100 Ohm while pure ECM, due to its insulating nature, had a much higher impedance of ~10,000 Ohm at 1 kHz.

In situ PEDOT deposition was conducted at a constant voltage of 2 V with different deposition times. As indicated in Fig 3.5, the impedance over the frequency range gradually decreased after PEDOT deposition. Longer polymerization time led to lower impedance as more conducting materials had been deposited. After 4 hrs of deposition, the PEDOT-ECM composite showed similar impedance improvement as intrinsic PEDOT coating.

It should be noted that the amount of PEDOT deposited is proportional to the charge delivered to the system. For potentiostatic deposition, as constant voltage was applied, the corresponding current depends on the system impedance. Due to insulated ECM film, the corresponding current of the ECM coated electrode shows much lower current compared to bare gold surface. After PEDOT deposition, the current gradually increase to its saturated value. Our experimental design employed a needle electrode inserted in the ECM film. It was observed that initially PEDOT deposited on the needle electrode and then into ECM afterwards. Therefore, it is difficult to estimate how much PEDOT was contributed to the impedance measurement due to the limited information of how much PEDOT was deposited on needle electrodes.

3.3.5 *In Vitro* Study-PC12 Adhesion Test

Differentiated PC-12 cells were employed to investigate the biocompatibility of PEDOT-ECM. PC12 is known as one of the non-adherent neural cells. Its non-adherent property is one of the challenges when culturing PC12 (Gilmour, Woolley, Poole-Warren, Thomson, & Green, 2016). Typically, a cell adhesion promoter coating such as collagen or poly-L-lysine is required when culturing PC12(Xiao, Li, Wang, Shi, & Ooi, 2010b). These coatings lead to complicated surface characteristics. In our study, ECM was functioned as a cell adhesion promoter layer to provide a better cell adhesion on to the electrodes. As shown in Figure 3.6, after 4 days of culture, the cells were essentially non-adherent to either gold or PEDOT surface. The unmodified ECM surface showed the highest cell densities (~450 per mm^2). When covered with PEDOT, the cell density decreased from 450 to 100 per mm^2. Nevertheless, a significant

portion of cells were still attached onto the composite. The detailed cell morphology on PEDOT-ECM composite was studied by SEM and fluorescence microscopy (Fig 3.7 (a) and (b)). We found that the cells grew well on the film surface, with abundant long axons. The processes of these axons tended to attach to the ECM-rich regions, which stresses the importance of these biologically active materials in promoting specific interactions with tissue.

3.4 Conclusions

The electroactive, biomimetic conducting polymer-ECM film that we describe in this study represent a novel *in situ* polymerization method to address the issue at tissue-electrode interface such as lacking of bioactivity and mechanical mismatch. This technology should help to retain a long-term communication between tissues and machines while alleviate typical inflammatory response.

FIGURES

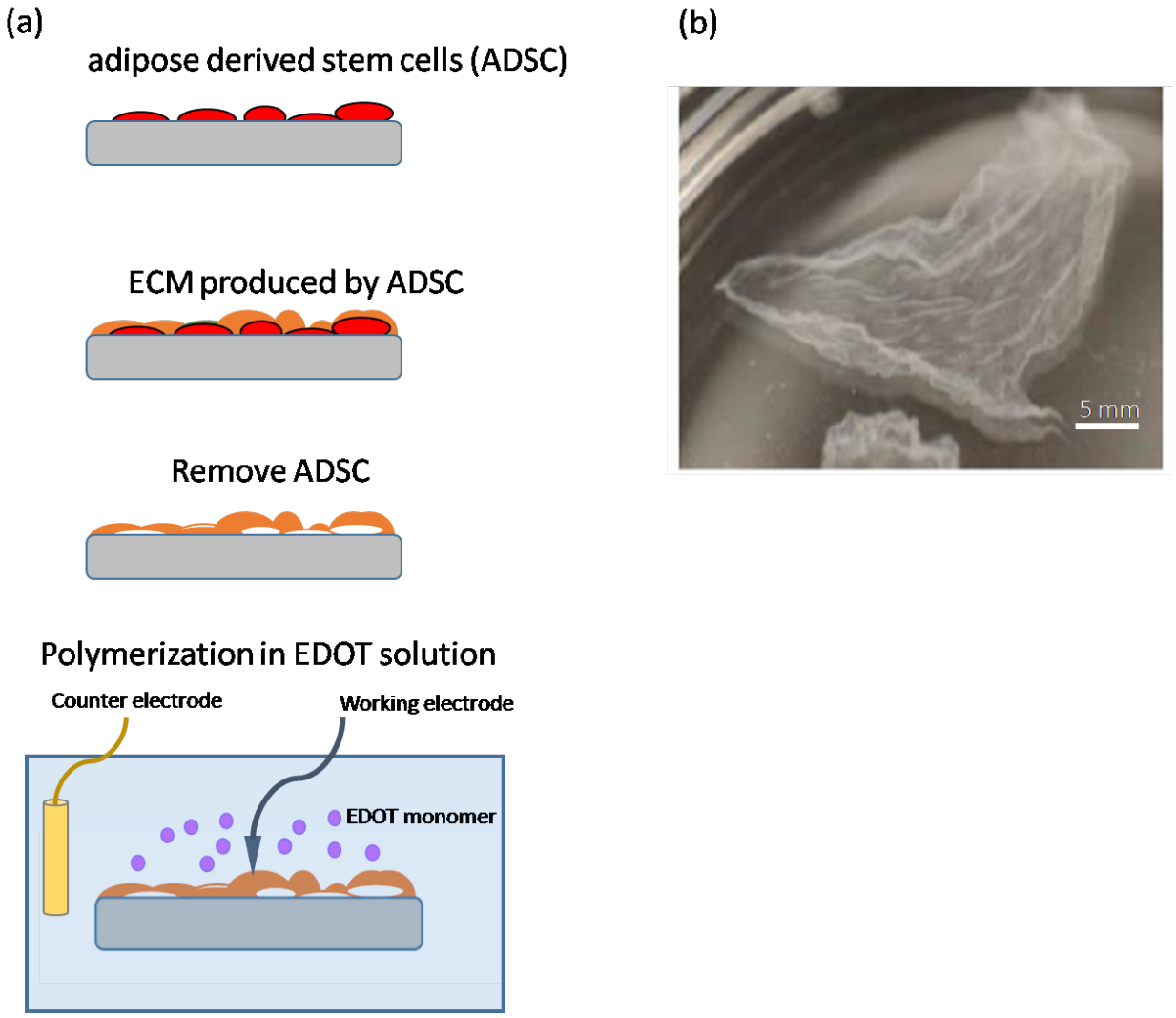

Figure 3.1 (a) preparation scheme for ECM scaffolds and *in situ* PEDOT polymerization in ECM (b) Optical image of a free standing ECM prepared with AA & A2P culture for 2 weeks.

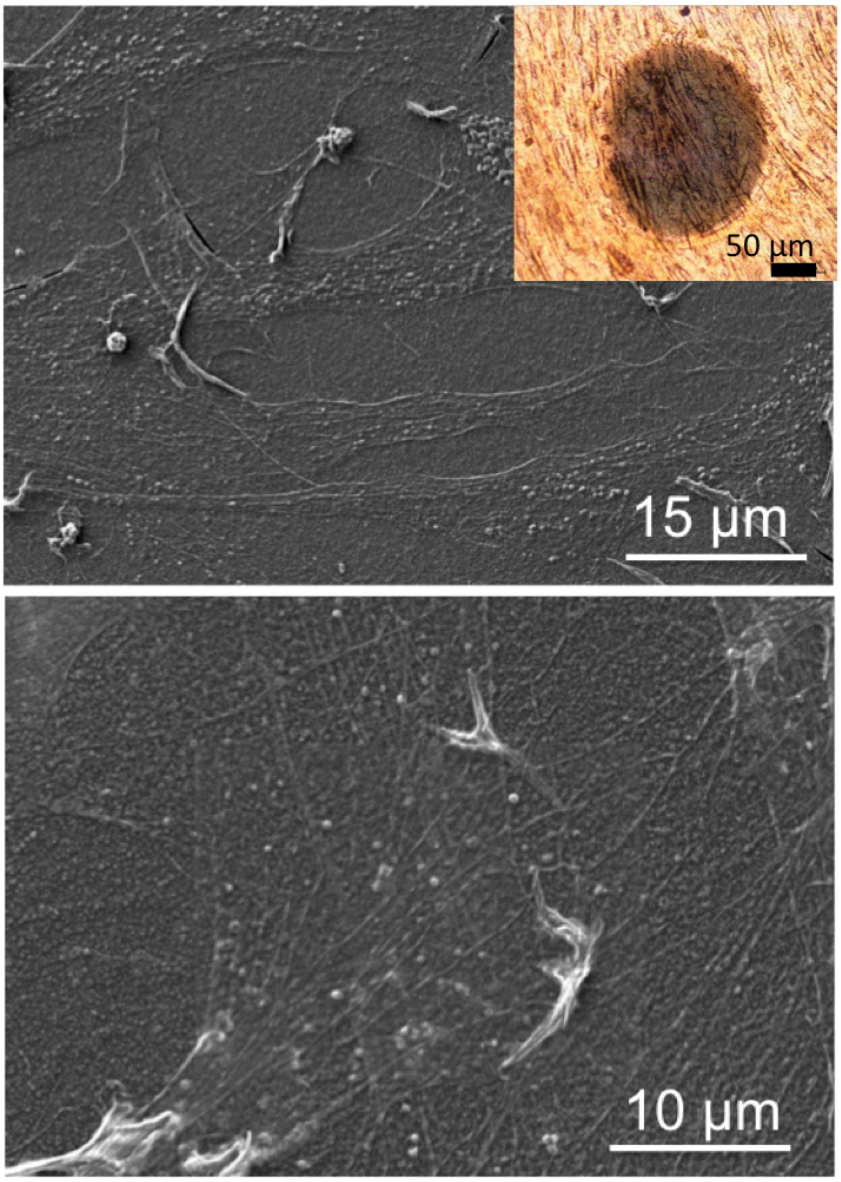

Figure 3.2 SEM images shows PEDOT deposition on gold electrode and under ECM film by using traditional electrode design. The insulated ECM film allows portion of the ions transportation but blocked all electron transportation limiting the conductive pathways during signal transmission.

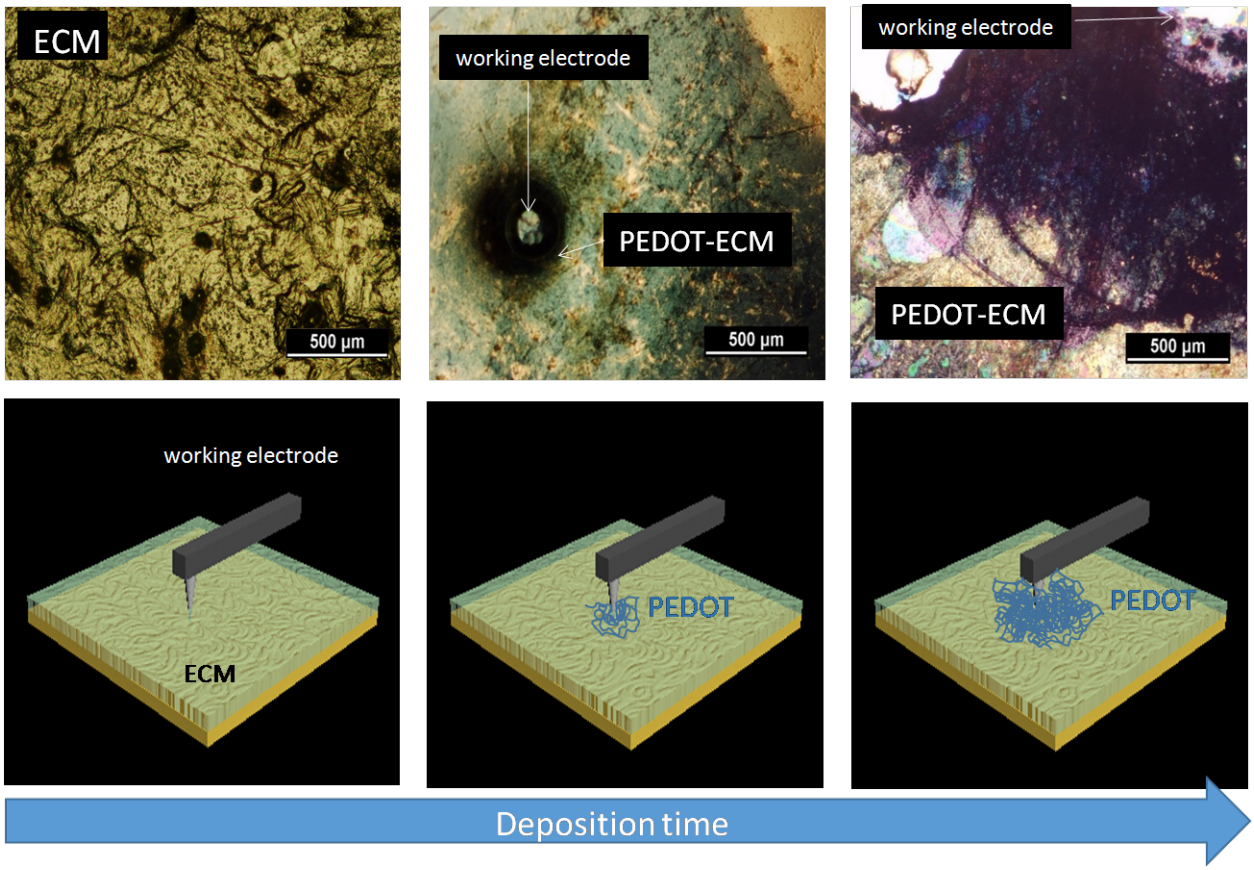

Figure 3.3 Bright-field images (top) and schematic diagram (bottom) of *in situ* PEDOT polymerization in ECM film with different deposition time

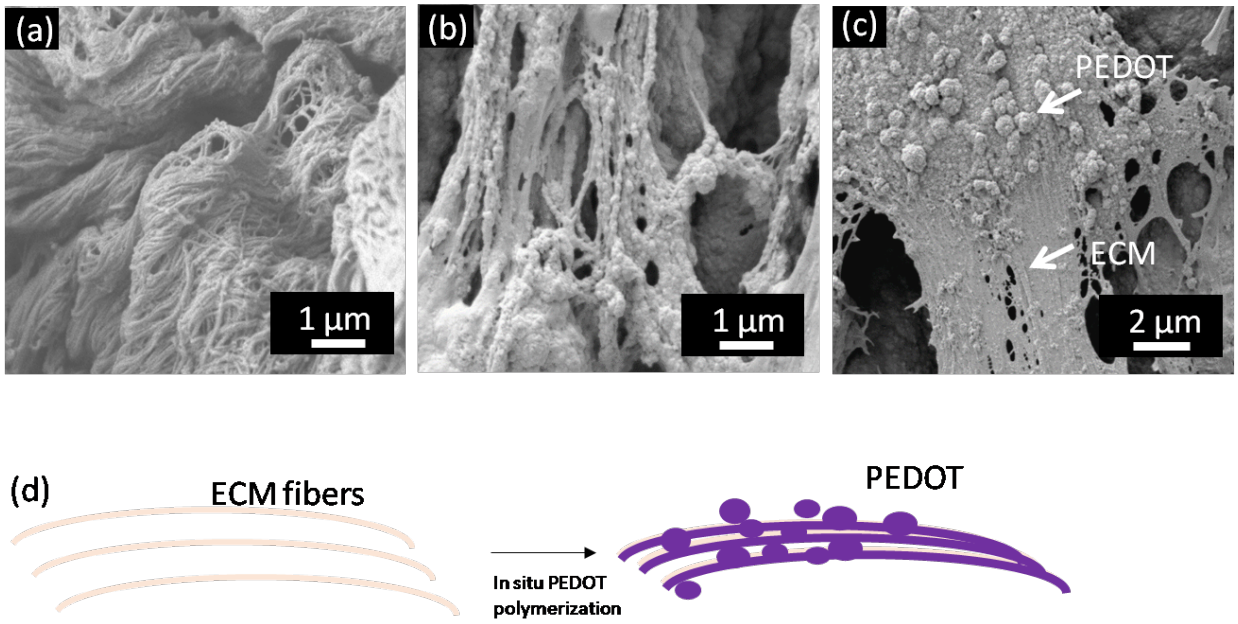

Figure 3.4 SEM images of (a) ECM, (b) PEDOT-ECM showing the PEDOT clusters aggregated along ECM fibers, (c) PEDOT-ECM with lower magnification showing that PEDOT filled up the space between ECM fibers and (d) the schematic diagram of PEDOT-ECM

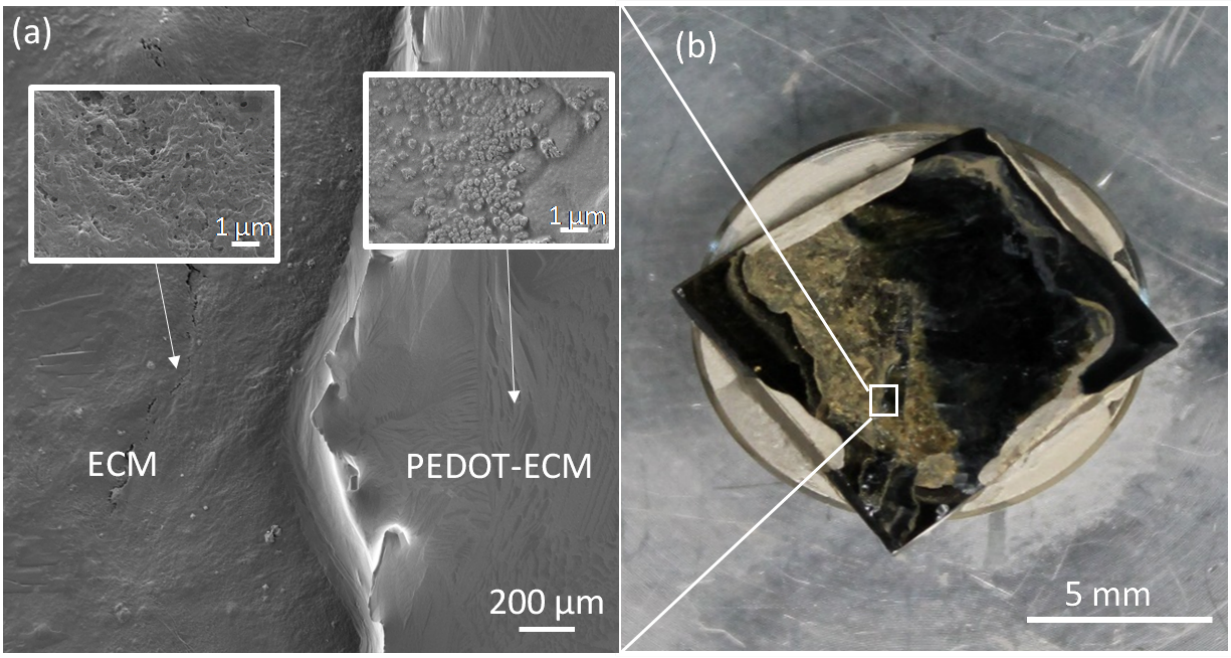

Figure 3.5 (a) SEM images of the interface between ECM and PEDOT-ECM with detail morphology correlated with (b) optical image of the sample.

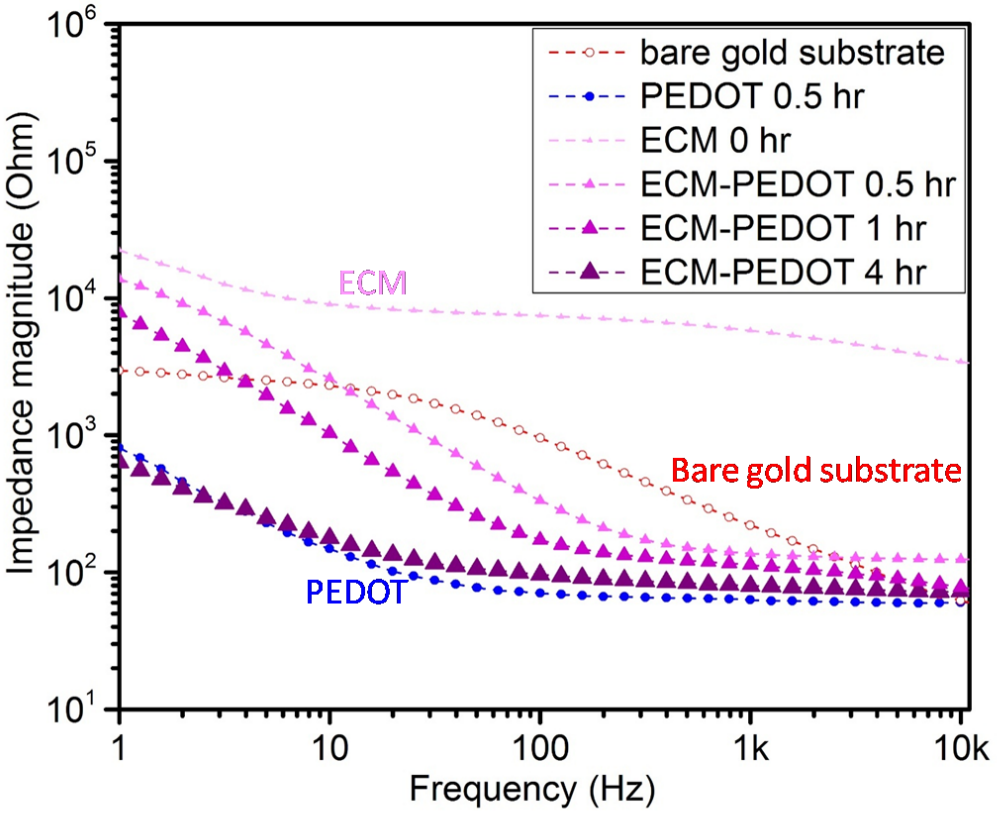

Figure 3.6 Impedance spectra for bare gold electrodes (red dash), PEDOT coated electrodes (blue), PEDOT-ECM coated electrodes (pink to red with respect to different deposition time) vs AC frequency.

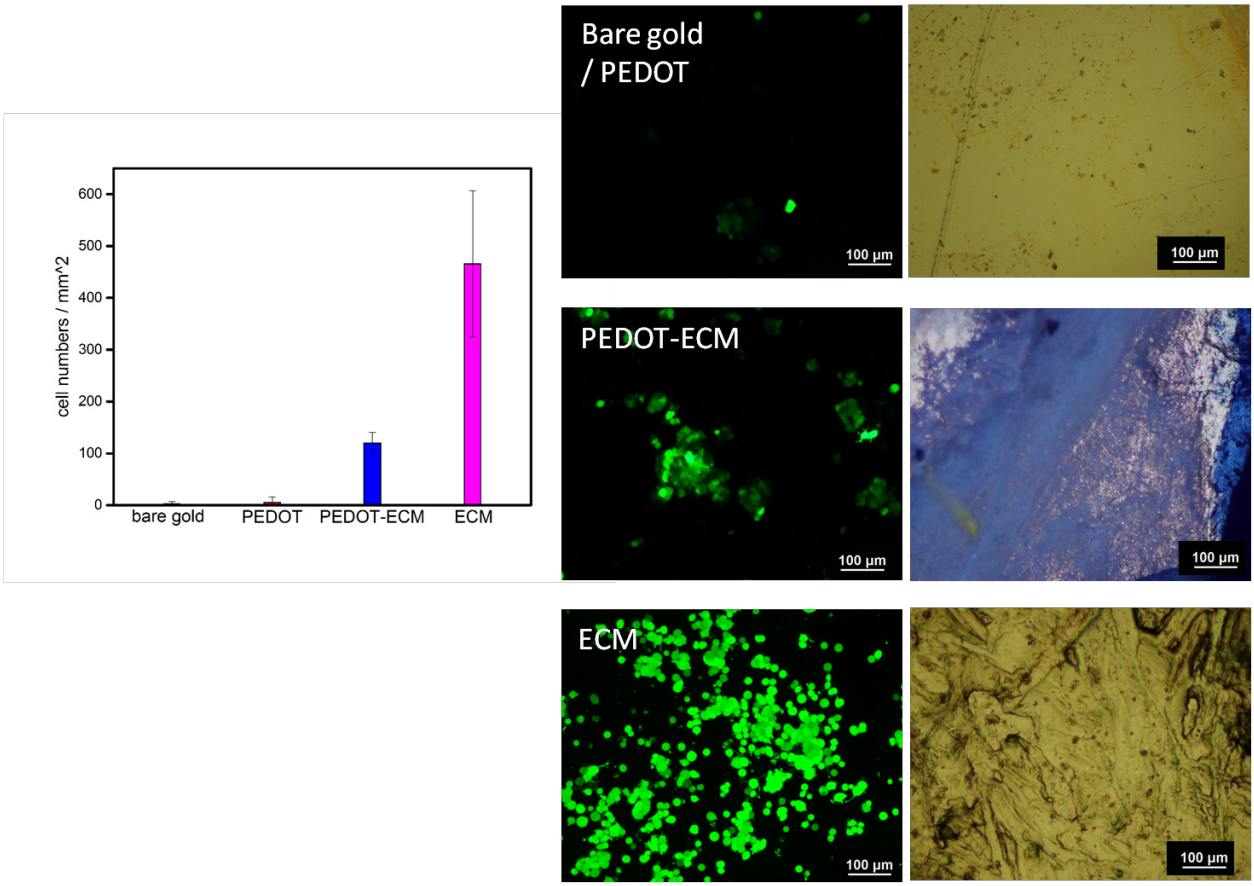

Figure 3.7 Differentiated PC12 attachment on various substrates for 4 days

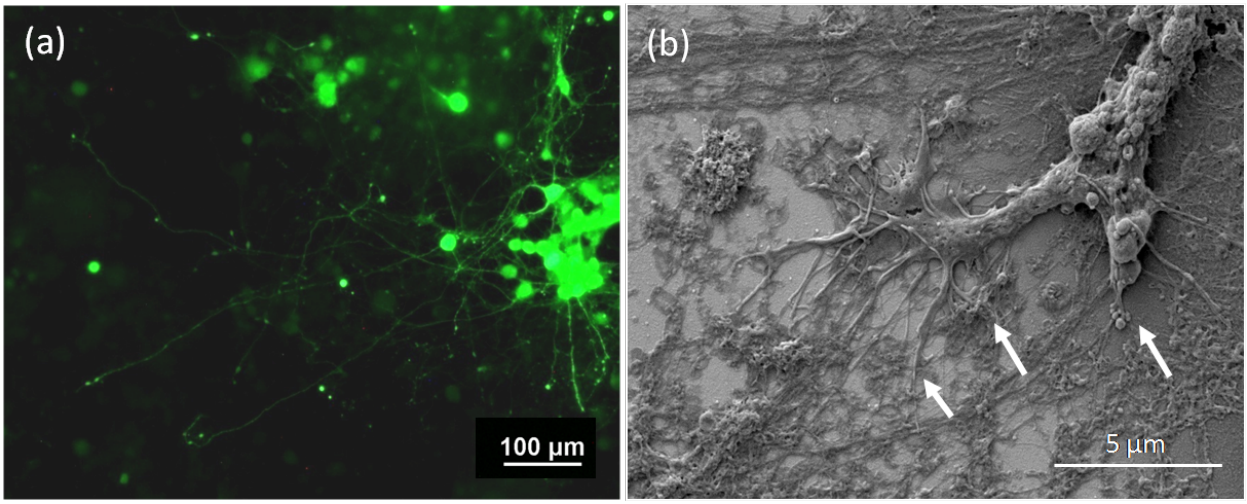

Figure 3.8 The differentiation of PC12s on PEDOT-ECM modified electrodes. PC12s were differentiated for 7 days in NGF added medium. (a) Fluorescence image of differentiated PC12 cells on PEDOT-ECM substrate. The long neuritis confirms the high degree of differentiation. (b) SEM images of the detailed neurites of cells interacting with PEDOT-ECM coating. The arrows indicate axons attached to the PEDOT-ECM coated surface, not on the bare electrode.

REFERENCES

Abidian, M. R., & Martin, D. C. (2009). Multifunctional nanobiomaterials for neural interfaces. *Advanced Functional Materials*, *19*(4), 573–585. http://doi.org/10.1002/adfm.200801473

Anderson, J. M., Rodriguez, A., & Chang, D. T. (2008). Foreign body reaction to biomaterials. *Seminars in Immunology*, *20*(2), 86–100. http://doi.org/10.1016/j.smim.2007.11.004

Badylak, S. F. (2002). The extracellular matrix as a scaffold for tissue reconstruction. *Seminars in Cell & Developmental Biology*, *13*(5), 377–383. http://doi.org/10.1016/S1084

Bhadra, S., Khastgir, D., Singha, N. K., & Lee, J. H. (2009). Progress in preparation, processing and applications of polyaniline. *Progress in Polymer Science*, *34*(8), 783–810. http://doi.org/10.1016/j.progpolymsci.2009.04.003

Biran, R., David C. Martin, & Tresco, P. A. (2007). The brain tissue response to implanted silicon microelectrode arrays is increased when the device is tethered to the skull. *Clinical and Experimental Rheumatology*, *82A*(1), 169–178. http://doi.org/10.1002/jbm.a

Chikar, J. a, Hendricks, J. L., Richardson-Burns, S. M., Raphael, Y., Pfingst, B. E., & Martin, D. C. (2012). The use of a dual PEDOT and RGD-functionalized alginate hydrogel coating to provide sustained drug delivery and improved cochlear implant function. *Biomaterials*, *33*(7), 1982–90. http://doi.org/10.1016/j.biomaterials.2011.11.052

Collier, J. H., Camp, J. P., Hudson, T. W., & Schmidt, C. E. (2000). Synthesis and

characterization of polypyrrole-hyaluronic acid composite biomaterials for tissue engineering applications. *Journal of Biomedical Materials Research*, *50*(4), 574–584. http://doi.org/10.1002/(SICI)1097-4636(20000615)50:4<574::AID-JBM13>3.0.CO;2-I

Crispin, X., & Marciniak, S. (2003). Conductivity, morphology, interfacial chemistry, and stability of poly (3, 4-ethylene dioxythiophene)–poly (styrene sulfonate): A photoelectron spectroscopy study. *Journal of Polymer …*, *41*(21), 2561–2583. http://doi.org/10.1002/polb.10659

Cui, X., Lee, V. a., Raphael, Y., Wiler, J. a., Hetke, J. F., Anderson, D. J., & Martin, D. C. (2001). Surface modification of neural recording electrodes with conducting polymer/biomolecule blends. *Journal of Biomedical Materials Research*, *56*, 261–272. http://doi.org/10.1002/1097-4636(200108)56:2<261::AID-JBM1094>3.0.CO;2-I

Cui, X., Wiler, J., Dzaman, M., Altschuler, R. a, & Martin, D. C. (2003). In vivo studies of polypyrrole/peptide coated neural probes. *Biomaterials*, *24*(5), 777–87. Retrieved from http://www.ncbi.nlm.nih.gov/pubmed/12485796

De Groot, C. J., Van Luyn, M. J. A., Van Dijk-Wolthuis, W. N. E., Cad??e, J. A., Plantinga, J. A., Otter, W. Den, & Hennink, W. E. (2001). In vitro biocompatibility of biodegradable dextran-based hydrogels tested with human fibroblasts. *Biomaterials*, *22*(11), 1197–1203. http://doi.org/10.1016/S0142-9612(00)00266-0

Farwell, D. G., Giachelli, C. M., Ph, D., & Ratner, B. D. (2006). Matrix Tissue Scaffold. *Tissue Engineering*, *12*(2).

Forrest, S. R. (2004). electronic appliances on plastic, 911–918.

Freed, L. E., Vunjak-Novakovic, G., Biron, R. J., Eagles, D. B., Lesnoy, D. C., Barlow, S. K., & Langer, R. (1994). Biodegradable Polymer Scaffolds for Tissue Engineering. *Nature Biotechnology*, *12*(7), 689–693. http://doi.org/10.1038/nbt0794-689

Gerard, M., Chaubey, A., & Malhotra, B. D. (2002). Application of conducting polymers to biosensors. *Biosensors and Bioelectronics*, *17*, 345–359. http://doi.org/10.1016/S0956-5663(01)00312-8

Gilmour, A. D., Woolley, A. J., Poole-Warren, L. A., Thomson, C. E., & Green, R. A. (2016). A critical review of cell culture strategies for modelling intracortical brain implant material reactions. *Biomaterials*, *91*, 23–43. http://doi.org/10.1016/j.biomaterials.2016.03.011

Green, R. a, Hassarati, R. T., Goding, J. a, Baek, S., Lovell, N. H., Martens, P. J., & Poole-Warren, L. a. (2012). Conductive hydrogels: mechanically robust hybrids for use as biomaterials. *Macromolecular Bioscience*, *12*(4), 494–501. http://doi.org/10.1002/mabi.201100490

Green, R. A., Lim, K. S., Henderson, W. C., Hassarati, R. T., Martens, P. J., Lovell, N. H., & Poole-Warren, L. A. (2013). Living electrodes: tissue engineering the neural interface. *Conference Proceedings : ... Annual International Conference of the IEEE Engineering in Medicine and Biology Society. IEEE Engineering in Medicine and Biology Society. Annual Conference*, *2013*, 6957–6960. http://doi.org/10.1109/EMBC.2013.6611158

Green, R. A., Lovell, N. H., Wallace, G. G., & Poole-Warren, L. A. (2008). Conducting polymers for neural interfaces: Challenges in developing an effective long-term implant. *Biomaterials*, *29*(24-25), 3393–3399. http://doi.org/10.1016/j.biomaterials.2008.04.047

Huynh, W. U. (2002). Hybrid Nanorod-Polymer Solar Cells. *Science*, *295*(5564), 2425–2427. http://doi.org/10.1126/science.1069156

Karumbaiah, L., Saxena, T., Carlson, D., Patil, K., Patkar, R., Gaupp, E. A., … Bellamkonda, R. V. (2013). Relationship between intracortical electrode design and chronic recording function. *Biomaterials*, *34*(33), 8061–8074. http://doi.org/10.1016/j.biomaterials.2013.07.016

Kim, D.-H., Wiler, J. a, Anderson, D. J., Kipke, D. R., & Martin, D. C. (2010). Conducting polymers on hydrogel-coated neural electrode provide sensitive

neural recordings in auditory cortex. *Acta Biomaterialia*, *6*(1), 57–62. http://doi.org/10.1016/j.actbio.2009.07.034

Kim, W. H., Mäkinen, A. J., Nikolov, N., Shashidhar, R., Kim, H., & Kafafi, Z. H. (2002). Molecular organic light-emitting diodes using highly conducting polymers as anodes. *Applied Physics Letters*, *80*(20), 3844–3846. http://doi.org/10.1063/1.1480100

Liu, X., Yue, Z., Higgins, M. J., & Wallace, G. G. (2011). Conducting polymers with immobilised fibrillar collagen for enhanced neural interfacing. *Biomaterials*, *32*(30), 7309–17. http://doi.org/10.1016/j.biomaterials.2011.06.047

Lu, H., Hoshiba, T., Kawazoe, N., & Chen, G. (2011). Autologous extracellular matrix scaffolds for tissue engineering. *Biomaterials*, *32*(10), 2489–99. http://doi.org/10.1016/j.biomaterials.2010.12.016

Martin, D. C., Wu, J., Shaw, C. M., King, Z., Spanninga, S. a., Richardson-Burns, S., … Yang, J. (2010). The Morphology of Poly(3,4-Ethylenedioxythiophene). *Polymer Reviews*, *50*(3), 340–384. http://doi.org/10.1080/15583724.2010.495440

Parenteau-Bareil, R., Gauvin, R., & Berthod, F. (2010). Collagen-based biomaterials for tissue engineering applications. *Materials*, *3*(3), 1863–1887. http://doi.org/10.3390/ma3031863

Richardson-Burns, S. M., Hendricks, J. L., Foster, B., Povlich, L. K., Kim, D. H., & Martin, D. C. (2007). Polymerization of the conducting polymer poly(3,4-ethylenedioxythiophene) (PEDOT) around living neural cells. *Biomaterials*, *28*(8), 1539–1552. http://doi.org/10.1016/j.biomaterials.2006.11.026

Subbaroyan, J., Martin, D. C., & Kipke, D. R. (2005). A finite-element model of the mechanical effects of implantable microelectrodes in the cerebral cortex. *Journal of Neural Engineering*, *2*(4), 103–13. http://doi.org/10.1088/1741-2560/2/4/006

Woolley, A. J., Desai, H. A., & Otto, K. J. (2013). Chronic intracortical microelectrode arrays induce non-uniform, depth-related tissue responses. *Journal of Neural Engineering*, *10*(2), 026007. http://doi.org/10.1088/1741-2560/10/2/026007

Xiao, Y., Li, C. M., Wang, S., Shi, J., & Ooi, C. P. (2010a). Incorporation of collagen in poly(3,4-ethylenedioxythiophene) for a bifunctional film with high bio- and electrochemical activity. *Journal of Biomedical Materials Research. Part A*, *92*(2), 766–72. http://doi.org/10.1002/jbm.a.32412

Xiao, Y., Li, C. M., Wang, S., Shi, J., & Ooi, C. P. (2010b). Incorporation of collagen in poly(3,4-ethylenedioxythiophene) for a bifunctional film with high bio- and electrochemical activity. *Journal of Biomedical Materials Research. Part A*, *92*(2), 766–72. http://doi.org/10.1002/jbm.a.32412

Yang, J., & Martin, D. C. (2004). Microporous conducting polymers on neural microelectrode arrays: I electrochemical deposition. *Sensors and Actuators, B: Chemical*, *101*(1-2), 133–142. http://doi.org/10.1016/j.snb.2004.02.056

Chapter 4

IN SITU POLYMERIZATION OF PEDOT IN LOW MODULUS HYDROGELS FOR NEURAL INTERFACES

4.1 Introduction

Conducting polymers have attracted considerable interest as a promising materials to replace traditional metals or semiconductors in a variety of applications such as organic light emitting diodes (OLED) (Kim et al., 2002), solar cells (Huynh, 2002), transistors and biosensors (Kim et al., 2010)(Gerard et al., 2002) (Forrest, 2004). Conducting polymers have shown particular potential for directly interfacing bionic devices with living neural tissue (Cui et al., 2003)(Cui, Lee, et al., 2001)(Richardson-Burns et al., 2007a)(Green et al., 2008) due to their excellent electronic and ionic conductivities and relatively low mechanical stiffness.

For neural interface applications, implantation typically involves inserting a hard, electronic conductive, metallic or semiconductive electrode into soft, living, ionically conductive tissues. In chronic applications, such implants are often associated with a glial scar encapsulation that leads to the loss of device function (Woolley et al., 2013). After device implantation, reactive microglia were found near the implantation site. Reactive microglia have M-1 and M-2 states. The M-1 state is known to secrete neurotoxic agents that may lead to neuronal death. On the other hand, astrocytes synthesize glial fibrillary acidic protein (GFAP) that accelerates their

proliferation and accumulation near the implantation site. The activated astrocytes replace the neurons and secrete bioactivate agents that inhibit further neuron growth, thus leading to scar formation. Previous work has shown that GFAP+ astrocytes accumulated about ~150 um near the electrode site after 2 weeks of implantation and kept growing over the next 8 weeks (Biran et al., 2005; Winslow et al., 2010). These processes form a glial sheath around the implanted electrode that blocks signal transmission between the device and tissue. It was hypothesized that the scar encapsulation is related to the large mechanical strains that inevitably arise near the interface of rigid device and soft tissue (Subbaroyan et al., 2005) (Karumbaiah et al., 2013)(Nguyen et al., 2014). The persistent, locally heterogeneous strain creates to a hostile environment for neural survival, therefore decreasing the neuron density near the implants. Lowering the mechanical mismatch between devices and tissues remains an ongoing challenge.

In chapter 3 of this thesis, we have shown that we are able to *in situ* polymerize PEDOT into an ECM template to lower the mechanical mismatch between devices and neighboring tissues. Figure 4.1 shows the DMT modulus of PEDOT-ECM film measured by AFM-QNM (Dokukin & Sokolov, 2012). In this figure, the modulus ranged from 900 MPa to several MPa showing a significant decrease in modulus compared with intrinsic PEDOT (which is typically about 1-5 GPa) (Hassarati et al., 2014)(Lang et al., 2009)(Qu et al., 2016). However, the typical modulus of cortex is about 400 Pa for 20-40 weeks old rats and about 1000 Pa for adult rats (Elkin, Ilankovan, & Morrison, 2010), so there is still a significant difference between PEDOT-ECM and cortex. In this chapter we examined the idea of utilizing an extremely soft hydrogel with PEDOT to further reduce the mechanical modulus.

Hydrogels have long been studied as tissue engineering scaffolds (Peppas et al., 2006)(Drury & Mooney, 2003). For the biomedical applications, hydrogel coatings should function as a mechanical buffer between the stiff electrodes and soft tissues. With proper stimulation, hydrogel can locally release bioactive agents such as anti-inflammatory drugs (Yi Luo, Kirker, & Prestwich, 2000) and growth factors (Tabata, Hijikata, & Ikada, 1994). The moduli of hydrogels can be tailored from 1 kPa to 100 kPa by controlling the crosslinking strength (Clark, Gidley, Richardson, & Ross-Murphy, 1989). We expect that soft hydrogels could better mitigate chronic foreign body response after implantation. *In vivo* study also showed that using Zwitterionic hydrogels could resist the scar encapsulation formation for at least 3 months (Zhang et al., 2013). These results support the idea of using hydrogel to mitigate chronic body reaction. However, hydrogels are not electrically-active materials making them not suitable for neural interfaces.

For neural interface applications, the materials must facilitate charge transport by both electronic and ionic conduction. Previous reports have demonstrated a variety of methods for creating conductive polymer hydrogels. Researchers have chemically developed intrinsically conducting hydrogels through chemical synthesis by utilizing conducting moieties on hydrogel monomers or by using suitable precursors (Pan et al., 2012) (Mawad et al., 2012). These chemically synthesized conductive hydrogels showed significantly lower conductivities than traditional CP films. Pan et al reported a conductivity of 0.11 S/cm from their hydrogels, which is 4 folders lower than PEDOT/PSS (>200 S/cm). In addition, the chemical synthesis involved several toxic chemicals which would likely present risks to potential hosts.

Other reports demonstrated physical methods, such as the mixing conducting polymer suspensions during crosslinking to create a conducting polymer blend in the gel (Press et al., 1999). This CP suspension is only electrostatically attached to the hydrogel backbone. The integration between the CP suspension and hydrogel matrix is likely too weak to maintain a reliable CP/hydrogel blend in such materials. Besides that, the results showed the conductivity of this CP/hydrogel blend was still much lower than intrinsic PEDOT (Åsberg & Inganäs, 2003). The decreased conductivity limits the use as a material for neural interfacing.

Another method is to combine both the chemical and physical approaches. The oxidant can be into the hydrogel solution with the monomer in order to polymerize the CP simultaneously with hydrogel crosslinking. These conducting polymer hydrogels presented high conductivity and could be uniformly deposited (Ismail et al., 2011). However, chemical deposition of the CP onto the hydrogel backbone caused the hydrogel to become more brittle and fragile. Dai at al. therefore developed a double layer hydrogel network to improve durability (Dai et al., 2010)(Dai et al., 2009). Although the conductive hydrogels made by this method provided good conductivities, the process required strong oxidizing agents for polymerization. These oxidants will also function as a dopants for the CP polymerized into the hydrogel. The oxidant is also able to diffuse out of the sample over time. Normal rinsing to the gel is not sufficient to totally remove the biologically hazardous oxidant. The residual chemicals could cause damage to tissues of hosts. Hence, these chemical depositions methods are not particularly suitable for biological applications.

Green et al. developed a hybrid of CP polymerized on an anionic hydrogel to make better integrated and more robust CP/hydrogel (Green et al., 2012a). However,

these conductive hydrogels presented relatively high moduli (in the range of 1000 MPa) which is about 2x larger than cortex tissues. The function of using hydrogel to lower the mechanical mismatch during implantation was limited due to its large modulus. Soichiro et al. have demonstrated electrochemically polymerized CP on hydrogels. However, from their results, most of the CP was concentrated near the electrode surface (~10 μm) (Sekine et al., 2010) (Ido et al., 2012). This CP/hydrogel thickness is far less than the known scar encapsulation characteristic thickness which makes it difficult for the CP/hydrogel to obtain signals when scar formation occurs (~150 μm).

Previously, our lab developed a CP-hydrogel with high conductivity by an electrochemical method (Kim et al., 2004). It was found that under the deposition of 506 mC/cm^2, the impedance was even lower (10^4 Ω at 1 kHz) than that of thin film CP deposition (10^5 Ω for PPy thin film) (Kim et al., 2004). Abidian et al. also used similar methods to fabricate conducting polymer-hydrogel conduits for axonal growth to provide an encapsulated environment for peripheral nerve regeneration (Abidian et al., 2012). This method was relatively easy to fabricate and avoided several chemical synthesis steps, hence improving the biocompatibility of this material.

In this study, we reproduced this method on an extremely low modulus agarose hydrogel (~2 kPa) to create a both electronic and ionic conductive hydrogel by the *in situ* polymerization of PEDOT. We found that PEDOT could polymerize into the hydrogel matrix as far as 350 μm in diameter. With this large size of the PEDOT-gel, the signal communication can easily go beyond the typical scar characteristic thickness (~150 μm), hence allowing the material to obtain an electrical signal even after scar encapsulation occurs. Additionally, agarose gels have been reported to

enhance cell adhesion, proliferation, as well as neural outgrowth (Ying Luo & Shoichet, 2004). A detailed study of the morphology, electrical properties, mechanical properties, and swelling properties of PEDOT-agarose gels are investigated in this chapter. This PEDOT-hydrogel construct exhibited a very low modulus which is expected to significantly reduce the chronic body reaction to the implanted material, as well as to provide electrical conductivity for effective neural interfaces between electronic biomedical devices and living tissue.

We examined the performance of the PEDOT-gel coated electrode *in vivo*. An animal study was employed and we used rats as the animal model. The experiment was designed to confirm the performance of the PEDOT-gel when implanted into the rat hippocampus. The *in vivo* impedance was measured every other day until 10 weeks.

4.2 Materials and Methods

4.2.1 Fabrication EDOT-gel Coated Electrodes

An EDOT monomer solution was prepared by dispersing 0.01 M EDOT monomer and 0.1 wt% polystyrene sulfonate (PSS) in DI water. Agarose powder (A9539, Sigma) was dissolved into the EDOT monomer solution at 70°C. After the solution became transparent, the temperature was maintained at 50°C to keep the agarose in the liquid state. The electrodes (Plastics One) were stored in 70% ethanol solution for pre-sterilization. A dip-coating method was used to coat EDOT-gel onto the tip of the electrodes. The room temperature electrodes were dipped in and pulled out from the warm EDOT-gel solution. As the temperature near the electrode rapidly drops, a gel forms allowing a thin coating of EDOT-gel to deposit on the electrode.

The final thickness of the coating could be readily controlled by the total number of dips and the speed of withdrawal of the electrode from the solution. The coated electrodes were examined with a stereo microscope (Nikon, SMZ800) to confirm the size and the integrity of the EDOT-gel coating during deposition.

4.2.2 *In Situ* Polymerization of PEDOT in Hydrogels

The EDOT-gel coated electrode was stored in EDOT monomer solution overnight to prevent dehydration as well as provide sufficient time for EDOT and PSS to diffuse into the coating. The same EDOT monomer solution was prepared for electrochemical deposition. The coated electrode was used as the working electrode while a large platinum/iridium foil was placed next to it as the counter electrode. A potentiostat (ModuLab, Solartron Analytical) was used to generate electrical potential in order to oxidize EDOT monomer in the system. The deposition proceeded at 2 V for up to 4 hours leading to a significant dark blue cloud forming around the tip of the electrode. The thickness of *in situ* PEDOT deposition could be directly observed by optical microscopy due to its significant dark color. Figure 4.2 (a-d) shows a schematic of *in situ* PEDOT polymerization into hydrogel and the implantation process. For the implantation, a dehydration process was required. The measured modulus of PEDOT-gel is lower than typical cortex tissue, which may lead to a PEDOT-gel damage during implantation. The dehydrated PEDOT-gel presents a larger modulus, preventing damage to the PEDOT-gel during implantation. After implantation, the body fluid from the tissues would re-swell and soften the PEDOT-gel.

4.2.3 PEDOT-gel Characterizations: Electrical Properties

Electrochemical characterizations including cyclic voltammetry (CV) and electrochemical impedance spectroscopy (EIS) were conducted with a Solartron using a three-electrode cell. For EIS, the samples themselves were used as the working electrode, an imbedded platinum/iridium foil acted as the counter electrode, and a saturated Ag/AgCl reference electrode was placed next to the working electrode. A 2 mV sinusoidal AC signal was applied to the system over frequency range from 1 to 10 kHz. Both impedance amplitude and phase angle were collected. For CV, the samples were scanned from -0.6 to 0.8 V to remain inside the water window.

4.2.4 PEDOT-gel Characterizations: Morphology

SEM images of PEDOT-gel coatings were acquired with a Zeiss Auriga 60 Focused Ion Beam- Scanning Electron Microscope (FIB-SEM). In order to examine the structure of PEDOT-gel, two different sample preparation methods were employed. First, the sample was prepared with critical point drying. Samples were soaked in an intermediate solution, ethanol, at 10%, 25%, 50%, 75%, and 90% each for 1 hour respectively and then stored in 100% ethanol. Samples were critical point dried to retain their structure for SEM imaging (name, model of the critical point dryer). In the second method, a liquid SEM sample capsule (QuantomiX WETSEM) was used. This capsule isolated the wet samples from the vacuum environment of the SEM chamber. A thin film of silicon nitride kept the liquid sample isolated from the chamber, but

allowed electrons for imaging. The capsule could then be loaded into SEM chamber for imaging.

Optical microscopy was performed on a Nikon Eclipse LV100 POL microscope equipped with a Nikon Intensilight C-HGFI lamp. The images were collected with a Nikon DS-Ri1 camera.

4.2.5 PEDOT-gel Characterizations: Mechanical Properties

An oscillatory rheometer (TA instrument ARG2) was used to confirm the modulus of the wet PEDOT-gel. A fully PEDOT polymerized hydrogel was scooped out form a bulk hydrogel for test.

The modulus of the dried hydrogel must be larger than the cortex in order to ensure successful implantation. A fully PEDOT polymerized gel was dehydrated in room temperature same as the procedure to prepare implanted electrode. Atomic Force Microscopy PeakForce Quantitative Nanoscale Mechanical Characterizations (AFM-QNM) was used to confirm the Derjagin, Muller, Toropov modulus (DMT modulus) of the dehydrated PEDOT-gel. The modulus was obtained with Nanoscope Dimension 3100 software on a Bioscope Catalyst (Bruker Nano/ Veeco) AFM. All samples were measured at room temperature in the dry state. A TAP150A electrode (force constant of 5 N/m) was used to indent the sample surface at a depth of about 1-2 nm. Taking the adhesion between the tip and the surface into account, the reduced Young's modulus E_r was calculated from

$$E_r = \frac{3(F_{tip} - F_{adh})}{4\sqrt{Rd^3}}$$

where F_{tip} and F_{adh} are the , R is the tip radius, and d is the deflection.

The actual Young's modulus can be calculated from

$$\frac{1}{E_r} = \frac{(1 - v_s^2)}{E_s} + \frac{(1 - v_I^2)}{E_I}$$

where E_S is the sample modulus, E_I is the indenter modulus, and v_s and v_I are the Poisson's ratio of the sample and the indenter, respectively. In our work $E_I >> E_S$, so we can neglect the second term in this equation. The condition of each tip is not consistent from manufacturing. The precise force constant K was calibrated by using thermal tuning with each measurement. To obtain the precise electrode radius R, TiO_2 standards with well-defined curved features were employed. By analysing the images generated from imaging the TiO_2 standards, an estimate of the tip radius R could be obtained. Since the tip may wear out after scanning, the calibrations were performed before each experiment. Three scans were taken at different spots for each sample. The modulus mapping was made by indenting 512 × 512 points over a 2 μm × 2 μm image area.

4.2.6 *In Vitro* Cell Culture Tests: PC12

The PC12 cell line was used to test the cytotoxicity of PEDOT-gel. Rat pheochromocytoma cells expressing green fluorescent protein (PC-12-Turbo-GFP, Marin Pharm) were seeded onto the samples at a density of 2×10^4 per well through a 22 gauge needle to dispense the cells. The cells were cultured in growth medium (RPMI 1640 (Corning Cellgro) plus 5% fetal calf serum (FCS), 10% horse serum (HS), 2 mM L-alanyl-L-glutamine, 1% Pen-Strep and 1% non-essential amino acids (NEAA)) for 3 days before staining with a live/dead viability assay (ThermoFisher

Scientific). The viability was obtained by calculating the ratio of live/dead cell numbers in the fluorescence image. Typical fluorescence images are provided in supplementary data. For each sample, 3-5 independent measurements were performed.

4.2.7 Animal Study Design

An animal study was employed to examine the function of PEDOT-gel coated electrodes in cortex including their contribution to the electrical communication as well as the chronic body reaction in vivo by analyzing the in vivo impedance.

All procedures were carried out in accordance with the University of Delaware Institutional Animal Care and Use Committee. A guide cannula electrode (Plastics One) with a 26 gauge cannula was inserted to 2 mm below the dura targeting the dorsal hippocampus of all rodent subjects (n=9). The counter electrode was set at the other hemisphere. The experimental set up is shown in Figure 4.3

There were three types of electrodes used for this experiment that were prepared and then sterilized with ethanol overnight before the surgery. The three types are bare, PEDOT coated and PEDOT-gel coated electrode. The surgery was unilateral for the electrode implant. The electrodes were implanted into the posterior hippocampus. There were three rats in each group, implanted with bare, PEDOT coated, and PEDOT-gel coated electrode respectively. The *in vivo* impedance measurements were recorded over a frequency range from 1 Hz to 10 kHz. A positive 0.1 V bias was applied. The *in vivo* impedance was recorded from these rats immediately after surgery and then three times a week up to 10 weeks. The data was averaged from 3 individual tests for each group.

4.3 Results and Discussion

Figure 4.4 (top a to f) represents the PEDOT growth into gel matrix in 0.6% agarose gel with respect to time. This confirms that PEDOT was grown into the gel matrix instead of only on the electrode surface. The delivered charge density was respectively 0, 0.79, 0.95, 1.02 and 1.20 C/cm^2. The working electrode was a Pt/Ir wire with diameter of 1 mm with an exposed surface area of 0.039 cm^2 and the counter electrode was approximately 2 cm away from the working electrode. The potentionstatic electrochemical deposition of 2V was conducted and the corresponding current density was averagely 0.1 mA with only minor fluctuations. From Figure 4.4, a thin film of PEDOT was initially deposited on the electrode surface until the delivered charge density reached 0.79 C/cm^2. PEDOT then started to grow out into the gel matrix with observance of significant thickness change, consequently forming a PEDOT-gel cloud. A dark blue cloud of PEDOT gel was observed as the reaction continued, confirming our hypothesis that the PEDOT would be deposited as a open gel, forming a fuzzier and more open structure instead of a solid, dense film on the electrode. The thickness change with respect to charge density delivered in the system is plotted in Figure 4.4 (bottom).

Another outstanding property of PEDOT was its dark blue color after polymerization. This is a simple and reliable way to confirm the boundary of PEDOT-gel cloud. An optical microscope was used to determine the deposition of PEDOT. The imbedded plot shows the thickness of PEDOT thin film on the electrode during the early stages of polymerization. The thickness of PEDOT thin film approached 5 μm before growing into hydrogel matrix. In this region, the thickness was almost linear with respect to the charge density below 0.8 C/cm^2. The PEDOT deposited

thickness in this region was an order of a few microns (~ 1-5 μm) implying the PEDOT deposited as traditional thin film first. After delivered charge density reached to 0.8 C/cm^2, the thickness significantly increased to hundreds of microns. After 0.8 C/cm^2 the thickness significantly increased to 250 μm with only an additional 0.2 C/cm^2 of charge density delivered to the system. The thickness gradually increased to ~350 μm then plateaued at this value. There was no significant thickness change after 1.5 C/cm^2 charge density.

These results are consistent with our presumption that PEDOT was deposited onto the gel backbones. With the concentration of 0.6% hydrogel, the surface area was about 150 times larger than a flat surface. While the same amount of charge density is applied, the same amount of PEDOT will be deposited onto the larger surface area which causes observable larger thickness.

4.3.1 Mechanical Properties

The mechanical mismatch of electrodes and tissues should be addressed to mitigate foreign body response. The modulus of hydrogel and PEDOT-gel were measured using the rheometer. To evaluate the modulus of PEDOT-gel, a total charge density of 1.5 C/cm^2 was applied in the system to ensure the PEDOT in situ polymerization reaches its saturation.

The rheometry data shows that the storage modulus of agarose hydrogel increased after PEDOT polymerization into hydrogel (Fig 4.5 (a)). After polymerization, the modulus of PEDOT-gel was about 4 kPa while the modulus of rat cortex is about 10 kPa (Hassarati et al., 2014). To prevent damage to the PEDOT-gel

coating during insertion, the PEDOT-gel coating was dehydrated before implantation. After implantation, the body fluid in the tissue swelled back the PEDOT-gel back to 30-50 % of its initial thickness (Figure 4.6). The ratio is calculated by the ratio of rehydrated thickness and dehydrated thickness among pure gel and PEDOT-gel. It was observed the presence of PEDOT in gels indeed inhibited the re-swelling ratio. The modulus of dehydrated PEDOT-gel could be obtained by AFM-QNM. Figure 4.5 (b) shows the DMT modulus of PEDOT-gel and intrinsic PEDOT measured from AFM-QNM. In figure 4.5 (b), the soft rat hippocampus and stiff stainless steel are marked for reference. Our results shows that the mechanical modulus of dehydrated PEDOT-gel is larger than rat hippocampus suggesting that the dehydrated PEDOT-gel can be inserted to the hippocampus without mechanical damage.

4.3.2 Morphologies of PEDOT-gel

In order to confirm the PEDOT-gel re-swelling condition, the morphology of gel structure was examined using SEM. However, to image in situ wet gel morphology is not trivial since SEM requires a high vacuum environment, so the imaging of wet samples imaging is difficult. In this study, we used two methods to examine the morphology of PEDOT gel; a critical point drying method and a WET SEM holder. Once the sample is critically point dried, it is ready to be observed under normal SEM.

One method is using WET SEM holder to image wet PEDOT-gel. The hydrated PEDOT-gel with water was put into the WET SEM holder with a screw cap. The cap was covered by a Si_3N_4 thin film that can block water and air while allowing electrons penetration. The holder was sealed with rubber to ensure an airtight condition. The holder was transferred to the SEM chamber for imaging. This

technique allows us to image the real wet sample. However, one drawback of this holder is its relatively low resolution as compared with tradition SEM images. It requires high accelerating voltage for the electrons to backscatter through the thin film to the detector. The amount of electrons that could be detected by the detector was limited. However, it was a reliable method to understand the swelling condition of our sample before and after the process of rehydration.

Figure 4.7 (a) and (b) shows SEM images of hydrated PEDOT-gel and re-hydrated PEDOT-gel. A fully polymerized PEDOT-gel was cut into small pieces and put in the WET SEM holder for imaging. After the dehydrated PEDOT-gel was imaged, the holder was uncapped leaving the sample air dry overnight. Then the holder was filled again with DI water to re-hydrate the PEDOT-gel. The same sample was imaged again after re-hydration process. From figure 4.7, we can observe that after dehydration-rehydration process the thickness of PEDOT-coated gel fibers was larger than ones before dehydration.

The air-dry dehydration collapses the gel structure. With following rehydration, the structure was not completely swollen back to its original structure. This is an important finding since the direct, local integration of PEDOT-gel and tissue is critical for signal recording. With better integration, the electrical signal can transmit more efficient and with better signal-to-noise ratio. While the rehydration process changes the gel structure of the PEDOT-gel, it still exhibits a crosslinked, open structure that should potentially provide good communication between the device and surrounding tissues.

The Critical point drying method required many steps of sample preparations but gave much better image quality since the sample could be observed without any

water. The PEDOT-gel was transferred from water to ethanol. Then liquid carbon dioxide was gradually infused to the chamber of critical point dryer at its critical point. The dryer maintained the temperature and pressure critical point allowing liquid carbon dioxide gradually replace ethanol in the system. The slow process makes it possible to retain the morphology of the PEDOT-gel. Figure 4.8 shows the SEM images of PEDOT-gel and agarose gel prepared by critical point drying. More detailed information of the PEDOT-gel morphology was obtained by this method. Fig 4.8 (a) shows the morphology of pure agarose gel. The diameter of gel fibers are about 10-20 nm. No rough surfaces were observed implying the absence of PEDOT. Fig 4.8 (b) shows the interface of PEDOT and PEDOT-gel. As we mentioned earlier, the PEDOT was deposited on the electrode surface as an intrinsic PEDOT film, then at certain condition, PEDOT started to deposit on gel backbones forming a PEDOT-gel matrix. From this image, we saw that the PEDOT clusters were deposited on the gel fibers giving them a rough surface (Fig 4.8 (b)).

4.3.3 Electrical Properties

Electrical properties of intrinsic PEDOT thin film and PEDOT-gels were characterized using EIS and CV. The typical frequency range of electrophysiological signals from neurons is at 0.1-1 kHz. With lower impedances, electrodes can provide better signal-to-noise ratios. Impedance is a characteristic value to evaluate the performance of electrodes both in vitro and in vivo. Electrode impedance is associated with the effective surface area between electrode and electrolyte. With larger surface area, the impedance of electrodes decreases. Fig 4.9 (a) shows the impedance magnitude of PEDOT-gel coated electrode, intrinsic coated electrode, and bare

electrodes over a frequency range of 1-10 kHz. Consistent with previous reports, coating the metal electrodes with intrinsic PEDOT drops the electrode impedance by about 1-2 orders of magnitude. This is due to the increase of effective surface area brought about by fuzzy and nano-porous morphology of PEDOT. Compared with intrinsic PEDOT, the impedance of the PEDOT-gel shows even lower impedances over the entire frequency range. Referring back to Fig 4.9 (b), the agarose gel matrix provided a more open template for PEDOT deposition. With the same amount of charge delivered to the system, the same amount of PEDOT was deposited on the substrate. The agarose gel template made it possible for more of the deposited PEDOT to be involved in charge transport than the PEDOT on the stainless surface. The effective surface between the electrode and electrolyte of PEDOT-gel was therefore significantly increased, leading to a lower impedance magnitude than intrinsic PEDOT alone.

Fig 4.9 (b) plots the phase angle with respect to frequency. In the high frequency range of higher than 1 kHz, the phase angles of each sample are consistently low, corresponding to a predominantly resistive response. The bare electrode exhibits a phase angle of about 75° at a frequency of 50 Hz or lower showing that the electrode was more capacitive. Coating with PEDOT brought down the phase angle to about 15° between 10-1 kHz and then raises to 40° at the frequency lower than 10°. It was more resistive than bare electrode. As for the coating of PEDOT-gel on the electrode, the phase angle was steady at 10-15° over the whole frequency range. This suggests that the PEDOT-gel coated electrode functioned primarily as a resistor. The results show that PEDOT-gel coated electrodes have lower impedances than either or the bare

metal or PEDOT-coated electrodes, suggesting that they will be more suitable materials for neural interfacing.

CV was used to analyze the charge transfer capacity of the intrinsic PEDOT and PEDOT-gel coated electrode. The charge capacity (the area under CV curves) increased dramatically after PEDOT deposition as compared with bare electrode, in a manner consistent with previous reports (Wilks, Richardson-Burns, et al., 2009) (Fig 4.9 (c)). From Fig 4.9 (c), the charge capacity of PEDOT-gel coating on the electrode was larger than intrinsic PEDOT. These results confirm that there is more charge transport possible with the PEDOT-gel matrix than with intrinsic PEDOT. Both EIS and CV support the assertion that PEDOT-gels are more promising candidates for neural interfaces than either bare metal electrodes or PEDOT-coatings alone.

4.3.4 *In Vivo* Study

Before the animal study, a pilot study of in vitro cell cytotoxicity test was performed to ensure the biocompatibility of PEDOT-gel. Figure 4.10 shows the live/dead cells ration on metal substrate, PEDOT coated substrate, and PEDOT-gel coated substrate. All of them present great biocompatibility with viability over 90% after 7 days culture. Figure 4.11 (top) shows the in vivo impedance of PEDOT-gel electrodes at week 1, 2, 4, and 9. Unlike the impedance of PEDOT-gel coated electrode measured in the PBS electrolyte, it shows some fluctuations during the measurement. It was hypothesized that those peaks or fluctuations may be associated with rats moving in the cage. For this reason, we typically regard these fluctuations as noise. In order to extract and analyze the data, a polynomial fitting line (red line) was

employed for each measurement to smooth the fluctuations. After fitting, the impedance magnitudes at 1 kHz and at 200 Hz were extracted and analyzed. The results are shown in Figure 4.11 (bottom) for the bare electrode, the PEDOT coated electrode, and the PEDOT-gel coated electrode. The impedance magnitude at 1 kHz was typically used to analyze single neuron activity since it is corresponds to the typical neural signal firing frequency. For neural interface applications, 1 kHz is the most representative frequency to evaluate the performance of biomedical devices. In addition, the impedance magnitude at 200 Hz was also examined here.

From Figure 4.11 (bottom), it is obvious that the impedance magnitude trends over the weeks of implantation are similar at both low and high frequencies. For the 1 kHz frequency, the impedance of bare electrode was the largest among the three groups for the first week. This is consistent with the EIS results shown in the earlier section. PEDOT and PEDOT-gel brought down the impedance therefore the impedance without PEDOT was less conductive than others. After the 2nd week, microglia and activated astrocytes aggregate at the interface leading to a impedance increase. Interestingly, the impedance magnitudes at 2nd week were extremely consistent among these three groups at both low frequencies (~1.5 MΩ) and high frequencies (0.5 MΩ). According to previous reports, it was suggested that scar encapsulations are formed in 2-4 weeks with bare metallic electrodes (Biran et al., 2005) (Nguyen et al., 2014). This is where the impedance goes to a maximum, presumably due to a layer of insulated glial scar blocking the conductive pathways. At this time point, both the impedance magnitude of the bare electrodes and PEDOT coated electrodes increased, but PEDOT-gel coated electrodes remained almost the same. This suggests that no significant scar encapsulation was formed at the interface

between PEDOT-gel electrode and tissues. In order to examine the long-term function of each electrode, we also analyzed the data at 9^{th} weeks after implantation. The impedance of the bare electrodes still retained their high impedance values, suggetings that the glial scars were still blocking signal transmission. Surprisingly, while the impedance of PEDOT-gel still remained at the same value (slightly lower than week 4), the impedance of PEDOT electrode bounced back to even lower values than the PEDOT-gel. The reason why the impedance of PEDOT electrodes decreased after 9 weeks implantation is still not known. Our hypothesis is that during the long term implantation, the PEDOT film on the electrodes may have suffered from the extensive movement causing some part of PEDOT to be delaminated from the electrode surface. The bare electrode surface or the inner layer of PEDOT film was then exposed to the system which hence provide better conductive pathways than the insulated glial scars. This hypothesis could be confirmed with another *in vivo* study with longer implantation time (perhaps up to 20 weeks). However, it is worth mentioning that even the impedance of PEDOT and PEDOT-gel coated electrode located at similar range after 9 weeks implantation, the mechanism behind these phenomena is quite different. The constant low impedance magnitude of PEDOT-gel suggests a delay of foreign body response after implantation, while the high impedance of PEDOT occurring at week 4 implies some glial scar encapsulations, as seen in the bare electrode.

4.4 Conclusions

This study demonstrated methods for creating soft, ionically and electronically conductive materials by *in situ* polymerizing PEDOT into hydrogels. The improved mechanical and electrical properties suggest that PEDOT-gels are more suitable materials for neural interface. The detailed morphology of the PEDOT-gel was examined by SEM, confirming the increased effective surface area that facilitates more efficient charge transport. Animal studies were employed to evaluate the performance of the PEDOT-gel coated electrode. The constant relatively lower impedance of the PEDOT-gel coated electrodes is consistent with a reduction of the foreign body response in vivo. These electrochemically polymerized PEDOT-gels have potential applications in neural recording, neural stimulation, neural regeneration, and controlled drug delivery.

FIGURES

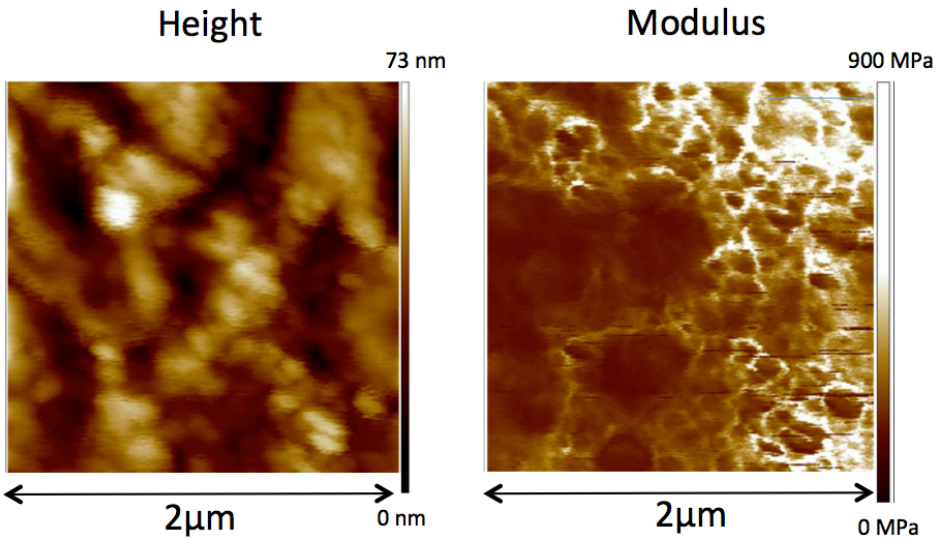

Figure 4.1 AFM QNM™ height and modulus distribution of dehydrated PEDOT-ECM. Scan size is 2 µm by 2 µm. The maximum of the DMT modulus of PEDOT-ECM is about 900 MPa which is significantly larger than cortex tissue.

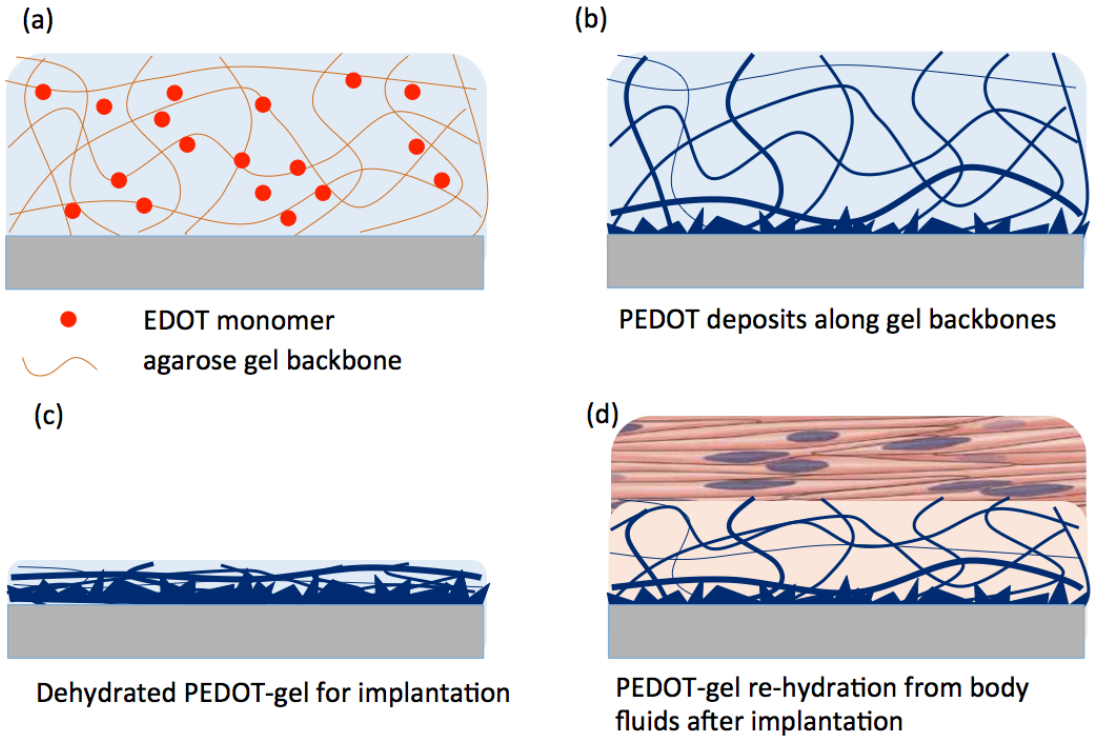

Figure 4.2 The schematic of in situ PEDOT polymerization into hydrogel. (a) premix EDOT monomer with with agarose gel to form a EDOT-agarose gel. (b) apply potential to the system to oxidize EDOT to PEDOT, deposited on substrate in the beginning and then on the gel fibers. (c) dehydrate PEDOT-ECM using air dry method to collapse the PEDOT-gel structure, raising the modulus to allow safe implantation. (d) After implantation, reswell the PEDOT-gels with body fluid from the tissue.

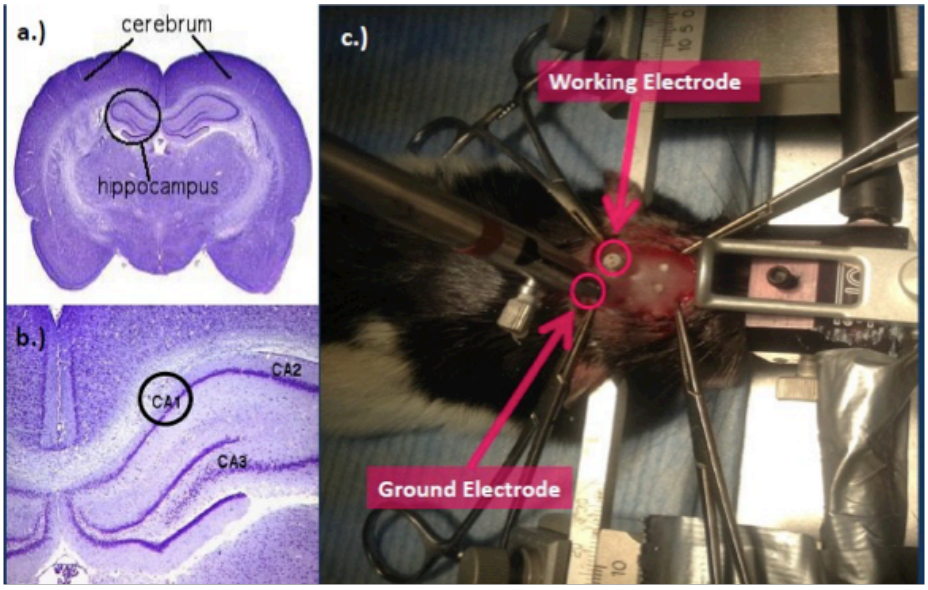

Figure 4.3 Set up of the working electrode and counter electrode. the position of the PEDOT-gel coated cannula tip (working) was inserted into one hemisphere and the bare electrode (counter) was inserted into the other.

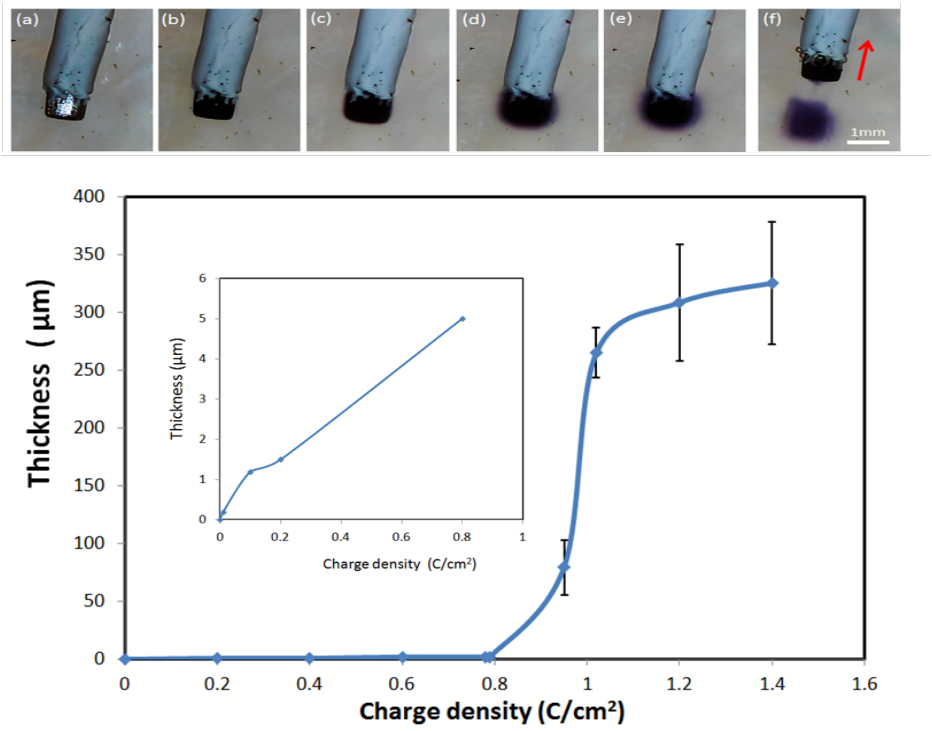

Figure 4.4 (Top) the optical images showing the progress of PEDOT polymerized into hydrogels. The maximum thickness of PEDOT cloud in the gel was about 350 µm. (bottom) the thickness plot with respect with charge density confirming that PEDOT was initially deposited on the electrode as a thin film then at charge density of 0.8 C/cm^2, PEDOT starts to grow out to the hydrogel matrix.

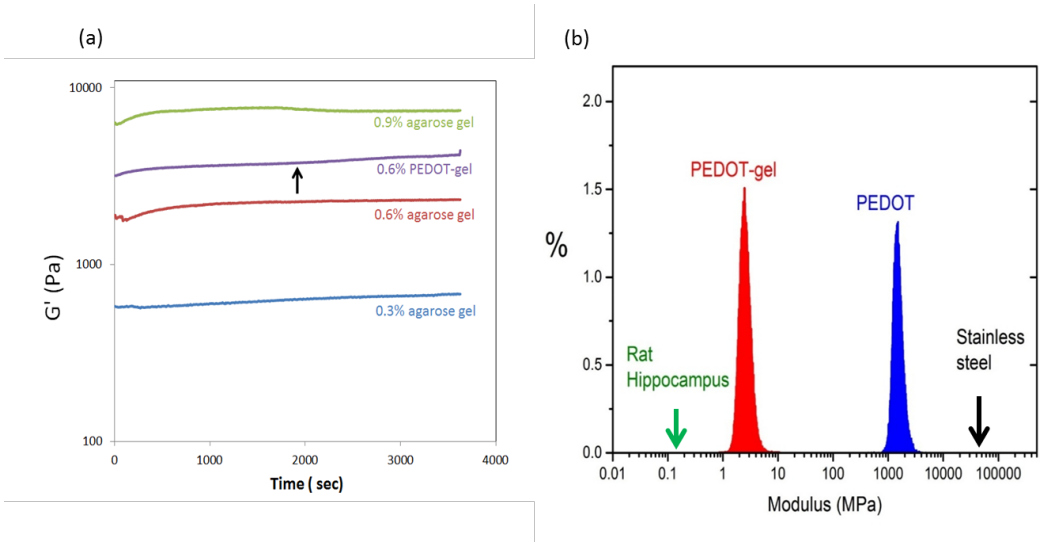

Figure 4.5 The mechanical analysis of PEDOT-gel in (a) hydrated condition by rheometer and (b) dehydrated condition by AFM-QNM. The arrows indicate the mechanical modulus of rat hippocampus and stainless steel for the reference.

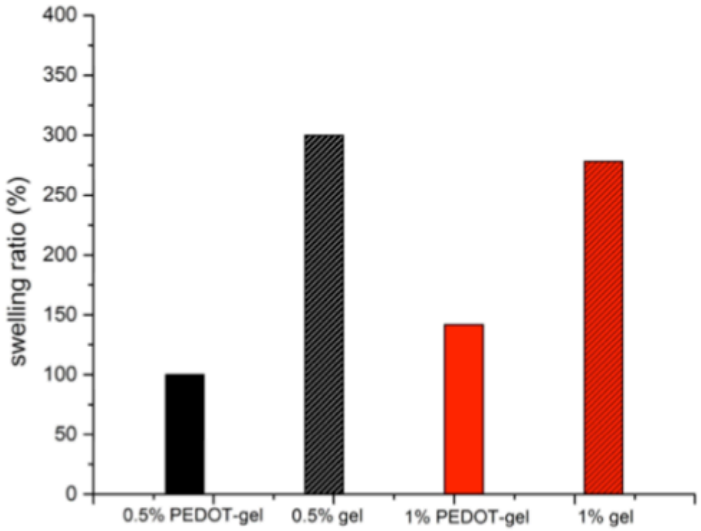

Figure 4.6 Swelling ratio of agarose gel and PEDOT-gel at different gel concentration at 0.5% and 1.0%. The presence of PEDOT inhibits the re-swelling ratio to about 30-50% of pure agarose gel.

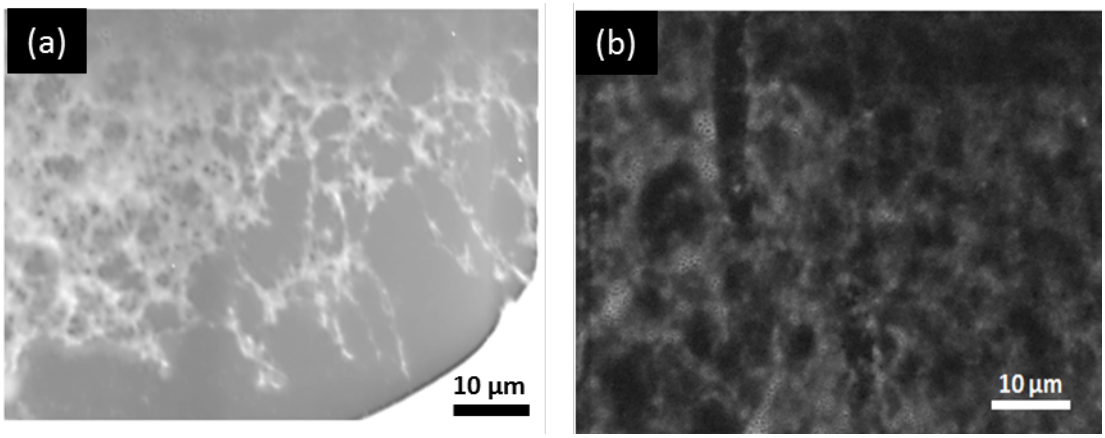

Figure 4.7 SEM images of (a) hydrated PEDOT-gel (b) re-hydrated PEDOT-gel in DI water obtained by using WET SEM holder. Samples were images in the initial hydrated condition and then air dried in the room temperature overnight. The same samples were then immersed in DI water and imaged by SEM.

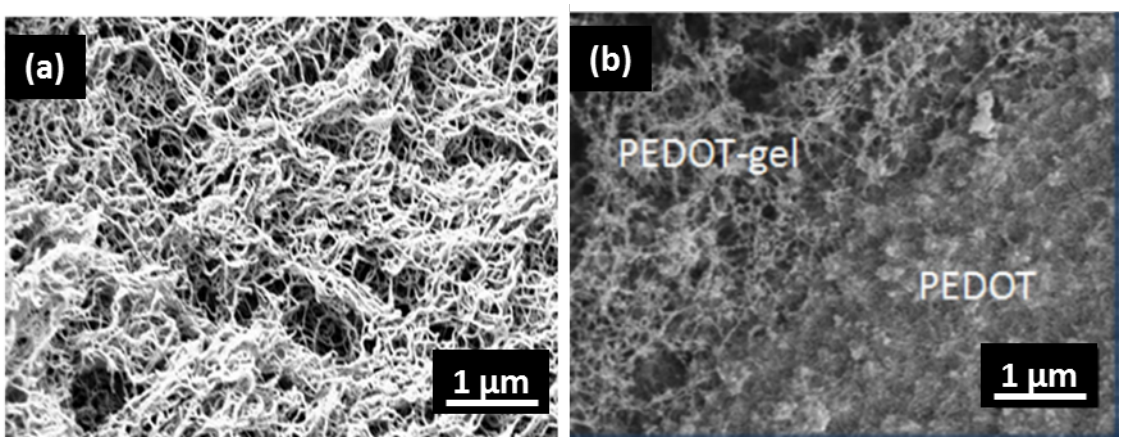

Figure 4.8 SEM images of (a) agarose gel and (b) PEDOT-gel prepared by critical point dry method. An obvious boundary between the PEDOT and PEDOT-gel interface was observed confirming the initial PEDOT thin film deposition on electrodes.

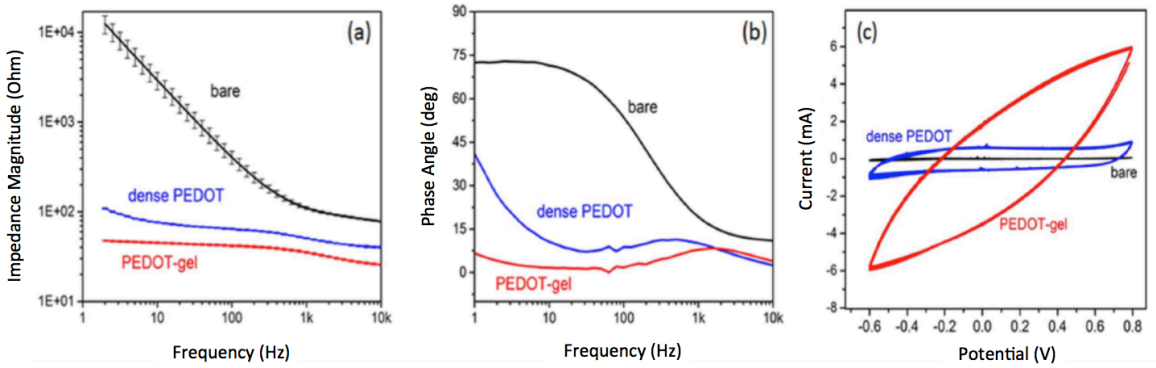

Figure 4.9 Electrical properties of PEDOT-gel was examined by EIS and CV. For EIS, (a) impedance amplitude and (b) phase angle of bare electrode, PEDOT coated, and PEDOT-gel coated electrode was compared over the frequency range between 1 Hz to 10kHz was. (c) CV was swept between -0.6 to 0.8 V for 20 cycles.

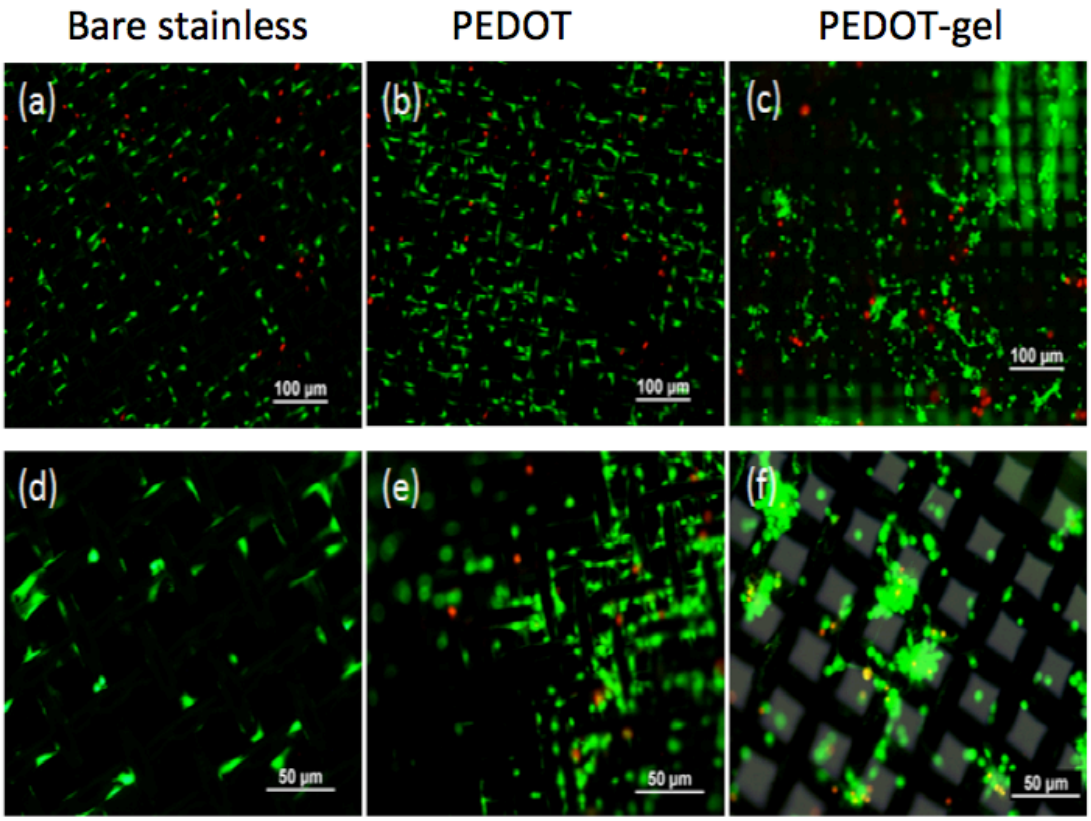

Figure 4.10 Viability tests of PC12 cells on bare, PEDOT coated and PEDOT-gel coated electrodes. PC12s were stained with live/dead viability kit where red represents dead cells and green represents live cells.

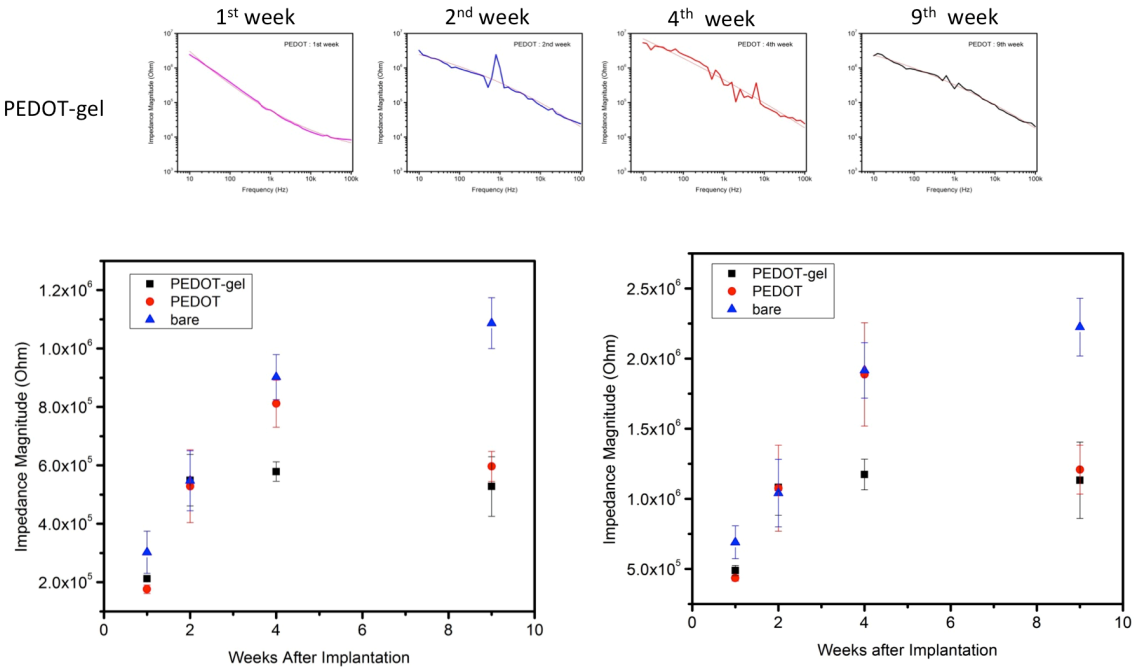

Figure 4.11 In vivo impedance of bare, PEDOT coated and PEDOT-gel coated electrodes implanted in rat hippocampus as working electrode in one hemisphere and a counter electrode in the other hemisphere. The recordings were taken and averaged every other day (three times a week) until 9 weeks of implantation. The data recorded at week 1, 2, 4 and 9 were plotted among 9 individual test (n=9).

REFERENCES

Abidian, M. R., Daneshvar, E. D., Egeland, B. M., Kipke, D. R., Cederna, P. S., & Urbanchek, M. G. (2012). Hybrid conducting polymer-hydrogel conduits for axonal growth and neural tissue engineering. *Advanced Healthcare Materials*, *1*(6), 762–7. http://doi.org/10.1002/adhm.201200182

Åsberg, P., & Inganäs, O. (2003). Hydrogels of a conducting conjugated polymer as 3-D enzyme electrode. *Biosensors and Bioelectronics*, *19*(3), 199–207. http://doi.org/10.1016/S0956-5663(03)00220-3

Biran, R., Martin, D. C., & Tresco, P. a. (2005). Neuronal cell loss accompanies the brain tissue response to chronically implanted silicon microelectrode arrays. *Experimental Neurology*, *195*(1), 115–26. http://doi.org/10.1016/j.expneurol.2005.04.020

Clark, A. H., Gidley, M. J., Richardson, R. K., & Ross-Murphy, S. B. (1989). Rheological studies of aqueous amylose gels: the effect of chain length and concentration on gel modulus. *Macromolecules*, *22*(1), 346–351. http://doi.org/10.1021/ma00191a063

Cui, X., Lee, V. a., Raphael, Y., Wiler, J. a., Hetke, J. F., Anderson, D. J., & Martin, D. C. (2001). Surface modification of neural recording electrodes with conducting polymer/biomolecule blends. *Journal of Biomedical Materials Research*, *56*, 261–272. http://doi.org/10.1002/1097-4636(200108)56:2<261::AID-JBM1094>3.0.CO;2-I

Cui, X., Wiler, J., Dzaman, M., Altschuler, R. a, & Martin, D. C. (2003). In vivo studies of polypyrrole/peptide coated neural probes. *Biomaterials*, *24*(5), 777–87. Retrieved from http://www.ncbi.nlm.nih.gov/pubmed/12485796

Dai, T., Qing, X., Lu, Y., & Xia, Y. (2009). Conducting hydrogels with enhanced mechanical strength. *Polymer*, *50*(22), 5236–5241. http://doi.org/10.1016/j.polymer.2009.09.025

Dai, T., Qing, X., Zhou, H., Shen, C., Wang, J., & Lu, Y. (2010). Mechanically strong conducting hydrogels with special double-network structure. *Synthetic Metals*, *160*(7-8), 791–796. http://doi.org/10.1016/j.synthmet.2010.01.024

Dokukin, M. E., & Sokolov, I. (2012). Quantitative mapping of the elastic modulus of soft materials with HarmoniX and PeakForce QNM AFM modes. *Langmuir : The ACS Journal of Surfaces and Colloids*, *28*(46), 16060–71. http://doi.org/10.1021/la302706b

Drury, J. L., & Mooney, D. J. (2003). Hydrogels for tissue engineering: scaffold design variables and applications. *Biomaterials*, *24*(24), 4337–4351. http://doi.org/10.1016/S0142-9612(03)00340-5

Elkin, B. S., Ilankovan, A., & Morrison, B. (2010). Age-dependent regional mechanical properties of the rat hippocampus and cortex. *Journal of Biomechanical Engineering*, *132*(1), 011010. http://doi.org/10.1115/1.4000164

Forrest, S. R. (2004). electronic appliances on plastic, 911–918.

Gerard, M., Chaubey, A., & Malhotra, B. D. (2002). Application of conducting polymers to biosensors. *Biosensors and Bioelectronics*, *17*, 345–359. http://doi.org/10.1016/S0956-5663(01)00312-8

Green, R. a, Hassarati, R. T., Goding, J. a, Baek, S., Lovell, N. H., Martens, P. J., & Poole-Warren, L. a. (2012). Conductive hydrogels: mechanically robust hybrids for use as biomaterials. *Macromolecular Bioscience*, *12*(4), 494–501. http://doi.org/10.1002/mabi.201100490

Green, R. A., Lovell, N. H., Wallace, G. G., & Poole-Warren, L. A. (2008). Conducting polymers for neural interfaces: Challenges in developing an effective long-term implant. *Biomaterials*, *29*(24-25), 3393–3399. http://doi.org/10.1016/j.biomaterials.2008.04.047

Hassarati, R. T., Goding, J. a., Baek, S., Patton, A. J., Poole-Warren, L. a., & Green, R. a. (2014). Stiffness quantification of conductive polymers for bioelectrodes. *Journal of Polymer Science Part B: Polymer Physics*, *52*(9), 666–675. http://doi.org/10.1002/polb.23465

Huynh, W. U. (2002). Hybrid Nanorod-Polymer Solar Cells. *Science*, *295*(5564), 2425–2427. http://doi.org/10.1126/science.1069156

Ido, Y., Takahashi, D., Sasaki, M., Nagamine, K., Miyake, T., Jasinski, P., & Nishizawa, M. (2012). Conducting Polymer Microelectrodes Anchored to Hydrogel Films. *ACS Macro Letters*, *1*(3), 400–403. http://doi.org/10.1021/mz2002406

Ismail, Y. a., Martínez, J. G., Al Harrasi, A. S., Kim, S. J., & Otero, T. F. (2011). Sensing characteristics of a conducting polymer/hydrogel hybrid microfiber artificial muscle. *Sensors and Actuators B: Chemical*, *160*(1), 1180–1190. http://doi.org/10.1016/j.snb.2011.09.044

Karumbaiah, L., Saxena, T., Carlson, D., Patil, K., Patkar, R., Gaupp, E. A., … Bellamkonda, R. V. (2013). Relationship between intracortical electrode design and chronic recording function. *Biomaterials*, *34*(33), 8061–8074. http://doi.org/10.1016/j.biomaterials.2013.07.016

Kim, D.-H., Abidian, M., & Martin, D. C. (2004). Conducting polymers grown in hydrogel scaffolds coated on neural prosthetic devices. *Journal of Biomedical Materials Research. Part A*, *71*(4), 577–85. http://doi.org/10.1002/jbm.a.30124

Kim, D.-H., Wiler, J. a, Anderson, D. J., Kipke, D. R., & Martin, D. C. (2010). Conducting polymers on hydrogel-coated neural electrode provide sensitive

neural recordings in auditory cortex. *Acta Biomaterialia*, *6*(1), 57–62. http://doi.org/10.1016/j.actbio.2009.07.034

Kim, W. H., Mäkinen, A. J., Nikolov, N., Shashidhar, R., Kim, H., & Kafafi, Z. H. (2002). Molecular organic light-emitting diodes using highly conducting polymers as anodes. *Applied Physics Letters*, *80*(20), 3844–3846. http://doi.org/10.1063/1.1480100

Lang, U., Naujoks, N., & Dual, J. (2009). Mechanical characterization of PEDOT:PSS thin films. *Synthetic Metals*, *159*, 473–479. http://doi.org/10.1016/j.synthmet.2008.11.005

Luo, Y., Kirker, K. R., & Prestwich, G. D. (2000). Cross-linked hyaluronic acid hydrogel films: New biomaterials for drug delivery. *Journal of Controlled Release*, *69*(1), 169–184. http://doi.org/10.1016/S0168-3659(00)00300-X

Luo, Y., & Shoichet, M. S. (2004). A photolabile hydrogel for guided three-dimensional cell growth and migration. *Nature Materials*, *3*(4), 249–53. http://doi.org/10.1038/nmat1092

Mawad, D., Stewart, E., Officer, D. L., Romeo, T., Wagner, P., Wagner, K., & Wallace, G. G. (2012). A Single Component Conducting Polymer Hydrogel as a Scaffold for Tissue Engineering. *Advanced Functional Materials*, *22*(13), 2692–2699. http://doi.org/10.1002/adfm.201102373

Nguyen, J. K., Park, D. J., Skousen, J. L., Hess-Dunning, A. E., Tyler, D. J., Rowan, S. J., … Capadona, J. R. (2014). Mechanically-compliant intracortical implants reduce the neuroinflammatory response. *Journal of Neural Engineering*, *11*, 056014. http://doi.org/10.1088/1741-2560/11/5/056014

Pan, L., Yu, G., Zhai, D., Lee, H. R., Zhao, W., Liu, N., … Bao, Z. (2012). Hierarchical nanostructured conducting polymer hydrogel with high electrochemical activity. *Proceedings of the National Academy of Sciences of the*

United States of America, *109*(24), 9287–92. http://doi.org/10.1073/pnas.1202636109

Peppas, N. a., Hilt, J. Z., Khademhosseini, a., & Langer, R. (2006). Hydrogels in Biology and Medicine: From Molecular Principles to Bionanotechnology. *Advanced Materials*, *18*(11), 1345–1360. http://doi.org/10.1002/adma.200501612

Press, A., Williams, D. J., Sohn, J. E., Marder, S. R., Josse, D., Zyss, J., … Goddard, W. A. (1999). Conducting Polymer Hydrogels as 3D Electrodes : Applications for Supercapacitors ** By Soumyadeb Ghosh * and Olle Inganäs, (14), 1214–1218.

Qu, J., Ouyang, L., Kuo, C. C., & Martin, D. C. (2016). Stiffness, strength and adhesion characterization of electrochemically deposited conjugated polymer films. *Acta Biomaterialia*, *31*, 114–121. http://doi.org/10.1016/j.actbio.2015.11.018

Richardson-Burns, S. M., Hendricks, J. L., Foster, B., Povlich, L. K., Kim, D. H., & Martin, D. C. (2007). Polymerization of the conducting polymer poly(3,4-ethylenedioxythiophene) (PEDOT) around living neural cells. *Biomaterials*, *28*(8), 1539–1552. http://doi.org/10.1016/j.biomaterials.2006.11.026

Sekine, S., Ido, Y., Miyake, T., Nagamine, K., & Nishizawa, M. (2010). Conducting polymer electrodes printed on hydrogel. *Journal of the American Chemical Society*, *132*(38), 13174–5. http://doi.org/10.1021/ja1062357

Subbaroyan, J., Martin, D. C., & Kipke, D. R. (2005). A finite-element model of the mechanical effects of implantable microelectrodes in the cerebral cortex. *Journal of Neural Engineering*, *2*(4), 103–13. http://doi.org/10.1088/1741-2560/2/4/006

Tabata, Y., Hijikata, S., & Ikada, Y. (1994). Enhanced vascularization and tissue granulation by basic fibroblast growth factor impregnated in gelatin hydrogels. *Journal of Controlled Release*, *31*(2), 189–199. http://doi.org/10.1016/0168-3659(94)00035-2

Wilks, S. J., Richardson-Burns, S. M., Hendricks, J. L., Martin, D. C., & Otto, K. J. (2009). Poly(3,4-ethylenedioxythiophene) as a Micro-Neural Interface Material for Electrostimulation. *Frontiers in Neuroengineering*, *2*(June), 7. http://doi.org/10.3389/neuro.16.007.2009

Winslow, B. D., Christensen, M. B., Yang, W.-K., Solzbacher, F., & Tresco, P. a. (2010). A comparison of the tissue response to chronically implanted Parylene-C-coated and uncoated planar silicon microelectrode arrays in rat cortex. *Biomaterials*, *31*(35), 9163–72. http://doi.org/10.1016/j.biomaterials.2010.05.050

Woolley, A. J., Desai, H. A., & Otto, K. J. (2013). Chronic intracortical microelectrode arrays induce non-uniform, depth-related tissue responses. *Journal of Neural Engineering*, *10*(2), 026007. http://doi.org/10.1088/1741-2560/10/2/026007

Zhang, L., Cao, Z., Bai, T., Carr, L., Ella-Menye, J.-R., Irvin, C., … Jiang, S. (2013). Zwitterionic hydrogels implanted in mice resist the foreign-body reaction. *Nature Biotechnology*, (October 2012). http://doi.org/10.1038/nbt.2580

Chapter 5

CONCLUSIONS AND FUTURE DIRECTIONS

5.1 Conclusions

This thesis discussed methods for preparing and characterizing hybrids of PEDOT as neural interfacing materials. There is a continuing need to build more robust, reliable, conductive and bio-friendly neural interfacing materials for efficient signal transmission (Ludwig et al., 2011)(R a Green et al., 2013a), neural regeneration (Christine E Schmidt, Shastri, & Vacanti, 2016) (Abidian et al., 2006) , and controlled drug delivery (Abidian et al., 2012). The challenges include the mechanical failures and the chronic foreign body response during implantation. In this thesis, we addressed those issues with various approaches.

The mechanical failures of PEDOT include delamination and cracking of coatings after chronic implantation. These mechanical failures contribute to dysfunction of PEDOT coated devices. There have been several reports describing the improvement of conducting polymer thin film coatings on devices, such as using EDOT-acid as an adhesion promoter to increase the adhesion strength between the coating and the solid substrate (Wei et al., 2015) and using crosslinked PEDOT to enhance the cohesive strength of PEDOT film itself (Ouyang et al., 2015a). For better

modifications of conducting polymer coatings we need to obtain quantitative data about the mechanical properties and failure modes of PEDOT films including their modulus, strength, strain-to-failure, and toughness. We developed and evaluated the performance of an in situ tensile test to directly evaluate the mechanical behavior of a PEDOT thin films. An electrochemically polymerized PEDOT thin film was machined with a FIB into a dog bone shape specimen and a tensile test conducting in-situ inside the SEM sample chamber. By utilizing Track and Engauge Digitizer software, precise stress-strain curves could be acquired. The Young's modulus was 5±1.0 GPa and the strength to failure was 270±70 MPa among 5 tests. The stress-strain curves of PEDOT thin film so obtained provided us with more comprehensive understandings about PEDOT's mechanical properties for future materials design and selection.

The chronic foreign body response is associated with an insulating glial sheath that encapsulates the implanted electrodes, as well as the loss of proximal neurons, leading to the loss of signal communications. The large mismatch in mechanical properties between the soft tissue and rigid electrode has been associated with the chronic body response. In addition to that, unlike natural tissue, PEDOT itself doesn't provide specific biological cues to promote neural interactions. In this thesis, we investigated the in situ polymerization of PEDOT in soft hydrogels and bioactive extracellular matrices in order to reduce the stiffness and improve the bioactivity of traditional PEDOT film.

In the later section of this thesis, we mainly discussed about the foreign body response. In our lab, we demonstrated that PEDOT could be electrochemically

polymerized into an extracellular matrix providing biological cues to implants. In vitro studies confirmed the improved cell adhesion properties over unmodified PEDOT, suggesting that it would be a bioactive material. Electrical measurements also confirmed its improve charge transport properties for neural interfacing applications. This idea can be elevated to the concept of autologous materials. Potential patients could cells extracted from their own bodies to produce an autologous ECM template which could potentially provide less immune responses during implantation.

Secondly, PEDOT could be polymerized into thermally solidified polysaccharide hydrogels for direct neural interfacing. With the benefit of low modulus of these conductive hydrogels, we could reduce the mechanical mismatch between the implants and neighboring tissues. Animal studies confirmed the performance of these PEDOT-gels as coatings for electrodes implanted in rat hippocampus. The impedances remained low, indicating that theses implants were able to improve the integration with the neural tissue.

5.2 Future Directions

5.2.1 Conductive Micro-organism Coated Electrodes

Exoelectrogens such as Geobacter are anaerobic bacteria that can directly transfer electrons in and out through hairy structures on their surfaces known as pili (Lovley et al., 2011). Their ability to harvest electrons from organic compounds and then transfer the electrons to metals makes them potential candidates for interfacing organic tissues with metallic electrodes (Lovley et al., 2011). Ramesh et al showed that the conductivity of individual pili is highly dependent upon pH. At pH=7, a

conductivity of 51 ± 19 mS cm^{-1} was measured (Adhikari, Malvankar, Tuominen, & Lovley, 2016). According to this report, the conductivity of the individual pili was comparable to organic conducting polymer wires of a similar size where 0.91 mS cm^{-1} of polypyrrole fibers with 80 nm diameter (L. Liu et al., 2006) and 90-600 mS cm^{-1} of PEDOT wire with 10 nm diameter (Samitsu et al., 2005). Considering its great conductivity and the living micro-organism properties, Geobacters may serve as means to create a biofriendly, soft, and conductive material for biomedical applications. Here, we investigated the idea of "electrochemical deposition" of these geobacter cultures directly onto metallic electrodes to bridge tissues and metals.

GS-15, Geobacter metallireducens (ATCC 53774) were chosen for this study. Two Pt-Ir rods were placed into a culture tube with sealed conditions maintaining the anaerobic environment. One electrode was used as the working electrode and the other as the counter electrode. A potentiostat (ModuLab, Solartron Analytical) was used to generate electrical potential needed to deposited Geobacters onto the working electrode. EIS spectra indicated that a material of some sort, evidently derived from the Geobacters, was deposited on the electrode, making the impedance lower with process time. Figure 5.2 shows the impedance of Geobacter coated electrode with different process times. The embedded plot shows the impedance of bare electrode before deposition. This preliminary data confirmed that electrochemically-deposited materials derived from Geobacter suspensions can significantly lower the impedance, and hence potentially can be used as the neural interfacing materials. Further studies are required to confirm the properties of this Geobacter coating such as its

composition, structure, mechanical properties, biocompatibility and potential reliability as an implant coating material.

5.2.2 *In Situ* Observations of PEDOT Electrochemical Polymerization

As described in this thesis, hydrogels have been used to modify the structure and properties of conducting polymers as a soft and open structure allowing both ionic and electronic transport (Martin et al., 2010). These conductive hydrogels have shown great promise as potential materials for direct neural interfaces. However, the detailed mechanism of their formation is still not yet studied. Without a comprehensive understating of the formation of these conductive hydrogels, it is difficult to optimize the properties of these new materials. This condition is even more complicated with conductive polymers involved in hydrogels considering the fluids in the gels and the complicated structure of gel backbones itself. This makes the analysis of their formation more challenging. Figure 5.2 shows optical microscope images monitoring the progress of PEDOT deposited in a template of 1% agarose hydrogel. It was found that after a certain period of time (typically ~30 mins) there were birefringent crystallites forming around the gold wire serving as the working electrode. The dark crystals increased in size with longer polymerization times. The size of crystals was controlled by many factors. Figure 5.3 shows the crystal length with respect with the hydrogel concentration and PSS concentration. The results indicate crystal size increased with gel concentration. It was found that without PSS, there were no crystals formed around electrode. The size of crystals decreased with PSS concentration. When the concentration of PSS was near 2.0% wt, no crystals were observed. Figure 5.4 shows TEM images of those crystals. A clear single-crystal texture could be observed

inside the crystals by electron diffraction and larger, reasonably regular "pore" structures were observed by density fluctuations in bright field images (Figure 5.4). The typical size of these regular structures was estimated to be around 10 nm. A series of experiments also confirmed that these crystals were associated with PEDOT deposition. However, the detailed composition of these crystals, and the mechanism of their formation is still unclear. Higher resolution microscopy capable to obtain in situ information during the process is required to obtain the detail information of the crystal formation process.

A recent report from our lab has shown high resolution images of PEDOT deposition process in aqueous solution can be obtained, providing an unprecedented degree of detail about the process (J. Liu et al., 2015). The experiments were conducted with a ProtoChips Poseidon 500 cell in a 300 kV JEOL 3010 Scanning Transmission Electron Microscope (STEM). By adapting and extended this method, we expect to reveal the detailed mechanisms involved in forming PEDOT and its related products in gels and in the presence of living cells.

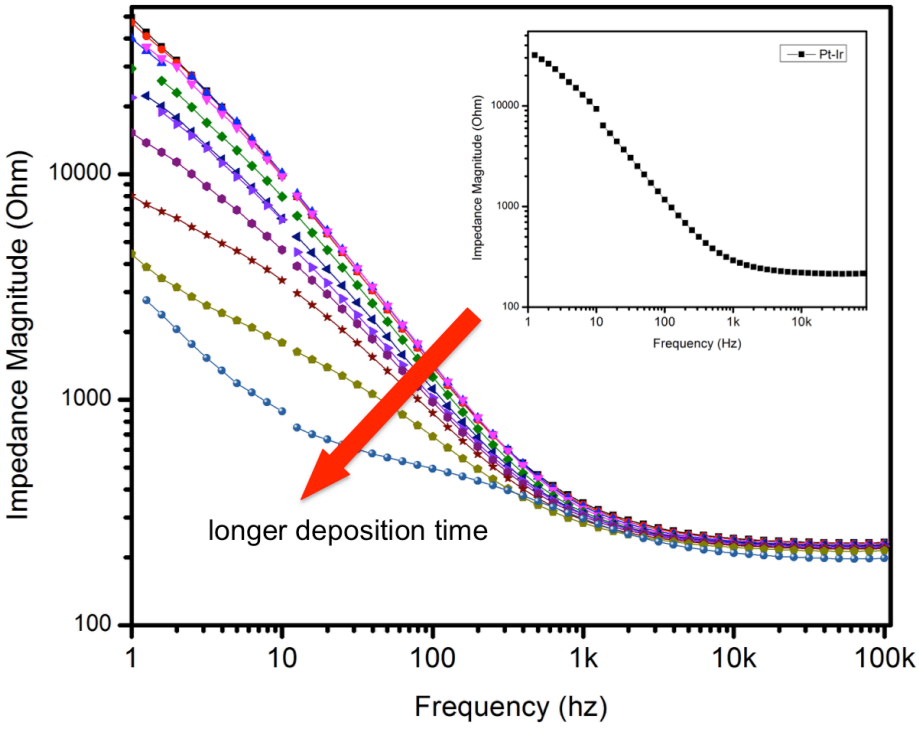

Figure 5.1 Impedance spectra with respect with processing time for Geobacter deposition on Pt-Ir electrode shows that the impedance is lower with more Geobacter-derived material deposited. The embedded plot is the impedance spectra of a bare Pt-Ir electrode for reference.

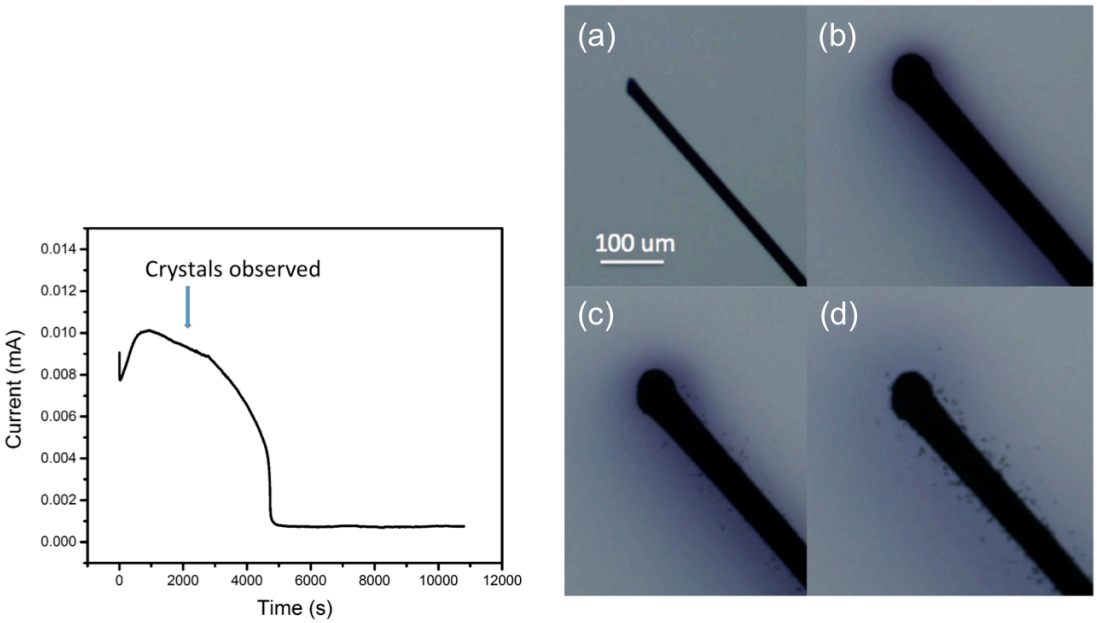

Figure 5.2 (Right) the corresponding current recording during crystals formation. A significant drop of current reading was recorded where crystals were observed under optical microscope. (left) optical micrographs of the electrochemical deposition of PEDOT on a 25 micron diameter gold wire in the presence of agarose gel under potentiostatic condition of (a) 0, (b) 10 minutes, (c) 20 minutes, and (d) 30 minutes deposition time. After 20 minutes, birefringent, needle-shaped crystals were initially observed and then saturated after 30 minutes deposition.

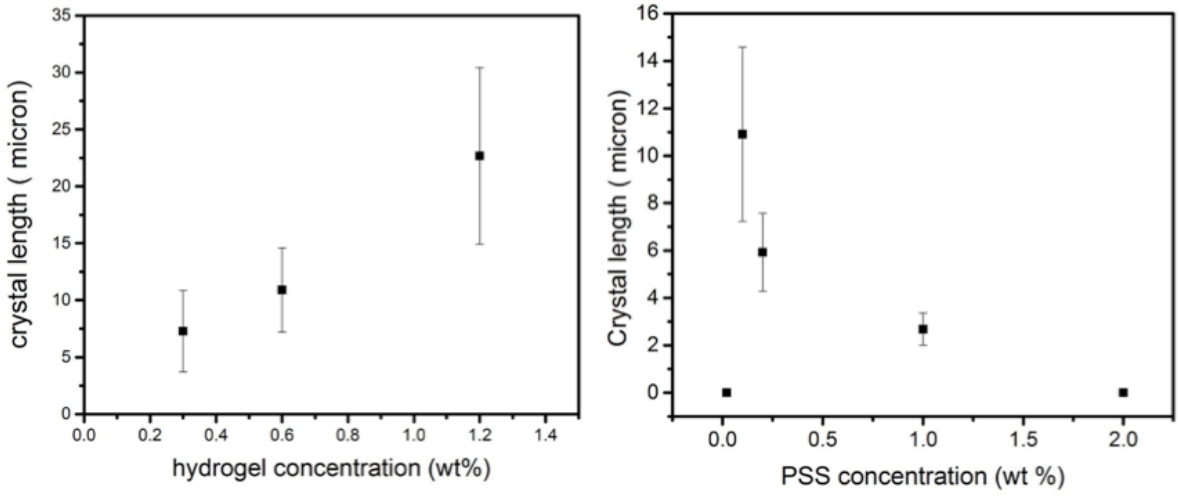

Figure 5.3 Crystal length with respect to the hydrogel concentration and PSS concentration. The results suggested that without PSS or higher concentration of PSS, no crystals were observed in the system. (N=2 for each group. 3 images were analyzed from each sample. There were about 60-80 counts from each image. The final value is averaged from 300-500 countings)

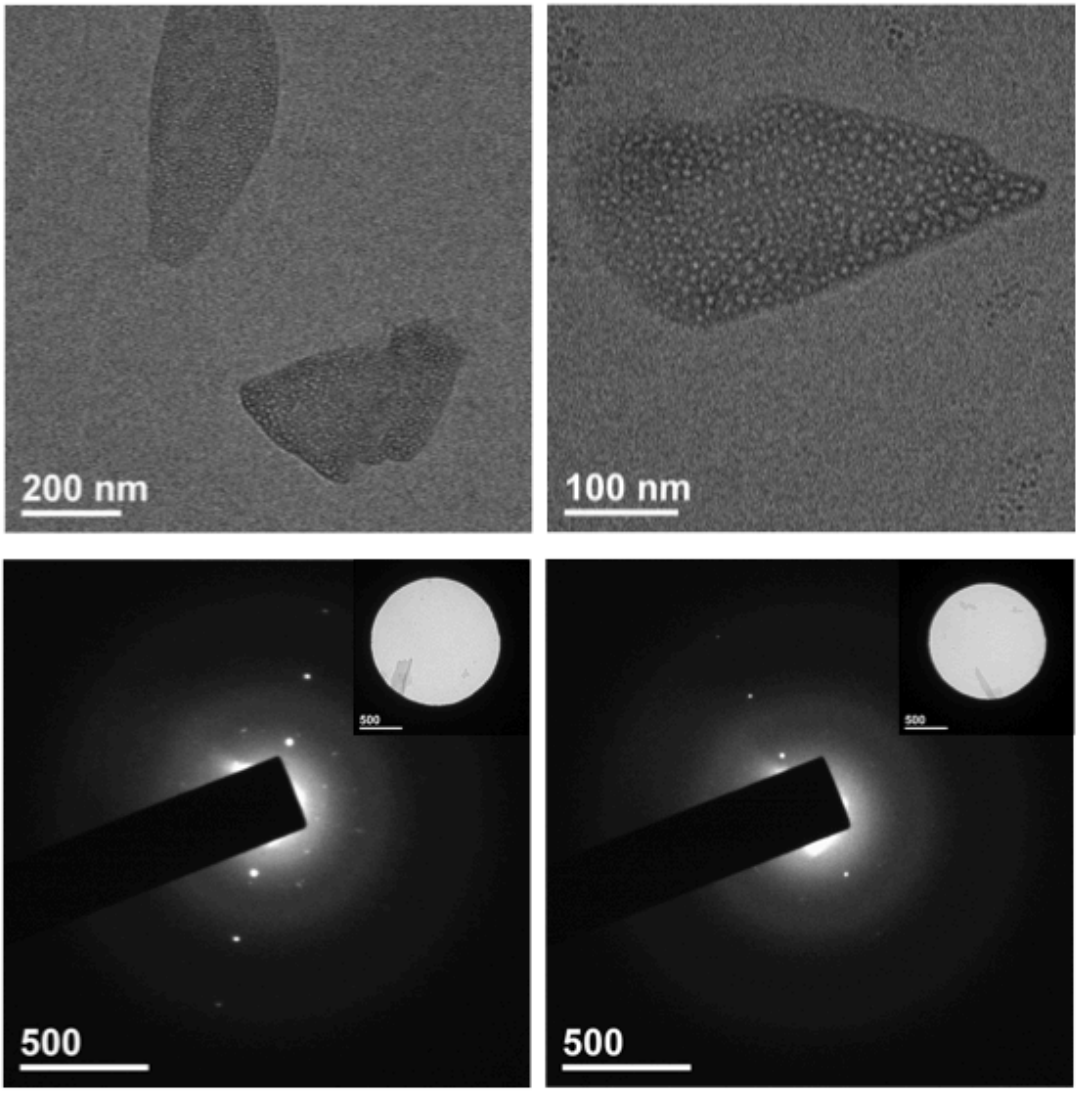

Figure 5.4 TEM micrographs of PEDOT-crystals formed in the hydrogel.

REFERENCES

Abidian, M. R., Daneshvar, E. D., Egeland, B. M., Kipke, D. R., Cederna, P. S., & Urbanchek, M. G. (2012). Hybrid conducting polymer-hydrogel conduits for axonal growth and neural tissue engineering. *Advanced Healthcare Materials*, *1*(6), 762–7. http://doi.org/10.1002/adhm.201200182

Abidian, M. R., Kim, D.-H., & Martin, D. C. (2006). Conducting-Polymer Nanotubes for Controlled Drug Release. *Advanced Materials (Deerfield Beach, Fla.)*, *18*(4), 405–409. http://doi.org/10.1002/adma.200501726

Adhikari, R. Y., Malvankar, N. S., Tuominen, M. T., & Lovley, D. R. (2016). Conductivity of individual Geobacter pili. *RSC Adv.*, *6*(10), 8354–8357. http://doi.org/10.1039/C5RA28092C

Green, R. a, Matteucci, P. B., Hassarati, R. T., Giraud, B., Dodds, C. W. D., Chen, S., … Lovell, N. H. (2013). Performance of conducting polymer electrodes for stimulating neuroprosthetics. *Journal of Neural Engineering*, *10*(1), 016009. http://doi.org/10.1088/1741-2560/10/1/016009

Liu, J., Wei, B., Sloppy, J. D., Ouyang, L., Ni, C., & Martin, D. C. (2015). Direct Imaging of the Electrochemical Deposition of Poly(3,4-ethylenedioxythiophene) by Transmission Electron Microscopy. *ACS Macro Letters*, *4*(9), 897–900. http://doi.org/10.1021/acsmacrolett.5b00479

Liu, L., Zhao, Y., Jia, N., Zhou, Q., Zhao, C., Yan, M., & Jiang, Z. (2006). Electrochemical fabrication and electronic behavior of polypyrrole nano-fiber array devices. *Thin Solid Films*, *503*(1-2), 241–245. http://doi.org/10.1016/j.tsf.2005.11.046

Lovley, D. R., Ueki, T., Zhang, T., Malvankar, N. S., Shrestha, P. M., Flanagan, K.

A., … Nevin, K. P. (2011). *Geobacter. The Microbe Electric's Physiology, Ecology, and Practical Applications*. *Advances in Microbial Physiology* (1st ed., Vol. 59). Elsevier Ltd. http://doi.org/10.1016/B978-0-12-387661-4.00004-5

Ludwig, K. a, Langhals, N. B., Joseph, M. D., Richardson-Burns, S. M., Hendricks, J. L., & Kipke, D. R. (2011). Poly(3,4-ethylenedioxythiophene) (PEDOT) polymer coatings facilitate smaller neural recording electrodes. *Journal of Neural Engineering*, *8*, 014001. http://doi.org/10.1088/1741-2560/8/1/014001

Martin, D. C., Wu, J., Shaw, C. M., King, Z., Spanninga, S. a., Richardson-Burns, S., … Yang, J. (2010). The Morphology of Poly(3,4-Ethylenedioxythiophene). *Polymer Reviews*, *50*(3), 340–384. http://doi.org/10.1080/15583724.2010.495440

Ouyang, L., Kuo, C., Farrell, B., Pathak, S., Wei, B., Qu, J., & Martin, D. C. (2015). Poly[3,4-ethylene dioxythiophene (EDOT)-co-1,3,5-tri[2-(3,4-ethylene dioxythienyl)]-benzene (EPh)] copolymers (PEDOT-co-EPh): optical, electrochemical and mechanical properties. *J. Mater. Chem. B*, *3*(25), 5010–5020. http://doi.org/10.1039/C5TB00053J

Samitsu, S., Shimomura, T., Ito, K., Fujimori, M., Heike, S., & Hashizume, T. (2005). Conductivity measurements of individual poly(3,4-ethylenedioxythiophene)/ poly(styrenesulfonate) nanowires on nanoelectrodes using manipulation with an atomic force microscope. *Applied Physics Letters*, *86*(23), 1–3. http://doi.org/10.1063/1.1940725

Schmidt, C. E., Shastri, V. R., & Vacanti, J. P. (2016). Stimulation of Neurite Outgrowth Using an Electrically Conducting Polymer Source : Proceedings of the National Academy of Sciences of the United States of America , Published by : National Academy of Sciences Stable URL : http://www.jstor.org/stable/42537 Stimulation of neurite outgrowt : hL using an electrically conducting polymer, *94*(17), 8948–8953.

Wei, B., Liu, J., Ouyang, L., Kuo, C.-C., & Martin, D. C. (2015). Significant Enhancement of PEDOT Thin Film Adhesion to Inorganic Solid Substrates with EDOT-Acid. *ACS Applied Materials & Interfaces*, *7*(28), 15388–94.

http://doi.org/10.1021/acsami.5b03350